uc3m | Universidad Carlos III de Madrid

Bachelor Thesis

Degree in Aerospace Engineering

Design and Validation of a 3D Magnetic Nozzle for Thrust Steering

Iñigo Alforja Ruiz

TUTOR

Jaume Navarro Cavallé

2017 - 2018

Abstract

Electric space propulsion is one of the main fields of study in space engineering nowadays. It is considered to be the future of space propulsion, already being implemented in one third of existent satellites. However, operating such motors requires expensive, heavy and complex steering platforms in order to orient the direction of the plasma, and thus the direction of the thrust vector.

The project presented aims to explain the development of a prototype of a 3-dimensional magnetic nozzle, which has been recently patented by the research group of EP2 (*Equipo de Propulsión Espacial y Plasmas*). This magnetic nozzle will allow to steer the thrust vector freely and without moving parts, and involves only slight modifications in thrusters which already have a magnetic nozzle.

In order to do so, the first prototype showing this technology presented has been designed in such a way that it is compatible with the plasma source of the EP2 laboratory. This model will be tested in the vacuum chamber simulating space conditions. The process of validating such a prototype is also presented.

The work presented shows the complete design process of such an innovative technology and the different achieved characteristics. This is followed by the development and verification of the validation process and the proposed experiments to completely validate the prototype. Since the model could not be manufactured for validation, different experiment proposals are given to prove the validity of the thrust-steering device.

Key words: 3D magnetic nozzle, electric propulsion, thrust vector control, design, validation process, magnetic field

Acknowledgements

First of all, I would like to thank the EP2 team for the opportunity to work with them in such an interesting project. In particular, Jaume and Pablo who have patiently guided me throughout the year, teaching me how to deal with actual engineering problems. Also, I would like to express my gratitude to Mick, without whom I would not have been able to perform any experiment. Thank you all for your help.

This project could not have been done without the support of my whole family. Thank you to my parents for listening to my continuous rants against all the problems that have surged throughout the project, but also for showing interest in it (even though we all know it was not so interesting to hear). Thank you also to my siblings, Ainhoa, Joaquin and Diego, for studying economics and making it so easy for me to be the intelligent one (you know I love you). Thank you all for believing in me.

I would also like to acknowledge the support of all my friends from Pamplona, who have always been happy to celebrate any good news I have given them. In particular, I want to thank Alzueta and Chusma for the great conversations in front of a beer and Decar for his encouragement from anywhere in world. And, of course, I have to thank Basiano, who has always been there to support me in all aspects of my life (although most conversations end up being about completely unrelated topics).

Special gratitude must be given to Juan and Diego, who have been amazing flatmates during this year. University worries are less tough with the company of friends (and of video games, of course).

I want to give my most special thanks to the person who has been there everyday to bear with all the details of this project. Pizza days, strolls and Parks and Rec have been essential to keep our sanity during this work. All the words in the world fail to express how grateful I am for your support in my life. I love you very much, Patricia.

Lastly, I would like to show my biggest gratitude to my Amatxi, Babela and Eliana. You have showed me the importance of working the best of oneself and overcome all the possible problems that may arise in our lives. You are life models.

Contents

List of Figures

List of Tables

1 Introduction

1.1 Motivation and Socio-Economic Impact

In the last two decades, the Space has become again one of the main spotlights for the development of Science and Technology. The interest in both knowing about the nature of the Universe (such as deep space missions, Earth observation missions, etc.) and using it (for example, for telecommunication purposes, climate change, etc.) has provoked immense efforts in the aerospace industry to achieve such purposes.

Among the main topics of study about space matters, space propulsion has been one of the most analyzed to ensure optimal performance by using the least amount of means. In such a way, electric propulsion is nowadays the principal subject of these studies, due to its clear advantages in weight and fuel economy against chemical propulsion in space maneuvering activities, as well as to its promising future in long distance space missions. In fact, these investigations are nowadays moving towards next-generation space plasma thrusters, such as the Helicon Plasma Thruster or the VASIMR. The acceleration stage of such thrusters depends on what are called *magnetic nozzles*; devices able to apply a convergent-divergent magnetic field which guides and accelerates the plasma jet into vacuum. In this way the internal energy of the plasma is converted into axially-directed kinetic energy, thus producing an effective thrust. Efforts are put nowadays in the understanding and development of these systems.

One of the most innovative proposals for the design of such a magnetic nozzle was presented by Mario Merino and Eduardo Ahedo [1]. They proposed a magnetic nozzle system composed of several coils at different angles, able to steer the plasma jet in different directions, allowing the deflection of the thrust vector without movable parts. The only requirement for this new system was its capability to modify the magnetic field generated by varying the intensity going through the coils, changing the direction in which the plasma is guided. This theoretical device was patented by both authors [2], although no actual experimental data sustaining its results has been shown yet.

Therefore, the scope of this work is to design, develop and validate a prototype following the description of the three-dimensional magnetic nozzle given by Merino and Ahedo both in their paper and in their patent to prove the validity of their idea. In fact, showing correct performance of this prototype will suppose a immense step in the electric propulsion technologies. It would provide a solution for plasma propulsion that has all the advantages of magnetic-nozzle-using thrusters as well as those related to the non-necessity of moving parts for the steering of plasma. Among all these advantages, one finds the contactless and electrodeless handling of plasma, reducing critical points of failure due to plasma-material interaction and increasing the lifetime of the space system; the tunable magnetic field in flight, which adapts to the necessities of the spacecraft at each moment; or the simplicity of the magnetic

nozzle, which by removing the moving parts reduces the failure probability due to malfunction of delicate pieces due to wear or fatigue.

Thus, this report summarizes the work performed in order to design and validate a real three-dimensional magnetic nozzle, in order to prove to the electric propulsion community the feasibility and performance of a "more compact", cheaper and more reliable system of maneuvering a spacecraft. This way, the international knowledge in space propulsion will increase and move towards a system that may push further the development of better and more advanced technologies to continue exploring space and making use of it.

Socio-Economic Impact

As part of the motivation for performing the study of a 3D magnetic nozzle, it is of interest to consider its socio-economic impact. The proposed three-dimensional magnetic nozzle for thrust steering would represent numerous benefits for the aerospace sector and to society in general [1, 3].

On the one hand, one must consider the advantages in terms of economic figures of electric propulsion with respect to chemical propulsion. Electric propulsion needs a much smaller amount of propellant in order to do maneuvers throughout the life of the space system [4], which reduces the overall weight of the spacecraft, and consequently the mission cost for the operating organization. However, costs regarding the auxiliary power source and power processing units to produce and accelerate the plasma must be weighed off against the savings in propellant *per se*. In general, positive balance is achieved when comparing them. Thus, further development in the electric propulsion sector, as the 3D magnetic nozzle, would reduce operation costs of space systems of all types, among which telecommunication satellites (which is the largest commercial segment) would be affected.

Considering the 3D magnetic nozzle, it implies a remarkable simplification at system and subsystem level, making easier the needs or requirements about thrust vectoring or avoiding plasma impingement to the solar panels. In fact, good performance of such a device implies the non-necessity of any moving part to direct the plasma source. Moving parts require complex and heavy mechanisms, which introduce higher required amounts of chemical propellant to put the space system in orbit, which at the same time would additionally increase the dry weight of the system to carry it. This translates directly into higher costs for just putting the system on orbit to start operating: a higher initial cost that could back down potential operators. The 3D magnetic nozzle only requires the mounting of the coils, which is not a significant additional mass as it has been seen. Lower amounts of propellant are needed to send space systems with such a nozzle into space, thus becoming a more attractive and cheaper solution when considering initial costs.

In addition, moving parts, in general, are expensive because their design com-

plexity and the need of mechanisms which imply more testing activities (to ensure each one of the mechanisms is behaving correctly). In addition, it rises several issues such as the necessity of flexible piping and connections, or the increased complexity for thermal control and the demand of a damping system. As the 3D magnetic nozzle only relies on operation of several fixed coils, the complexity in their mounting would only depend on how it is wanted to arrange the wires (whether introducing coils in each other or by interwining wires at different angles with the same radius). In fact, due to the simplicity of the design, few tests concerning measuring the deflection angle when different intensities are applied through the wires would suffice to prove its performance. Production and testing costs would be significantly reduced.

Another main characteristic of current mechanical moving parts controlling the plasma thrust vector is their lower mechanical useful life. This is due to the fact that the mechanical pieces are delicate and may fracture easier in moving conditions due to fatigue and wear. Breaking of any part during operation must be considered at all times when using these steering systems. Thus, their reliability during operation is affected. However, due to the not use of movable parts of the 3D magnetic nozzle, the probabilities of malfunctioning of any of the coils are considerably reduced. This increases the system useful life and its reliability. Higher reliability, for its part, implies greater performance, which is very attractive to potential operators of the system.

As stated before, one of the main types of systems affected would be the telecommunication satellites. In such a way, communications on Earth could become cheaper and more reliable. The market penetration of this device could remarkably reduce costs of space operations, and improve the knowledge of electric related propulsion and technologies, also useful in other sectors. In fact, the development of this device could be also useful for material processing [1], showing the interdisciplinarity of the technology.

In conclusion, three-dimensional magnetic nozzles suppose a cost-effective alternative to current plasma thrust steering technologies, requiring minor modifications in thrusters already working with a magnetic nozzle. Proving the performance of a prototype with such innovative steering device would consist a tremendous step in the development of electric propulsion systems, reducing further the weight and operation costs. This would reduce the costs of sending and operating space systems and the evolution of a space engineering area towards the future of electric propulsion.

1.2 Objectives

In order to properly prove the validity of the idea of a 3D magnetic nozzle proposed by Merino and Ahedo, it was decided to aim for several objectives, being each one a milestone in the process of developing and checking the prototype.

The objectives which the present work aims to fulfill are listed as follows:

- Study the possibilities and feasibility of the 3D magnetic nozzle.
- Size the required coils to generate a desired magnetic field at the exit of the plasma source.
- Design the three dimensional magnetic nozzle in terms of the sized coils and the structural needs to hold them together as a whole system.
- Contact with manufacturers and providers to construct the prototype.
- Study the possibilities of implementing the designed nozzle within the plasma thruster and design attachment solutions to it or existing structures around it.
- Design a validating process to study the performance of the prototype.
- Prove the effectiveness of the validating process.
- Propose experiments needed to validate the prototype.

The different objectives shown will be addressed and tried to fulfill in the following pages. Thus, the rest of the report is structured as follows. In section 2, the state of the art of electric propulsion will be presented, showing the current trends in plasma thrusters as well as the operation principles of a magnetic nozzle. In this same section, the theory underlying the 3D magnetic nozzle will be explained. Section 3 is devoted to the process of design of the 3D magnetic nozzle. A brief explanation showing the type of coils selected is given first. The different physical characteristics determining its features as well as the different design iterations are presented next. The final decided design is shown at the end of this section. In section 4, the validation of the prototype is explained. The validation method as a whole is explained first, followed by the measurement of the magnetic field of a coil to prove its effectiveness. This section ends with a description of the proposed experiments to validate the magnetic nozzle. Section 5 is completely dedicated to the regulatory framework under which the project is done. The following section 6 shows the budget of the project. Finally, in section 7, the conclusions of the work are presented, as well as the envisaged future perspectives.

2 State of the Art

2.1 Electric Propulsion

Electric propulsion has been a division under development in the spacecraft propulsion sector since the 1960s due to its beneficial characteristics in relation with chemical propulsion. However, it has begun to take a widespread impact since the mid-90s. Chemical propulsion is limited by the internal energy of the expanding gas used as propellant. This limit does not exist in general for electric propulsion. In fact, the latter is limited by the amount of electric potential that can be supplied to the gas, which must be ionized into a plasma so that it can react with the applied electromagnetic fields [5, 6, 4].

It is of interest to introduce three main propulsion parameters [4], to be able to explain the performance of both the electric and the chemical propulsion. Firstly, *thrust* is defined as the force obtained by the ejecting propellant which accelerates the vehicle. *Specific impulse (I_{sp})* is the total impulse (or thrust force integrated over burning time) per unit weight of propellant. Finally, one can define *thrust efficiency* as the ratio describing how much of the thrust-producing kinetic energy can be delivered with respect to the total power supplied to the propulsion system.

Electric propulsion systems are divided into four different subsystems for its correct development [4]. These subsystems are the raw energy source (e.g. energy provided by solar panels) and its auxiliaries (such as radiators, pumps, controls, etc.); the conversion devices (power processing units) which adapt the energy to electrical energy at the required conditions of intensity and voltage; the propellant system that stores and delivers the propellant; and the thruster itself which converts electric energy into kinetic energy.

This type of propulsion allows for generally high efficiency thrusters (although some technologies being used have efficiencies of the order of 60%) with low propellant consumption. In fact, with such a propulsion system, higher specific impulses can be achieved, relative to the ones of chemical propulsion. Therefore, a longer operational life for the satellites whose useful life depends on the propellant reservoir can be attained. The differences in maximum amount of specific impulse that can be gained in both propulsion types are due to the gas acceleration mechanism. The specific impulse of the chemical propulsion is limited by the maximum temperature achieved during the exothermic reaction which produces the necessary heat power (it is energy-limited). For electric propulsion, however, this one is related with the extent of external power that the space system can generate and convert, allowing for much higher specific impulse values. However, lower thrust forces can be achieved relative to chemical propulsion, as the rate at which energy is supplied to the propellant is lower. Therefore, electric propulsion systems perform best in space conditions, under the effect of reduced-gravity or gravity-free environments. In general, electric propulsion is useful for overcoming rotational and translational

perturbations of satellites in orbits (such as North-South station keeping; NSSK), and increase the speed of a spacecraft under weak gravity fields. It is envisaged as the power source for potential missions of interplanetary caliber.

Main electric propulsion types

According to how energy is transformed from electrical to kinetic energy, several types of electric propulsion systems can be identified [4, 5]: electrothermal, electrostatic and electromagnetic.

The electrothermal systems heat propellant electrically and then it is expanded thermodynamically to supersonic speeds through a nozzle. Two main propulsion systems of this type can be found [4, 7, 8]:

- *Resistojets*: in it, some components with a very high resistance dissipate power coming from electrical energy (Joule heating) which heats the propellant. It is based in heat exchange principally by convection.
- *Arcjets*: It consists of a central cathode and an annular anode around it. In these kind of devices, the propellant gas is ionized by means of an electrical discharge (or electric arc), such that the gas reaches higher temperatures than those provided in a typical combustion reaction. This hot gas then expands in a conventional nozzle.

On the other hand, electrostatic devices rely on Coulomb forces to accelerate the ionized gas. Although electrons are easier to produce, their small mass makes them carry insufficient momentum for thrusting. Thus, ions are more desirable for these devices operation. Among the most successful electrostatic thrusters, one finds the *gridded ion thruster* [9, 6]. In these systems, two biased parallel grids are used to apply an electric field which accelerates ions to great velocities. Plasma is generated by introducing an internal cathode emitting electrons which collide with the propellant atoms and ionize them (although maintaining quasineutrality of the overall plasma). Ions then enter though the first grid while electrons are repelled, after which they start accelerating due to the applied electric field. Downstream, after the second grid, another external cathode is introduced to emit electrons and neutralize the ion beam. An schematic sketch of such system is shown as follows:

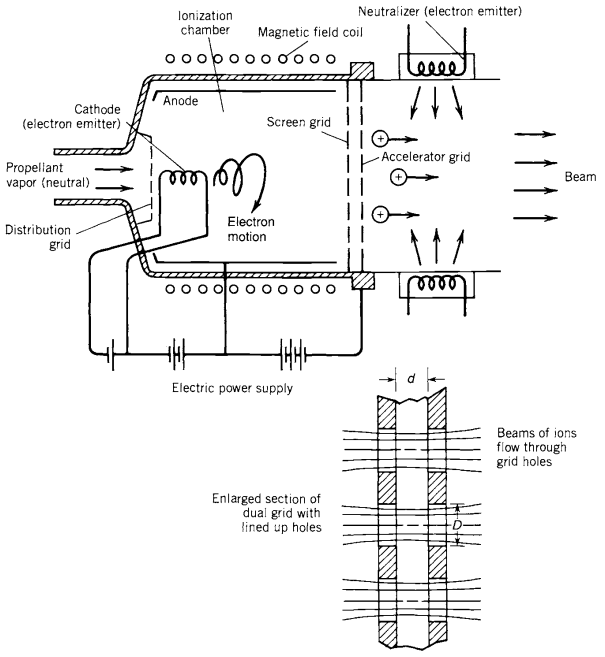

Figure 2.1: Sketch of a Gridded Ion Thruster. Retrieved from [4]

Finally, the remaining type of electric propulsion systems are the electromagnetic ones. These devices generate thrust by means of an interaction between the applied electromagnetic field and the ones within the used plasma. Thus, they rely on Lorentz forces to produce thrust, without the need of grids. Two main systems are worth noting among them [6, 4, 9]:

- *Pulsed plasma thruster*: in this system, a fast discharge between two metal plates is provoked which vaporizes and ionizes a thin layer of Teflon propellant. These particles are accelerated by the self-induced magnetic field produced by the discharge.
- *Hall effect thruster*: in such a device, an axial discharge is achieved inside an annular cavity by means of an anode on its rear-wall and a cathode located outside. Electrons emitted by the cathode try to move towards the internal anode, colliding with neutral gas atoms in their way and, therefore, ionizing them. In order to avoid electrons from short-circuiting the discharge, a radial magnetic field is applied in the annular channel. This produces electrons to drift azimuthally instead of striking the anode directly, this is known as the Hall effect, and it is mainly the electron particle drift due to the $\mathbf{E} \times \mathbf{B}$ term on the electron momentum equation. Produced ions are accelerated by the electric field, which appears due the potential fall established between the anode and the external cathode. Part of the emitted electrons flow with the accelerated ions, neutralizing the exiting plasma. A sketch of this Hall effect thruster is shown next.

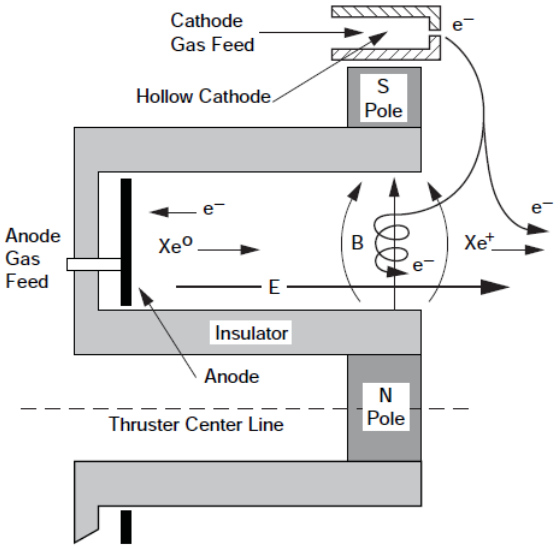

Figure 2.2: Sketch of the cross-section of a Hall Effect Thruster. Retrieved from [9]

However, all the proposed electric propulsion systems presented show certain issues, such as the wear and erosion of the electrodes necessary to generate the plasma. This limits notably the lifespan of such devices. Also, great loss of plasma is experienced by the interaction with the physical walls. In general, several problems rise with the explained propulsive systems by the interaction between plasma and material composing the system.

Next-generation plasma thrusters

In order to overcome such problems, a new generation of advanced plasma thrusters [10] is being investigated to achieve more long-lasting and more efficient propulsive systems. Some of these next-generation plasma thrusters use magnetic nozzles at their exit, limiting the interaction material-plasma and shaping the magnetic field modifying the plasma expansion. These magnetic nozzles are explained in the following section.

The first thruster to be commented is the Helicon Plasma Thruster. The mechanisms and performances of such a thruster are still being studied [11, 12], although the main characteristics can be explained. It consists of a cylindrical radio-frequency (RF) plasma source, followed by a magnetic nozzle. The source of plasma is composed on a cylindrical dielectric vessel, a gas feed, external coils (which unify the axial plasma field), and a RF (radio-frequency) antenna around the tube whose mission is to ionize and energize the gas when power is supplied. Such configuration can be seen in the following sketch:

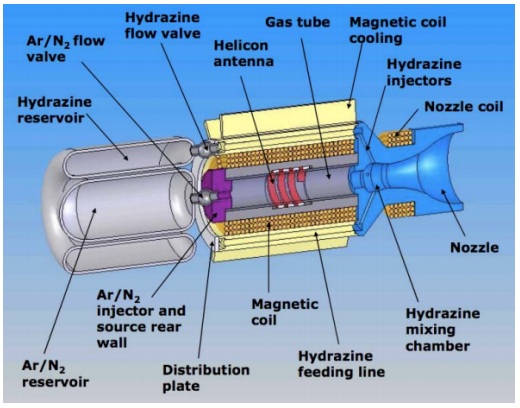

Figure 2.3: Sketch of the main parts of a Helicon Plasma Thruster (HPT). Retrieved from [13]

Helicon waves can produce very dense plasmas. Among the main advantages of this plasma source is the non-necessity of electrodes, which clearly improves the useful life of the thruster. Its simplicity is also a desirable characteristic, which allows for easy manufacturing. Also, it provides high thrust levels with respect to its size and can run with many different propellants (e.g. Xe, Ar, or Kr). However, this thruster is still under many analyses, and its efficiency has to be studied more profoundly, since for the moment it gives very low values [14].

Another interesting plasma thruster is the Applied-Field Magnetoplasmadynamic thruster [15], which still has not been used in any mission yet and thus is still under development. This system also relies on the magnetic nozzle to generate thrust. In this device a current is generated between central cathode and an annular anode which ionizes the propellant. The strong radial currents produce a magnetic field in the azimuthal direction, which in turn generates a Lorentz force in the axial direction, producing thrust. Also, a magnetic field is applied such that it superimposes the electrodes and protects them from erosion, creating at the same time a magnetic nozzle downstream. This is seen in the following sketch:

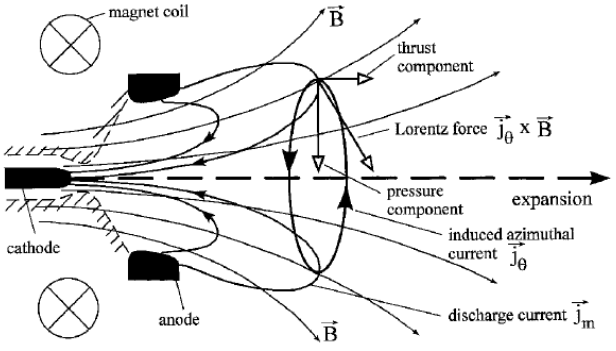

Figure 2.4: Sketch of the main parts of an Applied-Field Magnetoplasmadynamic Thruster. Retrieved from [15]

The presence of this applied axial magnetic field provokes ions and electrons to rotate, producing more acceleration and allowing operations at lower powers. The new magnetic field also pushes the discharges further downstream, such that most of the thrust is achieved in the magnetic nozzle. However, improvements in both the performance and the durability of the thruster are still necessary. To achieve them, further understanding of the physics under which the device operates must be attained.

The last next-generation plasma thruster to be discussed is the VASIMR (Variable Specific Impulse Magnetoplasma Rocket) [16, 17, 18]. Its configuration is very similar to that of the Helicon Plasma Thruster, although an ion cyclotron resonance heater (ICRH) is included, which heats ions at an intermediate stage. A sketch is shown next:

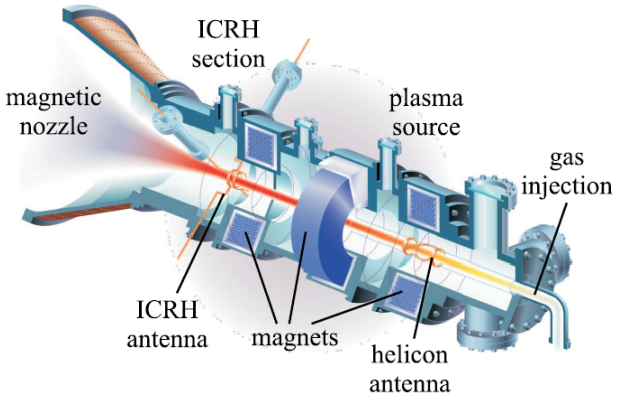

Figure 2.5: Sketch of the main parts of a VASIMR. Retrieved from [17]

The particularity of this propulsive thruster is that it is expected to vary both the thrust and the specific impulse by changing the magnetic nozzle, the power to the system and the mass flow of the propellant. However, it presents the technological problem of requiring very high magnetic fields to confine the highly-energetic ions, and also to be compatible with the ion cyclotron resonance. As for the previous one, this thruster is still under study and development, but shows a promising future with high efficiencies.

After explaining the last advances in electric propulsion, it is now of interest to explain how all these new-generation plasma thrusters actually achieve propulsive characteristics. Thus, magnetic nozzles must be studied now and the operating principles under which they work understood. This will be done in the following section.

2.2 Magnetic Nozzles

In order to properly introduce the topic of this work, it is of interest to explain what magnetic nozzles are and summarize their basic characteristics based on what is known about them currently.

Magnetic nozzles are convergent-divergent applied magnetic fields which can guide and accelerate supersonically a magnetized plasma jet into vacuum. In general, such magnetic fields are generated by magnetic coils or permanent magnets. This type of device allows for contactless, electrodeless and adaptable control of the plasma jet. They are being proposed as the acceleration stage of the next-generation space plasma thrusters explained in the previous section. The main characteristics of the magnetic nozzles are collected in the contribution of Merino and Ahedo to the *Encyclopedia of Plasma Technology* [3].

This type of nozzles mimic the way of working of the already well-known "de Laval" nozzle, although in this case the walls are considered to be the magnetic field applied. In the following parts of this section, the different characteristics of magnetic nozzles studied until now will be explained. The knowledge of the magnetic nozzle physics has been obtained by means of several experiments as well as of different theoretical models.

Fundamental Physics of the plasma in Magnetic Nozzles

In order to understand the physics behind the working of the magnetic nozzle, it is important to define a basic model of the plasma flow in the expanding magnetic field.

The general traits of plasma flows in the divergent part of a magnetic nozzle (outside the ionization chamber of the thruster) can be identified. It must be considered, firstly, that the plasma is sonically choked at the magnetic throat, achieving a supersonic expansion of ions at the divergent part. A second idea is the fact that most plasma sources considered for propulsion deposit most of the internal energy on electrons. In addition, electrons are considered to be well magnetized in a large region of the magnetic nozzle while ions would only be magnetized near the throat. For the magnetic nozzle, the divergent magnetic field, which is axisymmetric, created by coils or permanent magnets must be considered. However, another magnetic field is added to this applied one, which is the one induced by the plasma itself. Thus, taking into account the plasma and the magnetic field described, one finds a steady-state, fully-ionized plasma jet made of ions and electrons, which enters a divergent magnetic field generated by the magnetic nozzle at a throat (with characteristic radius R).

It is now of interest to understand how the magnetic nozzle confines the plasma generated by the thruster. According to R.A. Gerwin et al. [19], in the presence of a uniform magnetic field, the charged particles (electrons and ions) move helicoidally

about the magnetic field lines due to the magnetic force being applied on them. The particles move around the lines with a frequency (also called gyrofrequency) $\Omega = |qB/m|$ (where q is the charge of the particle, B is the magnitude of the magnetic field and m is the mass or inertia of the particle), and with a gyration radius (also called Larmor radius) $l = v_\perp m/(qB)$ (where $v_\perp$ is the perpendicular component of the particle to the magnetic field). When the particles are subject to an electric force perpendicular to the magnetic field, they tend to slowly drift in directions perpendicular to both the magnetic and the electric forces. In the macroscopic scale, the combination of the drift of all particles of a species generates a total diamagnetic drift. Another important effect of this electric field is the fact that it confines the particles in its direction (the radial one, considering magnetic nozzles). Thus, it only allows for movement of the particles in the direction of the magnetic lines or perpendicular to both magnetic and electric forces (azimuthal movement), hence channeling the flow. In order for this confinement to not be broken by possible collisions of the particles, the plasma must have a Larmor radius much smaller than the radius of the magnetic nozzle and collisions at a frequency much lower than the gyrofrequency. Under these two conditions, the particles are said to be magnetized and are fully confined by the magnetic field.

However, as stated before, the ions are not as magnetized as the electrons. This is due to the fact that their differences in masses (being the one of the ions much higher than the mass of electrons) provokes a more difficult magnetization in ions and produces a faster demagnetization within the magnetic nozzle.

A final characteristic of the plasma flow that remains to be discussed is its quasineutrality, meaning that the overall charge of the whole plasma tends to be neutral by having an equal or almost equal population densities of electrons and ions at all times ($n_e \simeq n_i$). However, local electric field may be generated whenever electrons or ions move, giving rise to the formation of an internal ambipolar field. This field appears to tend to maintain equal the population densities.

Principles of Operation

Based on the physics explained before, the principles of operation of a magnetic nozzle can now be described. In the ideal magnetic nozzle, most of the internal energy of the plasma is present as electron thermal energy, being these isotropic and Maxwellian, as presented in the work of Merino and Ahedo [3].

The magnetic field generated by this magnetic nozzle should be enough to fully magnetize the electrons. However, ions would be only partially magnetized, due to the reason explained before. This provokes that, when the magnetic nozzle is active, electrons will tend to follow the magnetic lines whereas ions will try to keep at rest (in principle), being almost unaffected by the magnetic field. Also, due to the electrons being much hotter than ions, they tend to move forward from the plasma source faster than ions, expanding into the vacuum ahead of the latter. As they

expand, in order to not breaking the overall quasineutrality of plasma, an ambipolar electric field is generated that tries to prevent this separation from occurring. The electric force generated then pulls the ions to follow the electrons downstream, so they are accelerated axially downstream and also radially, due to the field being divergent. In such a way, the thermal energy of the electrons is being transformed into kinetic energy of the ions.

Due to the confinement of these electrons, a macroscopic azimuthal current of electrons occurs within the plasma (confining it radially and accelerating it axially), which interacts with the magnetic field being applied. Ions present a similar behavior, although their contribution is smaller and the current goes in opposite direction to that of the electrons. Together, the contributions of both electrons and ions produce their own magnetic field opposing the one of the magnetic nozzle. Thrust is generated as the reaction force of the repulsive action between the two magnetic fields, generating what is called "magnetic thrust". However, the thrust is completely obtained due to the diamagnetic effect of the electron current, whereas the paramagnetic effect of the ion current generates some drag. This can be seen in the following figure:

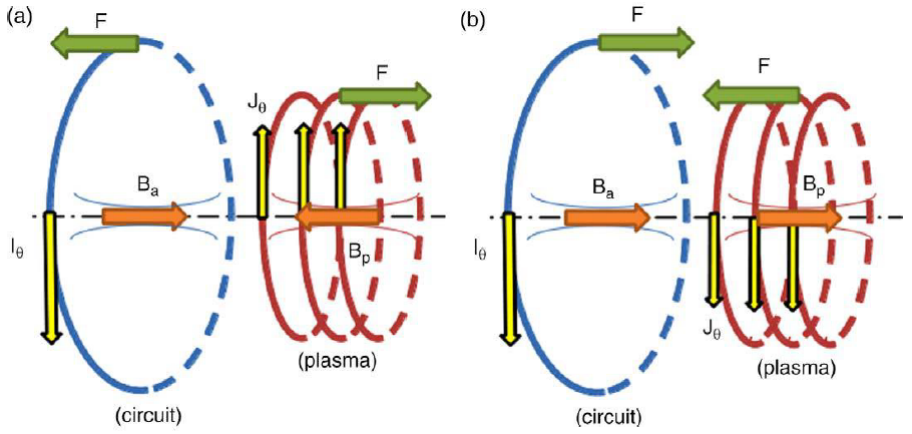

Figure 2.6: Applied plasma and induced plasma interaction. Left: Diamagnetic electron current effect (positive thrust). Right: Paramagnetic ion current effect (negative thrust or drag). Retrieved from [3]

As it can be observed, the opposing magnetic fields of the magnetic nozzle and the one generated by the electron currents repel each other, generating positive thrust in the thruster. In the other hand, the attraction between equal magnetic fields in the ones of the magnetic nozzle and the one generated by the ion current provokes a backwards force on the thruster, equal to a drag.

Studies of the plasma acceleration characteristics have been made both theoretically and experimentally. However, one of the most detailed discussions has been given by Merino and Ahedo [3] by means of a 2D simulation of plasma considering it as a two-fluid body of electrons and ions. Some of the main performance charac-

teristics of the magnetic nozzle are explained in their work. Among them, there are several worth mentioning [20]. The first one is the fact that plasma density decreases both axially and radially from the plasma source, as it expands along the magnetic field. Also, ions accelerate to supersonic speeds very fast downstream of the magnetic nozzle, decreasing the acceleration rate as they separate from it. However, continuous acceleration of the plasma is achieved by means of a magnetic nozzle. In fact, this acceleration is proportional to the temperature of the electrons, the hotter they are the higher speed can be achieved in ions. According to the study of Merino and Ahedo scale with the square root of the electron temperature ($\propto \sqrt{T_e}$). In addition to that, the thrust generated by the magnetic nozzle effect scales with the population density and temperature of electrons, as well as with the radius of the magnetic nozzle throat ($F \propto nT_eR^2$), meaning that hotter and denser plasma increases the total available thrust, as well as having a wider nozzle. Thrust forces twice as big as the ones of naked nozzles can be achieved by means of a magnetic nozzle. Finally, a last result is the fact that, although the induced magnetic field in the plasma is the one generating the magnetic thrust, it can also have some detrimental effects. If the induced magnetic field is of a magnitude comparable to that of the applied one, the one felt by the plasma decreases in magnitude, completely varying the topology of the desired magnetic nozzle. The ratio between induced and applied field scales proportional to population density and temperature of electrons and inversely proportional to the square of the magnitude of the applied field ($\propto nT_e/B^2$). If high thrust is wanted (high n, T_e) great magnetic fields must be applied. A weight-off between magnetic field applied and desired thrust must be considered then when designing a magnetic nozzle.

Plasma Detachment

In order to complete the discussion about magnetic nozzles, it is important to note how plasma detaches from the magnetic field in order to actually produce momentum. This has been a matter of study in the recent years and no clear justification theory for detachment has been decided yet. As of now, several theories have been proposed to explain the plasma detachment from the magnetic lines.

A good detachment of plasma is necessary in order to reduce to the minimum plasma losses, when it tries to go back with the turning magnetic field lines. A bad detachment process would not only handicap the operation of the magnetic nozzle (providing negative thrust) but also could damage the surfaces of the spacecraft by the returning ion particles. Several experiments have proven that under the guidance of a diverging magnetic nozzle, plasma does detach from the magnetic lines and does not return back to the thruster [21, 22]. Among the most important proposed mechanisms explaining this detachment process, one may find the ones explained as follows.

The first mechanism was proposed by Gerwin et al. [19], in which it is discussed the idea that detachment is due to recombination of the plasma species, making

again a neutral gas. Being neutral, it would not be affected by the applied magnetic field and would continue straight downstream. Another theory that was proposed [19, 23] asserted the idea that detachment was produced by internal collisions of the plasma particles that would force them to leave the magnetic lines (however this is not congruent with what has been already explained of low frequency collisions needed in magnetic nozzles). Another popular theory was proposed by Breizman et al. [24], according to whom the plasma is able to generate an induced magnetic field which pulls the magnetic field of the magnetic nozzle, stretching it so it becomes less divergent. In fact, in such a way, particles would follow the stretched lines up to infinity, without the need to actually detach from them.

However, the work made by Merino and Ahedo presented in many reports [3, 25, 26, 27], demonstrates that these theories do not accurately explain the detachment process in propulsive magnetic nozzles. In fact, according to them, the process of detachment is mainly due to the demagnetization of ions downstream from the plasma source. Apart from that, the motion of ion particles becomes dominated by their inertia, thus separating from the magnetic lines inwards. In order to ensure that this detachment is experienced early and minimum plume divergence is generated, the lowest possible magnetic field at the magnetic nozzle center must be applied, ensuring a lower magnetization level of ions (and faster demagnetization). However, enough magnetic field must be applied in order to fulfill previously explained conditions (such as total magnetization of electrons).

2.3 The 3D Magnetic Nozzle

The three-dimensional magnetic nozzle (3D MN) is an innovative thrust vector control concept for next-generation plasma thrusters first proposed by Mario Merino and Eduardo Ahedo [1, 28] and already patented by them [2].

Present devices of thrust vector control in electric propulsion depend on the mounting of the thrusters in mechanical bodies such as gimbaled platforms [29] or robotic arms [30]. This type of control is complex and expensive, as well as requiring very special characteristics such as flexible connections or shock damping. This affects the reliability that these systems have during space maneuvers in missions.

However, this type of magnetic nozzle allows to guide and expand the plasma jet, as explained in the previous section, but also enables steering of the thrust vector by means of a non-symmetric configuration. Thus, the main idea is to generate a magnetic nozzle composed of three or more interwined magnetic coils, each one at an angle α from the axis of the plasma source and separated in equal angles between each other. This way it creates a symmetric configuration in the plane perpendicular to the plasma source. Contrary to current thrust vector control alternatives, which rely on physical moving parts such as complex gimbaled platforms [29], the 3D magnetic nozzle has its coils at a fixed position and the magnetic field is changed by varying independently the current going through them. Installation in thrusters that already present a magnetic nozzle would be straight-forward, according to the references.

In order to construct this type of magnetic nozzle, there are two possible ways. In the first one, it could be achieved by winding simultaneously the different coils in the same spool, in such a way that the turns may not be exactly circular but more like ellipses. An example is shown in figure 2.7-Left. Another possible way is to interlock the different coils one into another by means of them having slightly different radii or being slightly offset from the central axis. An example is shown in figure 2.7-Right.

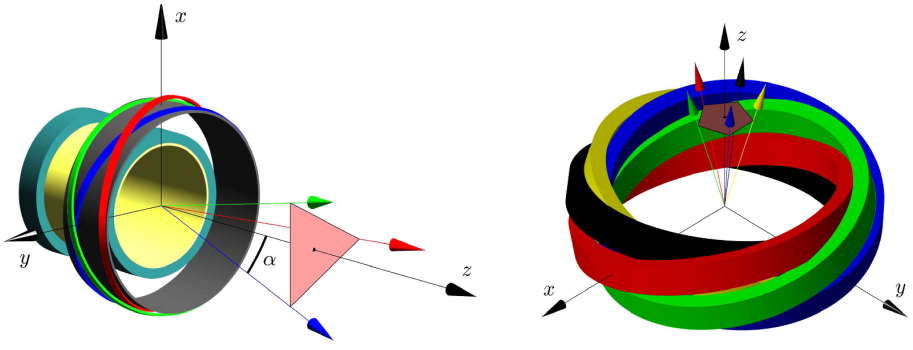

Figure 2.7: Left: Example of interwinded elliptical coils on MN. Right: example of interlocked circular coils whose center is offset from origin of coordinates. Retrieved from [1]

According to Merino and Ahedo, one may control the Ampere-turns of each one of the coils to modify the magnetic field generated at the exit of the thruster. However, this changes follow several principles to be considered:

- If the current going through all the coils is equal, the magnetic nozzle generated coincides with the axis of the plasma source, although some slight asymmetries may exist far from the axis. The larger α and the lower the number of coils, the more asymmetric it becomes. In such configuration, the net magnetic field would be axisymmetric at the exit of the thruster.
- Different intensities in the coils generate oriented magnetic nozzles
- When all electric currents have the same sign, the magnetic field can be oriented anywhere within a polygon with the same number of sides as number of coils the magnetic nozzle has. The maximum deflection α is achieved at the vertices of this polygon, since they are located at the directions of the central axes of the coils. This polygons can be seen in figure 2.7

As explained in [1], it is important that the magnetic field generated by the 3D magnetic nozzle does not affect the internal physics of the thrusting plasma, or that it does it in the minimum possible way, reducing the impact on the thruster efficiency. For those whose applied magnetic field in the plasma source is mainly axial, minimum effect is achieved by locating the magnetic nozzle at the exit plane. The higher the magnetic field intensity of the magnetic nozzle, the more it affects the internal magnetic field configuration of the thruster.

This novel magnetic nozzle idea was tested theoretically by means of the fully magnetized plasma model used in [3] adapted for 3D magnetic configurations. As explained before, for the computation of the plasma expansion in the near-region plume is assumed to be composed of single-charged electrons and ions, quasineutral, collisionless and with negligible induced magnetic field effects. The temperature of ions is neglected relative to the one of electrons and the inertia of the latter ones neglected with respect to the one of the ions. In addition, the electron temperature is considered constant, by assuming Maxwellian, isotropic and isothermal electron population. The same steady-state equations as explained for magnetic nozzles are thus used. Finally, both electrons and ions are considered to be fully magnetized.

If the fully magnetized species condition is assumed, the ion Larmor radius based on the sonic velocity must be small. Expanding about this zero limit, in such a way that motion of the species is done mainly along the magnetic lines of the magnetic nozzle, such that the drift velocities are negligible, making their streamlines equal to these magnetic lines. Thus, the mass conservation equation and the momentum conservation equation, projected along the direction parallel to the magnetic lines, of ions and electrons can be simplified and integrated along the magnetic streamlines yielding:

$$nu_{\|i}/B = G_i \tag{1}$$

$$nu_{\parallel e}/B = G_e \tag{2}$$

$$\frac{1}{2}m_i u_{\parallel i}^2 + e\phi = H_i \tag{3}$$

$$T_e \ln n - e\phi = H_e \tag{4}$$

Where G_i, G_e, H_i, H_e are integration constants that have to be evaluated from initial conditions on each magnetic line coming from the magnetic nozzle. It is observed how the problem with the assumptions made is algebraic and the different characteristics of the plasma expansion in the magnetic nozzle ($u_{\parallel i}$ ion speed, $u_{\parallel e}$ electron speed, n density, ϕ electric potential) can be obtained from solving those equations. The solution will depend exclusively on the local value of magnetic field B.

Thus, taking into account all these fully magnetized model considerations, the theoretical performance of a magnetic nozzle was evaluated by means of the open-source code *FUMAGNO* [31]. To close the model, a given set of boundary conditions must be introduced , which result from the coupling of the 3D magnetic nozzle and the plasma model.

By means of this fully-magnetized plasma model, Merino and Ahedo were able to predict the plasma density response of a magnetic nozzle comprised of three coils at different Ampere-turns configurations, showing that the plasma really deflected from the thruster axis when a directed magnetic field was located at its exit [1]. In fact, they showed how greater Amepere-turns produce a greater deflection, as they generate stronger magnetic fields which force ions to stay attached to the magnetic lines longer. The evolution of plasma density along the axis of the magnetic nozzle for the simple case in which one coil had 15 Ampere-turns going through it while the others had none is also shown in their work:

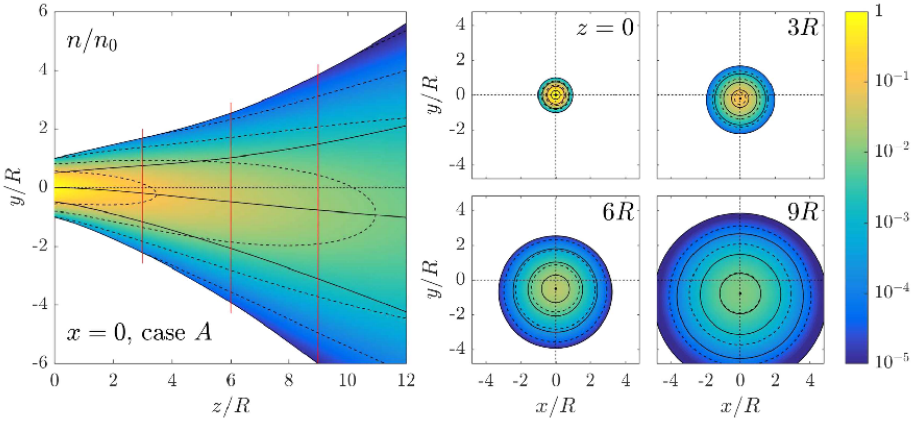

Figure 2.8: Evolution of plasma density in case where intensity through one wire is 15 Ampere-turns, while through the other two is zero. Left: Plot meridional section of maximum deflection. Right: Plots on z=const. sections of the plume. Retrieved from [1]

It is observed how the density maximum follows the line of the magnetic field generated by the 3D magnetic nozzle, achieving thus the deflection of plasma intended.

Considering now the performance of the 3D magnetic nozzle, the thrust force generated by each of the arrangements analyzed was evaluated and normalized with respect to the force at the exit of the thruster. Also, the azimuthal (on x-y plane) and polar (with respect to the axis of the plasma source) angles of this thrust vector were obtained for each of the cases, in order to check exactly how much thrust vectoring was being achieved. The results for the cases showed concordance with the principles of 3D magnetic nozzle explained before. Equal number of Ampere-turns in all the coils generates a thrust vector aligned with the thruster axis, thus being equal to any normal magnetic nozzle. As the intensities were changed, azimuthal and polar deflections were successfully achieved. Polar deflection capability was greater towards the vertices than towards the edges of the confining polygon (as expected). Also, as explained before, increasing the Ampere-turns increased the magnetic field at the exit of the plasma source, producing a higher deflection angle in the polar direction, approaching the maximum possible deflection. However, the cost of this greater deflection is a detrimental effect of the coils magnetic field in the plasma topology. In fact, in these cases, the total thrust generated is considerably lower than those in which lower deflection angles were achieved by lower intensities.

A characteristic worth noting of these 3D magnetic nozzles, as explained by Merino and Ahedo, is the fact that the power needed to operate the complete nozzle is about $(1/\cos\alpha)$ times larger than the corresponding coil magnetic nozzle with same mean radius and total mass. Thus, increasing α also increases the necessary power supply budget of the thruster. The same happens when increasing the number of coils composing the 3D magnetic nozzle.

The magnetization levels of ion species affect the plasma detachment in the far-region, as explained for magnetic nozzles. This effect could impact, in fact, the lateral deflection capabilities of a 3D magnetic nozzle. In such a way, a smaller polar angle deflection is expected in plasmas with partially magnetized ions, being the results obtained by Merino and Ahedo in their work the upper limit of the possible deflections (the most favorable scenario).

An experimental analysis is, therefore, of interest in order to study the practical usefulness of such a magnetic nozzle. In fact, the study of the magnetic nozzle with real plasma, which may not fulfill the fully-magnetized ions condition, is necessary to check the validity of the idea.

3 Design of the Protoype

3.1 Preliminary Design

The process of design of the 3D magnetic nozzle is mainly centered in the obtainment of a directed magnetic field. It is of interest to develop a nozzle able to steer plasma in three dimensions by introducing three different magnetic fields of diverse intensities.

Based on the actual magnetic nozzles and on the properties of solenoids, a magnetic coil was considered the best option to generate a uniform magnetic field. By means of this electromagnetic device, the field that can be achieved in its center is always in the direction of its axis, as it can be seen in the following diagram:

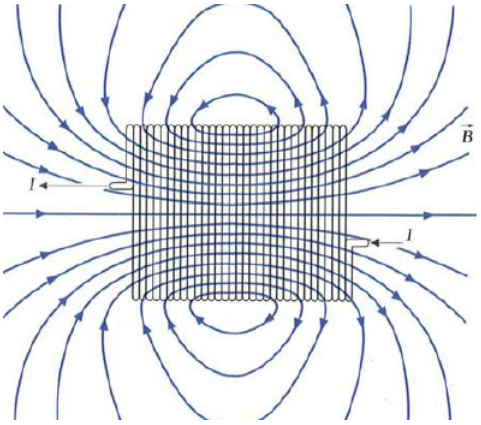

Figure 3.1: Theoretical magnetic field due to a soil. Retrieved from [32]

Thus, a design considering three coils is considered, as it is the minimum number of coils needed for full 3D steering.

The idyllic configuration in which the three coils are mounted would be one in which they are interlaced. This is mainly due to the fact that the three would have the same amount of turns and with the same radii. Thus, equal intensities through them would generate the same magnetic field, which provides a much simpler control of the thrust vector. However, due to technological limitations, this was not a possibility. As a first design consideration, this arrangement was concluded to not be viable. Therefore, it was decided to design a magnetic nozzle consisting of three different independent coils. Their symmetry axes would be oriented forming a certain angle with the central axis of the nozzle (or thruster axis). In a parallel way, the axis of each one of the coils would be at a en equal angle, rotating about the thruster axis, from the other two, thus forming a shape similar to a triangle. The disposition of these axes could be summarized into the following diagrams:

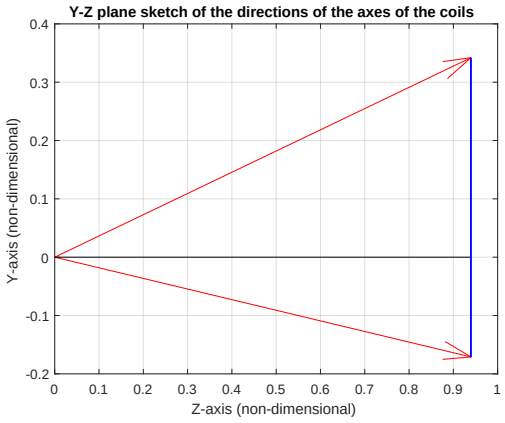

Figure 3.2: Y-Z plane view of the axes of the coils

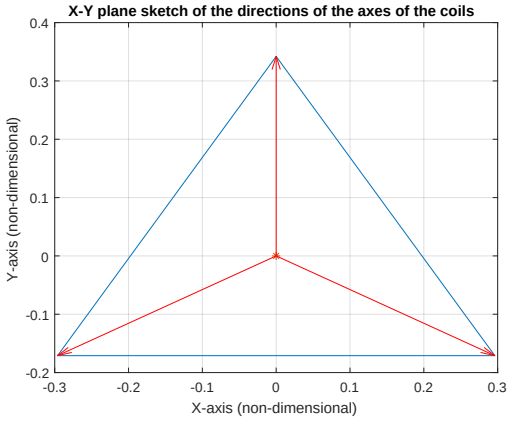

Figure 3.3: X-Y plane view of the axes of the coils

The basic idea to locate the coils in such a way relies on the fact that the effect of single coil would be a maximum deflection of the magnetic field of α degrees from the axis of the nozzle in its axis direction. Thus, three maximum direction points (located at 120^{o} each in the x-y plane) can be obtained. However, as discussed in the paper of Merino and Ahedo [1], each combination of such three magnetic fields would produce a smaller angle deflection. In fact, all the possible combinations of directed magnetic field lie within a triangle in the x-y plane delimited by the maximum points specified by the direction of the three basic coils. It is of interest, therefore, to restrain the locations of these three axes to a position in which the shape of the formed triangle is equilateral, as it maximizes the distribution of points around the axis of the nozzle which can be covered.

In such a way, although the maximum deflection would be α, there is a limit on

the maximum deflection angle that can be achieved in certain directions. This is due to the theory of the 3D magnetic nozzle [1], according to which the direction of the generated magnetic field is forced to point within a polygon with the same number of sides as number of coils composing the magnetic nozzle. Such limit is given when only two coils are active and generating the same magnetic field, moving the thrust vector direction to the middle of one side. This deflection can be calculated taking into consideration an equilateral triangle formed by the three coils. Knowing that the incenter (intersection of the bisectors and center of the incircle) is located at one third of the height of the triangle in its axis of symmetry, one can obtain the semiangle of the cone whose base is such circumference.

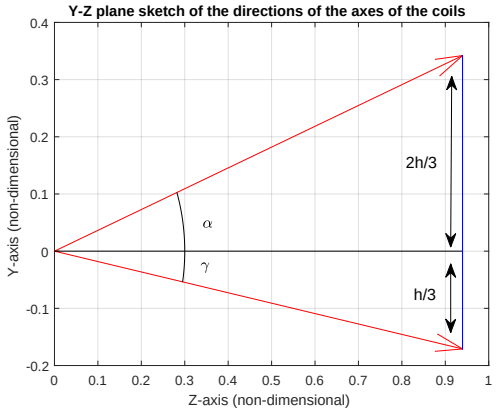

Figure 3.4: Cone deflection: Plane Y-Z

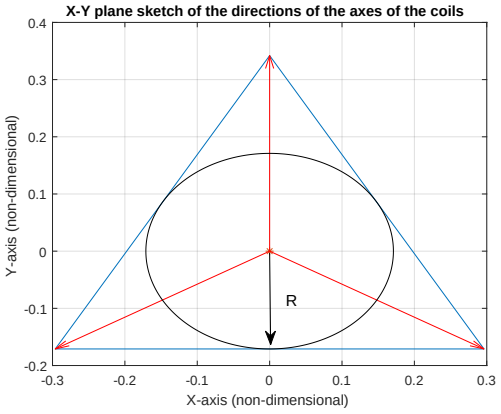

Figure 3.5: Cone deflection: Plane X-Y

By geometry, and if R=h/3:

$$\frac{2h/3}{tan(\alpha)} = \frac{h/3}{tan(\gamma)} \tag{5}$$

$$\gamma = \arctan\left(\frac{1}{2} \cdot \tan\alpha\right) \tag{6}$$

Therefore, a deflection γ degrees is the maximum deflection that can be achieved in the most restrictive case of the 3D magnetic nozzle in a configuration such as the preliminary design considered. Showing that the desired α is not achievable in all directions. It is remarkable how these deflection characteristics depend completely on the geometry of the axes of the coils and are completely independent from the strength of the magnetic field generated. Nonetheless, the plasma deflection will depend on both, as it will be seen.

3.2 Magnetic Field Calculation

It is now of interest to determine the amount of magnetic field that can be generated in the middle of the coil in order to size the whole system of three coils. To do so, a MatLab code was produced based on the functions for calculating the magnetic field of a single loop anywhere in space created by Mario Merino [33]. This code starts by solving the 2D problem of the magnetic field located off the axis in a plane perpendicular to the loop containing its axis. Due to the nature of a loop, this plane can be in any angular position with respect to the canonical axes and so, it will be placed in one that contains the point of calculation P.

The magnetic field generated by a single loop can be obtained according to Biot-Savart's law [32]:

$$\overrightarrow{dB} = \frac{\mu_0}{4\pi} \frac{I\overrightarrow{dl} \times \widehat{r}}{r^2} \tag{7}$$

Where $\overrightarrow{dB}$ is the differential magnetic field, $I\overrightarrow{dl}$ is the current element, $\widehat{r}$ is the distance from the element to the point of study, and μ_0 is the magnetic permeability of the medium ($\mu_0 = 1.2566 \cdot 10^{-6} NA^{-2}$) [34]. A schematic drawing of these properties is shown as follows:

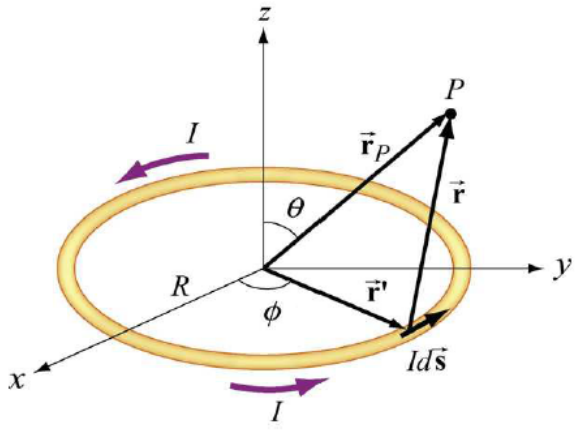

Figure 3.6: Schematic drawing to obtain the magnetic field of a point off the axis of a loop. Taken from [35]

Taking into account the image, one can obtain the magnetic field generated by a loop in its plane of symmetry [35]. The differential current element can be expressed as:

$$I\overrightarrow{dl} = Rd\phi(-\sin\phi\hat{i} + \cos\phi\hat{j}) \tag{8}$$

Where ϕ is the angle of circumference of the loop. The position of this differential current element can be described as:

$$\overrightarrow{r}' = R(\cos\phi\hat{i} + \sin\phi\hat{j}) \tag{9}$$

On the other hand, if it is considered that the plane of symmetry on which the point of calculation is the y-z plane as shown in the drawing (this is done for simplicity in the explanation, although this plane is the one explained before perpendicular to the loop containing its axis and the point P), one can represent its position as:

$$\overrightarrow{r_p} = y\hat{j} + z\hat{k} \tag{10}$$

Thus, one can readily obtain the position vector of the point with respect to the differential current element, as well as its magnitude and the unit vector in such direction:

$$\overrightarrow{r} = \overrightarrow{r_p} - \overrightarrow{r}' = -R\cos\phi\hat{i} + (y - R\sin\phi)\hat{j} + z\hat{k} \tag{11}$$

$$r = |\overrightarrow{r}| = \sqrt{R^2 + y^2 + z^2 - 2yR\sin\phi} \tag{12}$$

$$\hat{r} = \frac{\overrightarrow{r}}{r} \tag{13}$$

Taking into account all these data, one can easily substitute into Biot-Savart's law to obtain the contribution of the differential current element to the magnetic field at the point of calculation:

$$\overrightarrow{dB} = \frac{\mu_0}{4\pi}\frac{I\overrightarrow{dl}\times\widehat{r}}{r^2} = \frac{\mu_0}{4\pi}\frac{I\overrightarrow{dl}\times\overrightarrow{r}}{r^3} = \frac{\mu_0 IR}{4\pi}\frac{z\cos\phi\hat{i} + z\sin\phi\hat{j} + (R - y\sin\phi)\hat{k}}{(R^2 + y^2 + z^2 - 2yR\sin\phi)^{3/2}}d\phi \tag{14}$$

Thus, the magnetic field at the point off the axis is obtained by integrating the contributions of the differential current elements along the whole loop:

$$\overrightarrow{B}(0, y, z) = \frac{\mu_0 IR}{4\pi}\int_0^{2\pi}\frac{z\cos\phi\hat{i} + z\sin\phi\hat{j} + (R - y\sin\phi)\hat{k}}{(R^2 + y^2 + z^2 - 2yR\sin\phi)^{3/2}}d\phi \tag{15}$$

One can easily come into the conclusion that $B_x = 0$ (contribution perpendicular to the plane y-z in which the point lies) due to symmetry conditions (the contribution of the differential current element at $\phi = a$ is cancelled by the contribution of the element at $\phi = \pi - a$. The magnetic field in the plane y-z can be calculated, however, as follows:

$$B_y = \frac{\mu_0 I R z}{4\pi} \int_0^{2\pi} \frac{\sin\phi d\phi}{(R^2 + y^2 + z^2 - 2yR\sin\phi)^{3/2}} \tag{16}$$

$$B_z = \frac{\mu_0 I R}{4\pi} \int_0^{2\pi} \frac{(R - y\sin\phi)d\phi}{(R^2 + y^2 + z^2 - 2yR\sin\phi)^{3/2}} \tag{17}$$

These two equations involve elliptic integrals that can be calculated numerically [36]. In fact, MatLab already has a function for solving such type of integrals, which is how the code of M. Merino solves the equations. Once this 2D problem is solved, the function [33], converts it to a 3D solution by projecting the result of the 2D problem in the plane of the point of calculation and the axis into the canonical planes. Remarkable comments about this function comprise the fact that the loop can be defined to have any given radius and any intensity going through it, as well as being positioned in any point in space and having an axis pointing in any direction. All these variables are inputs for the user to implement.

This simple function for calculation the magnetic field of a single loop in any point of a 3D space is, therefore, the main resource for obtaining the design dimensions of the coils to be made.

In order to dimension the coils, the previously explained MatLab function is used in order to generate a coil of n loops and m arrays, all with an axis pointing towards the same direction. The sum of the contributions to the magnetic field at the center of the axis of the coil is obtained, in such a way that n and m are increased or decreased accordingly to obtain the desired amount of magnetic field at the center. A schematic figure explaining their position can be as follows:

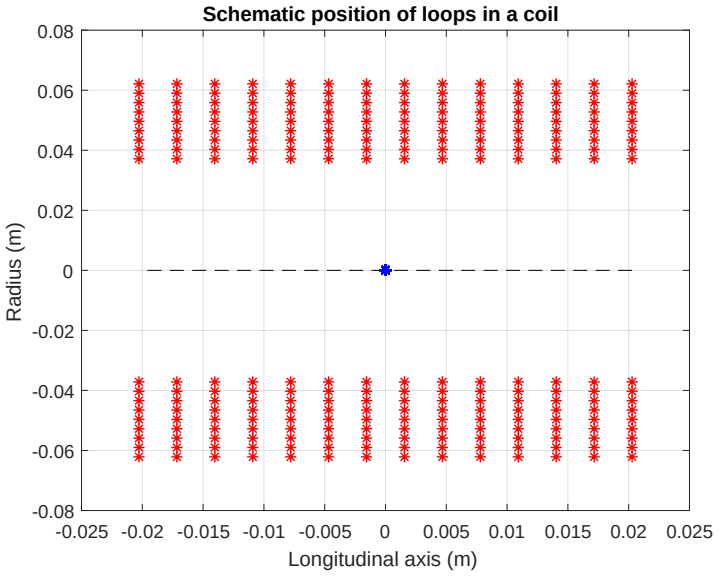

Figure 3.7: Example of arrangement of loops in a coil

As it can be seen from the figure, a number of loops (turns per row) $n = 14$ and a number of arrays (number of rows) $m = 9$ has been selected in the exemplifying coil. The magnetic field is then calculated in the middle of the coil, in its central axis (shown by the point colored in blue) by adding the contributions of each of the loops. The red points show the position of the center of the wire's cross-section of each of the loops (both upwards and downwards, showing as a longitudinal cut through a plane of symmetry). The spacing between these centers is given by the total diameter of the wire used to generate the coil. This diameter depends on the wire selected, which will be shown to have been repeatedly changed throughout the design process.

One can easily calculate the magnetic field around the whole plane shown for the given coil. Doing so, the following vector field of the magnetic components is obtained:

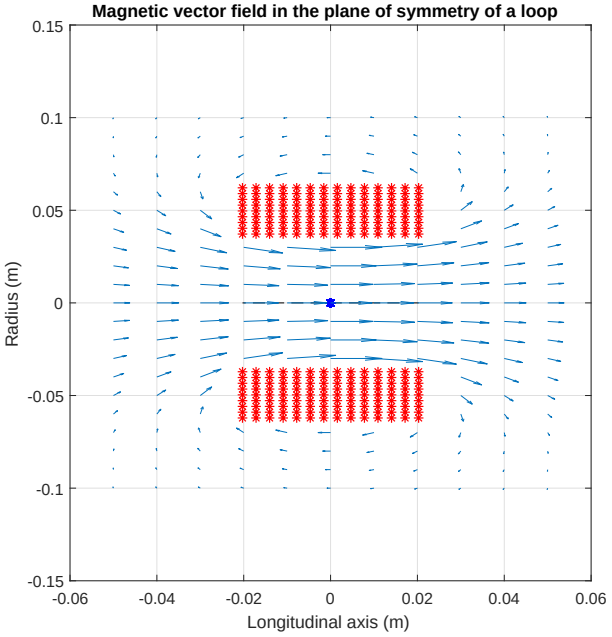

Figure 3.8: Vector field of the magnetic field of a coil in its plane of symmetry

The results on the plane are expected to be equal in all longitudinal planes of the coil due to symmetry properties. It is observable how the magnetic field lines followed by the arrows are as expected from the theoretical drawing of a coil. In fact, it can be observed how the magnetic field at the axis is completely parallel to the axis of the coil. This is the characteristic that was looked for when it was decided to use coils for the 3D magnetic nozzle. In a parallel way, it can be seen how magnetic lines far from the axis but inside of the coil turn around at the exit, generating closed lines with those of the entrance of the coil. It works similarly to a magnetized bar, being the exit of the coil equivalent to the north pole and the entrance equivalent to the south pole [32]. The intensity of the magnetic field in the plane can also be plotted:

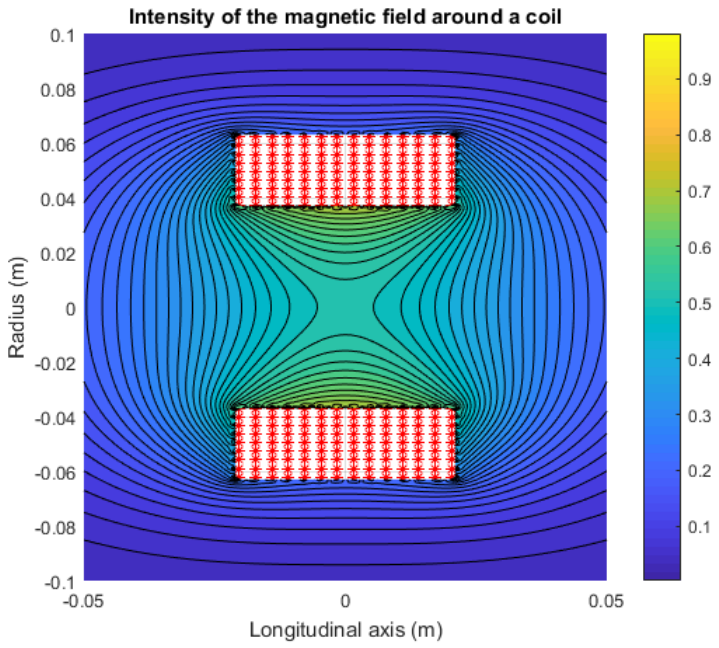

Figure 3.9: Normalized intensity of the magnetic field of a coil

The magnetic field intensities in the previous plot have been normalized to the maximum magnetic field generated, such that it can be generalized to any coil. As for the previous one, due to symmetry characteristics, these intensities are expected to be equal in every longitudinal plane of the coil. It can be observed how the maximum magnetic field is generated close to the wires. This goes in concordance with the equation of the magnetic field, as it is inversely proportional to the square of the distance of the current element to the point of calculation. However, the effect of the closeness to the wires creates a magnetic field whose direction is very variable along the axis. In the axis of the coil, the interesting region of study, it can be seen that the maximum magnetic field is towards the center of the coil. In fact, due to symmetry reasons, the exact center of the coil is the point of the axis in which the magnetic field is maximum.

Therefore, taking into account all these characteristics of the magnetic field of a single coil, it is clear that in order to obtain the maximum magnetic field with a certain desired direction, the point in which all calculations must be done is the center of the coil axis. In fact, in order for the coils of the magnetic nozzle to be the most effective as possible, the their centers must coincide with the center of the exit of the plasma source.

3.3 Coil Design

Although the idea of using coils to direct the magnetic field in a certain direction has been already discussed, it was studied the possibility of making them in two different ways.

The first one, as explained before, is such that the loops are perpendicular to the axis of the structure supporting them, which is completely straight. The magnetic field is directed, therefore, by locating this coil with a certain geometric angle with respect to the axis of the plasma source. This coil would be such as that showed in figure 3.7. This type of design provides several construction advantages, since the tube supporting the wires is completely straight (easily manufactured) and the winding around it presents no problems, as it is just as any typical coil. However, due to the necessity to locate the coil at a certain angle, interference with outer coils is a significant problem, which enforces oversizing and loss of space. In addition to that, the support needed for this type of arrangement would require holes in the structure of the coils with an already determined angle (does not allow for changes in the maximum angle of deflection with respect to the axis of the plasma source). However, this problem will be explained further in the report.

A second arrangement was considered in which the loops of the wire would be winded around a straight cylinder in the angle of the maximum deflection. In such a way, the structure supporting the wires would be completely aligned with the axis of the plasma source and it would be the geometry of the position of the loops itself what would be giving the direction of the magnetic field at the center of the exit. This type of arrangement has several benefits, since it allows for a much more compact device (no space is lost between the coils) and the mounting would be completely straight (no need for angles holes on the structure). However, this type of device presents some manufacturing problems, since it would need a structure whose center cylinder is straight but the loops (and thus the side restraining plates to keep them packed) must be oblique. This difficulties extremely the manufacturing of the support structure. Also, it demands a special winding operation, which is not certain whether a winding company can perform it. This is mainly due to the fact that the winding machines operate perpendicular to the surface of the cylinder about which they are winding the wire and this structure would require loops which are not perpendicular to the structure but oblique at α maximum deflection. A schematic arrangement of such a coil would be as presented in the following figure:

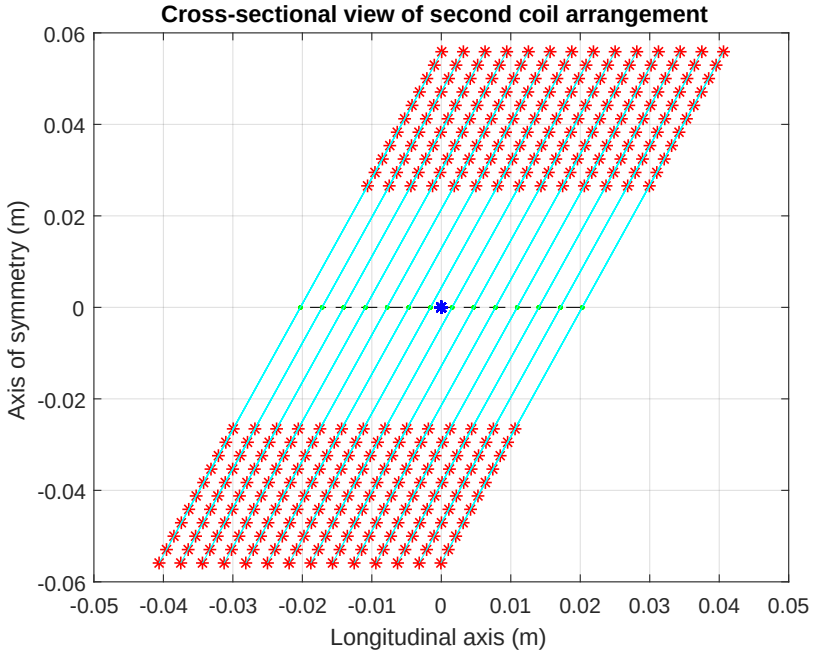

Figure 3.10: Example of arrangement of different coil proposition for $\alpha = -20^{o}$

For the example arrangement, a deflection of $\alpha = -20^{o}$ has been selected, thus the axes of the loops are tilted -20^{o} with respect to the central axis of the coil. It is easily observable how the limits of the coil in the radial direction are completely straight, which allows for an easier mounting and space optimization. Also, for the example shown, it has been selected a number of loops (turns per row) $n = 14$ and a number of arrays (number of rows) $m = 11$

It is of interest now to see how these two types of coils actually deflect the magnetic field in the middle of the axis of the coil. In order to do so, two different magnetic nozzles consisting of two coils each one will be simulated. Only two coils are introduced in the nozzle for the sake of simplicity, since in order to see the the effects of each of the configurations qualitative results are enough. The first one will consist on two straight coils deflected $+\alpha$ and $-\alpha$ from the plasma source axis and the second will consist on two straight coils with tilted loops in $+\alpha$ and $-\alpha$ inclination with respect to the axis. For this analysis, $\alpha = 20^{o}$ has been selected. These arrangements can be observed in the following figures.

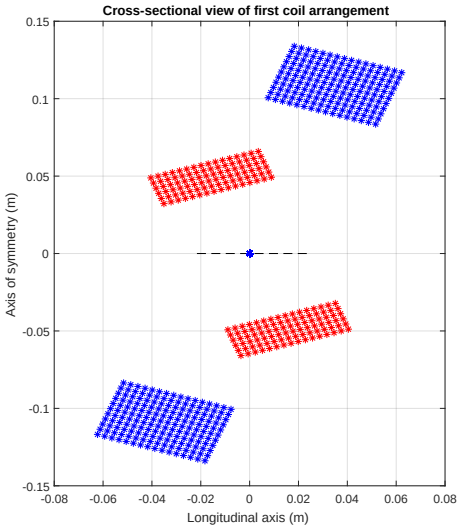

Figure 3.11: First magnetic nozzle coils

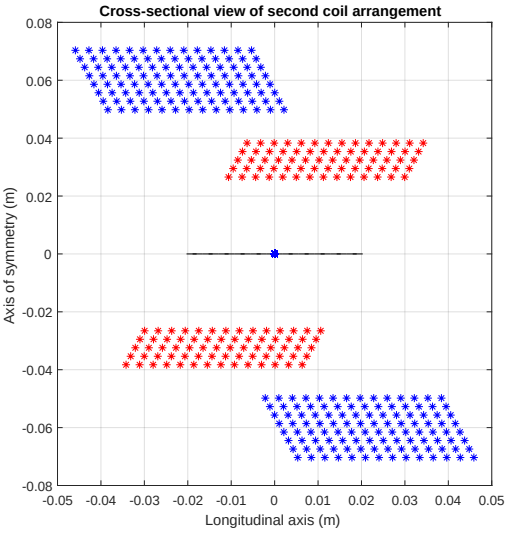

Figure 3.12: Second magnetic nozzle coils

The simulated magnetic nozzles are such that all the coils generate the same magnetic field intensity at the middle of the axis of the plasma source (represented by a blue point in both figures). Now, according to this, one can check which is the maximum deflection allowed by the magnetic field generated by the coils. Three cases are thus, considered, to check which is the direction of the magnetic field at the center of the plasma source in both magnetic nozzles. The first one where only the inner coil generates the maximum magnetic field, the second one where the outer coil generates the maximum magnetic field, and a third one in which both coils generate their maximum magnetic field. By means of the magnetic field calculator for a coil explained in the previous section, one can keep the components of the total magnetic field at the center of the coil. Thus, by retaining B_x and B_z at the point (0,0,0) (considered to be the center of the plasma source exit) of the contributions of magnetic field of all loops (of both coils), the direction of the magnetic field at such point can be simply calculated according to:

$$\alpha = \arctan\left(\frac{B_x}{B_z}\right) \tag{18}$$

Where the z-axis is the longitudinal axis of the coils and the x-axis is the one of symmetry, being positive upwards. In the following table it has been summarized the directions of the magnetic field at the center of the coils in the three different cases explained before. The angle of direction is included in terms of absolute value, since the angle with respect to the central axis is the important magnitude.

Case	α First Arrangement	α Second Arrangement
Only inner coil	20^{o}	17.11^{o}
Only outer coil	20^{o}	18.97^{o}
Both coils	0^{o}	0.93^{o}

Table 3.1: Direction of magnetic field at the center of the plasma source exit in both magnetic nozzle arrangements for several cases

The results for the case in which the nozzle is made by two straight coils whose structure is in a geometric angle with respect to the axis of the plasma source (first arrangement) is consistent with the results obtained in the previous section. In fact, the magnetic field generated by a single coil is exactly aligned with its axis in its center point. Thus, magnetic field generated only by a coil tilted α with respect to the axis would also be tilted that amount. Taking into account the case of magnetic fields generated by both coils (both equal in magnitude), it is expected for the B_x contributions of both coils to cancel out and the B_z contributions to add up, generating a strong field completely aligned with the axis of the plasma source (0^{o}).

The results obtained for the second arrangement, however, are not so straight forward. The result obtained is due to the characteristics of the magnetic field around a loop. Consider, for instance, the two loops located closest to the axis and in the extremes. Both loops are tilted α degrees from the plasma source axis, and so are their respective axes (perpendicular to the loop cross section shown).

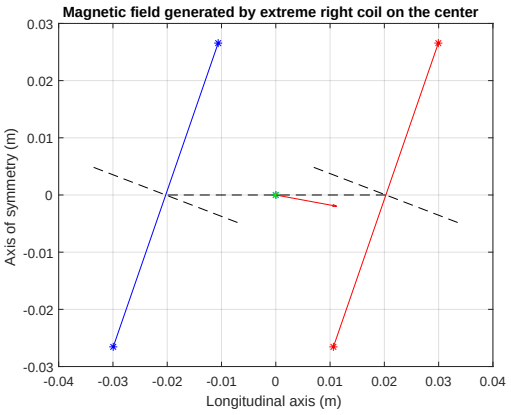

Figure 3.13: Magnetic field direction generated by outermost right loop

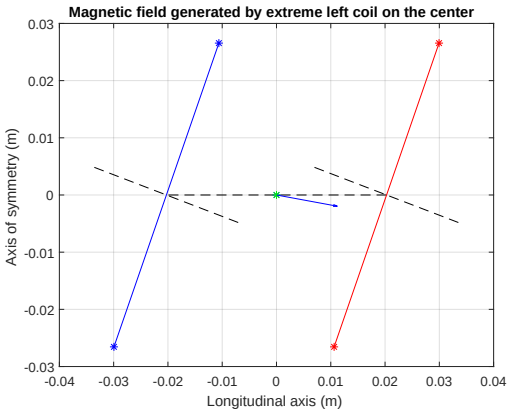

Figure 3.14: Magnetic field direction generated by outermost left loop

It is observed how both loops generate, in fact, the same magnetic field at the center, which is not aligned with their respective axes. A small upwards tilt can be seen. This is due to the shape of the magnetic field of the loop. For the right hand

side loop, the middle point happens to be behind it and lower than its axis. Due to the closing of magnetic lines, the magnetic field in such a region will tend to go up towards the center of the loop, provoking such a field in the specified point. The behaviour is opposite in the left hand side loop, since the center is in front of it and upwards from its axis. However, the same tendency of the magnetic lines of the field to close upon themselves makes the lines in such region to go up in order to start turning and go back to the entrance of the loop, provoking such behaviour.

It is then expected that, the closer the loop is to the center of the coil and the larger its radius, the smaller the effect in the magnetic field direction would be. In fact, if the radius of the loop is much larger than its distance to the point of calculation, the effects of the closing magnetic field lines would be almost unnoticeable and the field would be almost aligned with the loop axis. In the other hand, a loop with a radius comparable in size to the distance between its axis and the point of calculation would generate an effect in the magnetic field which would significantly effect its direction. Thus, in order for this type of coil to be useful, the relationship between its width (length between the centers of the outermost loops) and the radii of such loops must be considered as explained. Taking into account the results of Table 3.1, such proportions generate angles close enough to the imposed maximum angle and could be useful.

To decide which arrangement to use, it was taken into account the easier manufacturing of the first design and its more accurate output angles for the magnetic field generated, as well as the fact that the second design was not confirmed to be windable by the winding company. Thus, the first arrangement with straight coils was selected as the prototype one.

3.4 The Design Process

The design process of the prototype is a complicated one, in which many different agents take part. Many different iterations must be done before reconciling all the agents and, thus, reaching a feasible solution. This whole process can be summarized into the following flowchart.

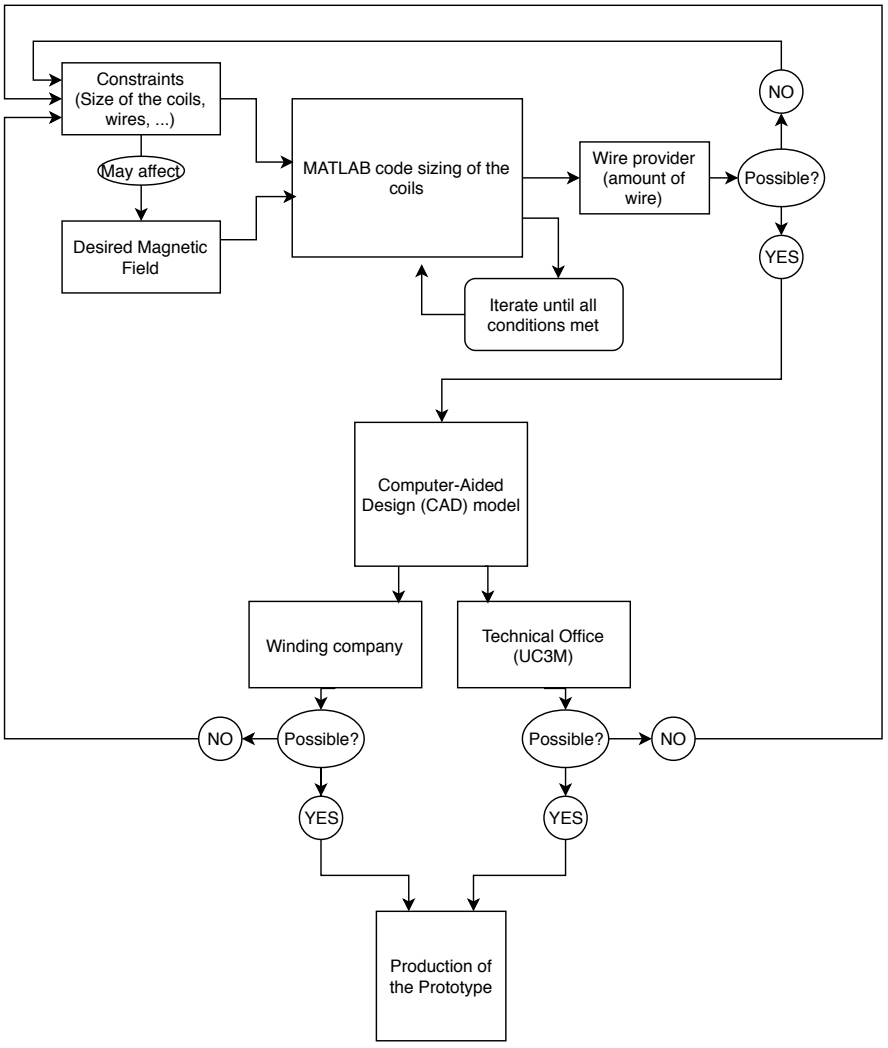

Figure 3.15: Flowchart describing the design process

As it can be seen, the design process starts from the desired magnetic field generated by the magnetic nozzle (both in terms of direction and magnitude) as well as the different constraints that affect the process. Among these, the type of wire, the space available or the possibility of winding are some examples. In fact, many times these restrictions affect the magnetic field that can be generated.

Once these considerations are taken into account, the MatLab code for sizing the coils is used. This one is iterated until all the desired characteristics and restrictions

are met (by varying number of turns per row n and the number of rows m, as well as current through the wire, type of wire, etc.). Once the sizing is done, the wire provider must be contacted in order to know the feasibility of obtaining the wire with which all calculations were performed and in the amounts desired. The latter condition is important, since if the provider does not offer enough wire or, in turn, can only deliver an amount much higher than the needed one, alternative wires or suppliers must be considered. In this case, the design process would have to restart again with new constraints.

When all the design is determined, a Computer-Aided Design (CAD) model of the sized magnetic nozzle is generated in order to transfer the drawing both to the Technical Office at the Universidad Carlos III de Madrid (UC3M), which is in charge of the manufacturing of the coils structure, and to the winding company, which determines whether the design can be winded or not. As for the previous case, a negative answer from any of these (they cannot perform the desired design) would create a new constraint and the design process would have to restart. An affirmative answer from both would mean that the design is entirely manufactured and, thus, the prototype can be constructed.

Taking into account this whole process, several characteristics of the magnetic nozzle and procedures where studied in each iteration. These can be summarized as follows.

Sizing the Coils: Magnetic Field and Energetic Cost

In order to size the coils of the magnetic nozzle, the magnetic field calculator MatLab code explained in section 3.2 was used. In addition to that, some geometric constraints were considered given the arrangement selected in the previous section 3.3. In order to fulfill the latter, some additional restraints were added to the code.

Four main geometric characteristics had to be considered:

- An exit of plasma source of 33 mm of outer diameter (OD) is located at the center of the system.
- The length of the coil must be as close as possible to 5 cm for the magnetic nozzle to fit around the already existing plasma source.
- The coil must take into account an aluminum structure of spool shape with a given thickness, which is the same for the center cylinder thickness and the limit plates ones.
- The α deflection of each of the coils must be allowed without any interference between the coils or with the plasma source exit. Thus an additional spacing between the coil at maximum deflection and its neighbour structures at the most critical geometry for interference must be included. This allows for easier

mounting of the magnetic nozzle, enabling independent mounting of each of the coils.

Thus, the sizing starts by determining the minimum distance of the first coil closest point to the central axis of the system when in its maximum deflection.

$$d_{min} = R_{plasmasource} + GAP \tag{19}$$

Where the GAP is the minimum spacing for no-interference between the two consecutive structures at the critical geometry (maximum deflection). Once this is done, the amount of number of turns per row n and the number of rows m of the coil must be defined for future calculations. These values are iterated constantly to change the size and magnetic field of the coil according to the desired characteristics and the constraints. At this point, the aluminum structure width must also be defined, as well as the total section diameter of the wire (comprising both the conducting material and its insulation). With these data, the length of the coil can be determined as:

$$L_{coil} = 2 \cdot \text{Width}_{structure} + n \cdot D_{section-total} \tag{20}$$

Which is the value wanted to be close to 5 cm, as explained before. One can now calculate the minimum inner radius of the aluminum structure supporting the coil so that it fulfills the condition of its minimum distance to the center of the system to be equal to d_{min}. By means of geometric calculations, one can obtain such radius, taking into account the following sketch:

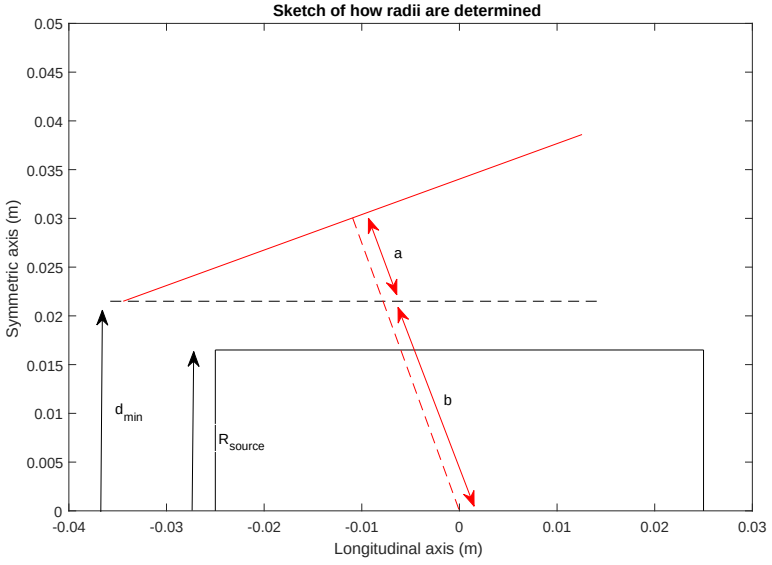

Figure 3.16: Sketch of how the radii of the coils are determined

The minimum inner radius is then obtained as:

$$R_{min-structure} = a + b \tag{21}$$

$$\cos(\alpha) = \frac{d_{min}}{b} \tag{22}$$

$$\tan(\alpha) = \frac{a}{L/2} \tag{23}$$

Thus;

$$R_{min-structure} = a + b = \frac{1}{\cos(\alpha)} \cdot \left(d_{min} + \frac{L}{2} \sin(\alpha) \right) \tag{24}$$

Using this radius, the outer radius of the aluminum is calculated as

$$R_{max-structure} = R_{min-structure} + \text{Width}_{structure} \tag{25}$$

Thus, the radius of the closest array of loops of the coil will be given by

$$R_{min-array} = R_{max-structure} + D_{section-total}/2 \tag{26}$$

The process of calculating the magnetic field at the center then follows exactly the explanation given in section 3.2. Once this is done, the maximum outer radius of the whole coil is calculated as

$$R_{max-coil} = R_{max-structure} + D_{section-total} * m \tag{27}$$

where m is, as explained before, the number of arrays of loops specified. Once this maximum radius is known, the maximum distance of the coil to the central axis can be calculated in a similar manner to the process explained before obtaining:

$$d_{max} = \frac{1}{\cos(\alpha)} + \frac{L}{2} \tag{28}$$

In order to continue the sizing, for the second coil, the minimum distance to the axis must be the maximum distance of the first one plus the space for non-interference. The rest of the sizing is exactly equal. The same exact process is done for the third coil based on the size of the second one.

Once the sizing is done, several more characteristics of the magnetic nozzle can be retrieved. It is interesting to obtain first the amount of wire needed to generate the three coils and its total mass. The length of the total amount of wire is estimated by obtaining the perimeter of each of the loops composing the coils:

$$p = 2\pi R \tag{29}$$

By adding up the perimeters of all the loops of each of the coils, one obtains the total length of wire needed (in an approximate way). This process is included in the *for* loops of the coils, which provides the information of the given radius of the loop (as it is necessary to calculate its magnetic field). The mass is simply obtained the as:

$$m_{coil} = \rho_{material} \cdot L_{wire-coil} \cdot A_{cross-section} \tag{30}$$

Where $\rho_{material}$ is the density of the conducting material, $L_{wire-coil}$ is the length of the wire needed for that coil, and $A_{cross-section}$ is the cross-sectional area of the conductive material (and not of the total wire). The total mass of the magnetic nozzle is then approximated by adding the masses of the wires needed in the three coils.

Another important set of measures needed in the design process are those of the energetic cost. As such, it is interesting to see the resistance generated by the wire, the voltage needed to maintain the intended current through it, and the dissipated power that it consumes. According to Tipler-Mosca [32], the resistance can be calculated as:

$$R = \rho \frac{L}{A} \tag{31}$$

Where ρ is the resistivity of the conductive material, L is its length (calculated before) and A is its cross-sectional area. Once this value is obtained, one can obtain the voltage and power straight forward if the intensity going through the wire is known [32] (which is a controllable parameter by definition of the magnetic nozzle):

$$V = I \cdot R \tag{32}$$

$$P = I \cdot V = I^2 R \tag{33}$$

All these parameters also affect the sizing of the magnetic nozzle, since the system cannot be very heavy, the maximum length of wire usable depends on the wire provider, and the maximum voltage and power deliverable to the coils depend on the characteristics of the motors already owned by the EP2 laboratory.

Wire Selection

Determining the wire to be used is crucial in the design process, since it will constraint the number of turns that are needed, the weight of the magnetic nozzle and the maximum current that can go through it. To decide which wire to use, the

American Wire Gauge (AWG) system has been considered, since it is an international standard for wire sizing. The dimensions for each type of wire were retrieved from ASTM standard B 258 [37]. In a parallel way, the MIL-STD-975M standard [38] was considered, according to which the maximum intensities going through the wires should follow:

$$I_{max} = \frac{29 - N_{\text{bundles}}}{28} \cdot 10.4(A_{\text{wire}})^{0.7};\ \ if\ \ N_{\text{bundles}} < 15 \tag{34}$$

$$I_{max} = 5.6176(A_{\text{wire}})^{0.6839};\ \ if\ \ N_{\text{bundles}} \geqslant 15 \tag{35}$$

Where N_{bundles} is the number of wires in the bundle considered and A_{wire} the cross-sectional area of the conductor. Although this gives a recommended maximum for the currents through the wires, previous experience ensures that greater amperages can be used up to the maximum of the correspondent AWG.

Considering the material of the wires, it is very important to determine which will be the conductive material to use. This is mainly due to the fact that the densities and resistivities of the materials change, as well as the maximum amperage that they can resist. A study to determine whether aluminum or copper were the best conductive candidate for the wire material was performed.

An equally important characteristic of the wires is the material used for its insulation. Since the conductive part will heat up due to the Joule effect (equation 33), it is important to select an insulating material which allows for long operation before reaching its critical temperature. Also, the fact that the wires will be used in vacuum is very important to select this insulating material, since they all do not perform equally in such conditions.

Finally, the last characteristic of the wires to be considered is the availability from the supplier. The wire selected must be deliverable from the supplier, which highly constraints the selection spectrum.

Deflection Angle Control: Maximum Magnetic Field Available

Being a magnetic nozzle whose ultimate use will be controlling the direction of the thrust vector in three dimensions, it is for crucial importance to study the necessary current that must go through each of the coils to achieve a certain angle and the maximum magnetic field that can be generated in such direction.

Since the magnetic field generated at the center of the magnetic nozzle generated by each coil follows the direction, determining the direction of the field due to their contributions is just a simple proportionality problem of sum of vectors. In order to do so, one must know the deflection angle of the coils with respect to the center axis (α) as well as the rotation angle of the second and third coils in the x-y plane

projection (β_2 and β_3, respectively) from the projection of the first coil (which is assumed to be aligned with the y-axis). Such angles are shown as follows:

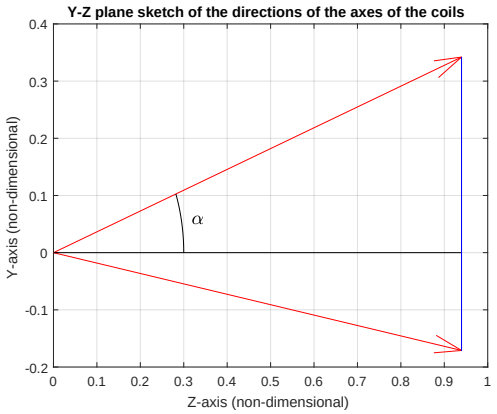

Figure 3.17: Sketch of angles: Plane Y-Z

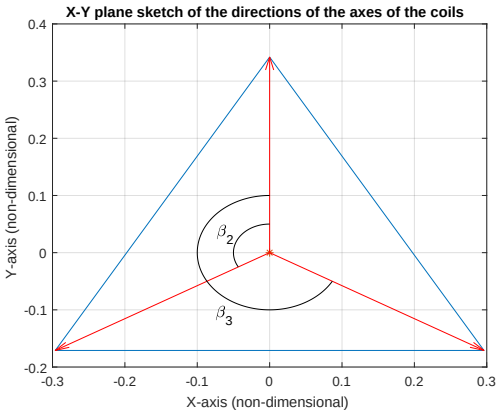

Figure 3.18: Sketch of angles: Plane X-Y

One can define a direction by means of two angles: α' (with respect to the z-axis) and β' (azimuthal angle with respect to the y-axis in the x-y plane projection, positive in the counter-clockwise direction). Thus, this direction can be converted into a point in the canonical axes (in the normalized case in which the maximum magnetic field of each coil at the center is 1 Gauss) as:

$$x = -\sin(\alpha') \cdot \sin(\beta') \tag{36}$$

$$y = \sin(\alpha') \cdot \cos(\beta') \tag{37}$$

$$z = \cos(\alpha') \tag{38}$$

Then, this position can be obtained as the addition of a linear combination of the vectors determining the direction of the coils. The constant of proportionality of the contributions would be the magnetic field generated by its respective coil. This can be expressed as a matrix equation:

$$\begin{bmatrix} \sin\alpha & \sin\alpha\cos\beta_2 & \sin\alpha\cos\beta_3 \\ 0 & \sin\alpha\sin\beta_2 & \sin\alpha\sin\beta_3 \\ \cos\alpha & \cos\alpha & \cos\alpha \end{bmatrix} \begin{bmatrix} B_1 \\ B_2 \\ B_3 \end{bmatrix} = \begin{bmatrix} -\sin(\alpha')\sin(\beta') \\ \sin(\alpha')\cos(\beta') \\ \cos(\alpha') \end{bmatrix} \tag{39}$$

Where B_1, B_2, B_3 are the magnetic field magnitudes at the center of the axis by each of the coils. Thus, these are the unknowns to be solved by this equation. Since the objective is to obtain the maximum magnetic field for such direction and the result for $[B_1, B_2, B_3]$ can be any arbitrary one if it keeps the necessary

proportionality, a correction for this result must be made. In order to do so, a check of this result with respect to the maximum possible magnetic field of each of the coils must be made by dividing $B_{i,max}/B_i$, which states how many times that result can be increased up to reaching the maximum available magnetic field. Thus, the result of $[B_1, B_2, B_3]$ is multiplied by the minimum value of these increment coefficients (since it would mean that the maximum magnetic field of one of the coils is reached) $[B_{1,max}/B_1, B_{2,max}/B_2, B_{3,max}/B_3]$.

$$\begin{bmatrix} B_1' \\ B_2' \\ B_3' \end{bmatrix} = \begin{bmatrix} B_1 \\ B_2 \\ B_3 \end{bmatrix} \min\left[B_{1,max}/B_1, B_{2,max}/B_2, B_{3,max}/B_3\right] \tag{40}$$

This way, the maximum proportional magnetic field $[B_1', B_2', B_3']$ is obtained to reach the direction determined by α', β'.

Knowing the magnetic field magnitudes needed to reach a certain direction, one can use the proportional relationship between the magnetic field of a coil and the intensity going through it [32] in order to know the intensities that must go through each of the coils to reach that position. This way, the control of the magnetic nozzle is created: a direction is specified and the intensities through the coils are changed accordingly to reach it. Such intensities are obtained as:

$$I_1 = I_{1,max} \cdot B_1'/B_{1,max} \tag{41}$$

$$I_2 = I_{2,ma}x \cdot B_2'/B_{2,max} \tag{42}$$

$$I_3 = I_{3,ma}x \cdot B_3'/B_{3,max} \tag{43}$$

Where B_i' is already the maximum possible magnetic field intensity needed to reach the desired direction. However, it is not always necessary to generate the maximum magnetic field. Thus, this can be scalable proportionally. For example, if only an x % of the magnetic field is wanted, all can be changed into:

$$B_1'' = B_1'\frac{x}{100}; \qquad I_1' = I_1\frac{x}{100} \tag{44}$$

$$B_2'' = B_2'\frac{x}{100}; \qquad I_2' = I_2\frac{x}{100} \tag{45}$$

$$B_3'' = B_3'\frac{x}{100}; \qquad I_3' = I_3\frac{x}{100} \tag{46}$$

The control of the magnetic nozzle is an important part of the design of the system since it allows to know which are the maximum magnetic field that can be generated to reach all available positions.

Heating Analysis

Another important design consideration is the heating of the coils and heat dissipation of the system. Since the magnetic nozzle will be in vacuum, the heat dissipation through convection is non-existent. Also, the dissipation through radiation can be considered negligible. For simplicity, and in a very conservative manner, the system will be considered in such a way that no dissipation of heat through conduction is produced, so that it only heats up.

One can then write the heat equation for the conductive part of the wire [39] as:

$$m \cdot c \cdot \frac{dT}{dt} = P(T) = I^2 R(T) \tag{47}$$

Where m is the mass of the wire, c is the specific heat of the conductive material and *P(t)* is the dissipated heat due to the Joule effect. However, the resistivity of a given material changes with its temperature and can be approximated by a linear equation [40]:

$$\rho(T) = \rho_0(T_0)[1 + \alpha_0(T - T_0)] \tag{48}$$

Where α_0 is the temperature coefficient of resistivity of the material of the wire, T_0 is the initial temperature and $\rho_0(T_0)$ is the resistivity at such temperature. Considering also 31, one may express the heat equation as:

$$m \cdot c \cdot \frac{dT}{dt} = I^2 \rho_0(T_0)[1 + \alpha_0(T - T_0)]\frac{L}{A} \tag{49}$$

Considering that $m = L \cdot A \cdot \rho$,

$$L \cdot A \cdot \rho \cdot c \cdot \frac{dT}{dt} = I^2 \rho_0(T_0)[1 + \alpha_0(T - T_0)]\frac{L}{A} \tag{50}$$

Or, rearranging:

$$\frac{dT}{[1 + \alpha_0(T - T_0)]} = \frac{I^2 \rho_0(T_0)}{\rho c A^2} dt \tag{51}$$

Which is an ordinary differential equation of first order, whose analytic solution is straight forward to obtain:

$$T = T_0 + \frac{1}{\alpha_0}\left[\exp\left(\alpha_0 \frac{I^2 \rho_0(T_0)}{\rho c A^2}(t - t_0)\right) - 1\right] \tag{52}$$

Which allows obtaining the time to reach a certain temperature T^*:

$$t = \frac{\rho c A^2}{\alpha_0 I^2 \rho_0(T_0)} \ln[\alpha_0(T^* - T_0) + 1] \tag{53}$$

This information is crucial to know for how much time the magnetic nozzle can be operated without reaching a maximum thermal limit imposed by the insulating material of the wire. It is important to notice how the evolution of temperature does not depend on how much wire is used. The only geometrical characteristic of relevance is the cross-sectional area.

CAD model

Generating the CAD model was the last of the design iteration parts. It consisted in generating the drawings of the magnetic nozzle parts according to the dimensions obtained in the previous steps, checking for possible interferences or other physical constraints. These drawings are the output of the process, what is given to both the Technical Office and the winding company to check whether it can be manufactured. However there are other characteristics that must be considered when designing the final model which are not part of the technical characteristics of the magnetic nozzle.

On the one hand, the manufacturing process of the aluminum structure which was going to support the wires had to be taken into account. Depending on how the Technical Office was considering its mechanization, one type of shapes could be done or not.

On the other hand, it had to be considered the already existing structure for the plasma source that the EP2 laboratory has as well as the structure already exiting for some coils. The supporting structure to hold the magnetic nozzle had to be designed in order to not produce interference. In fact, the best possible design would consist on one which could benefit from that already existing structure. In general, the holding mechanism of the magnetic nozzle had to be considered in this part of the process.

All these design steps had to be fulfilled in every iteration in order to reach a final prototype design.

3.5 Design Iterations

In order to explain the final design of the magnetic nozzle prototype, some of the most relevant iterations and changes that had to be done will be explained. Most of such changes are due to the encountering of specific problems and additional restrictions.

It must be considered that for all iterations it was decided that the angle between the coils axes and the central coil of the magnetic nozzle was $\alpha = 20^{\text{o}}$. This is due to the fact that, as explained in the paper by Merino and Ahedo [1], actual deflection of the thrust vector does not completely follow the maximum deflection imposed by the magnetic field.

Three Coil Magnetic Nozzle (600/600/600)

In the first iteration of the prototype design, it was decided to try to generate a magnetic nozzle composed of three coils whose maximum magnetic field at the center was 600 Gauss for each one of them. The closest resemblance to the theoretical model explained by Merino and Ahedo [1] was intended.

It was decided that the maximum current going through the wires would be of $I_{max} = 20$ A, based on previous experiences of the EP2 with magnetic coils. Taking this into account, the first analysis performed was the study of the best conductive material for the magnetic wires. The materials considered were based on already existing wires, which are mainly aluminum and copper. Thus, the following physical characteristics of these materials were used (retrieved from the *CRC Handbook of Chemistry and Physics* [41]):

Property	Copper (Cu)	Aluminum (Al)
Density	8960 kg/m^3	2700 kg/m^3
Resistivity (at 20$^{\text{o}}$C)	1.678·10^{-8} Ωm	2.65·10^{-8} Ωm

Table 3.2: Material Properties for the Wire Selection

With these data, and knowing the amount of current that it is desired to go through the wires, one can obtain the necessary AWG caliber using the *National Electrical Code* [42]. Some margin with the maximum allowable current intended and the one of the calibers selected has been left for security reasons. For this first preliminary design an insulator thickness of $\epsilon = D_{sec}/10$ has been selected (one tenth of the conductor section diameter). Also, the minimum radius for the inner coil has been selected to be $R_{min} = 4$ cm and no internal structure around which the wire will be wrapped has been considered (it is just a preliminary view of the possibilities of the coils). Thus, the design results for both materials in the inner coil are summarizes as follows:

Property	Copper (Cu)	Aluminum (Al)
Intensity (I)	20 A	20 A
Wire Caliber [42]	AWG 12	AWG 8
Conductor Section Diameter (D) [37]	2.053 mm	3.2639 mm
Insulator thickness (ϵ)	0.2053 mm	0.32639 mm
Coil width (L)	4.93 cm	5.09 cm
Inner radius (R_i)	4 cm	4 cm
Outer radius (R_o)	7.449 cm	17.317 cm
Packing factor (R_o/R_i)	1.862	4.329
Turns by row (n)	20	13
Number of rows (m)	15	35
Mass (m)	3.20 kg	6.88 kg
Magnetic field at center (B_0)	618.60 Gauss	598.37 Gauss
Resistance (R)	0.547 Ω	0.965 Ω
Necessary Voltage (V)	10.94 V	19.30 V
Necessary Power (P)	218.79 W	386.03 W

Table 3.3: Comparison of performance of Aluminum and Copper as wire conductors

It is easily observable how, although the density of the aluminum is much lower that the one of copper, it needs a higher amount of mass in order to obtain the desired magnetic field at its center. This is due to its higher resistivity and the need for it to have a higher cross-section size to allow for the same intensity through it. In such a way, it needs a much higher amount of turns to generate a similar magnetic field intensity to that of copper, making such coil have more than twice the weight of the copper one. Observing the energetic cost, it is seen how the aluminum coil requires higher voltages, and thus power, to maintain the intended current through it. In conclusion, it is easily determined that copper is the better material for the conductive part of the wires.

Using the selected conducting material (copper), the same current and caliber are used to generate the magnetic nozzle of three consecutive coils. For this preliminary design, a distance between the outer radius of a coil and the inner radius of the consecutive coil is selected to be three times the conductive part cross-section diameter:

$$R_{in-j} - R_{out-i} = 3D_{sec}$$

Taking this into account, the following results are obtained for the three coils:

Property	Coil 1	Coil 2	Coil 3
Intensity (I)		20 A	
Wire Caliber [42]		AWG 12	
Cond. Section Diameter (D) [37]		2.053 mm	
Insulator thickness (ϵ)		0.2053 mm	
Coil width (L)	4.93 cm	4.93 cm	4.93 cm
Inner radius (R_i)	4 cm	8.065 cm	15.086 cm
Outer radius (R_o)	7.449 cm	14.470	26.911 cm
Packing factor (R_o/R_i)	1.862	1.794	1.784
Turns by row (n)	20	20	20
Number of rows (m)	15	27	49
Mass (m)	3.20 kg	11.34 kg	38.35 kg
Magnetic field at center (B_0)	618.60 Gauss	604.13 Gauss	598.71 Gauss
Resistance (R)	0.547 Ω	1.938 Ω	6.554 Ω
Necessary Voltage (V)	10.94 V	38.76 V	131.09 V
Necessary Power (P)	218.79 W	775.16 W	2621.71 W

Table 3.4: Results for 600/600/600 Copper Magnetic Nozzle for I=20 A and AWG 12

It can be observed from the results of the table that the energetic requirements for both the second and the third coils are too high. In fact, this presented a problem since the available power supplies of the EP2 laboratory could not reach that amount of electrical DC power. This design fails in the constraints fulfillment. Therefore, it was of interest to check the maximum amount of magnetic field that could be generated for a maximum of 20 V, a magnitude maintainable by the already existing power supplies of the laboratory. Thus, obtaining the current that can go through the designed coils so that the maximum voltage is 20V can be easily obtained. Since the coils are already sized, the total resistance of each one of them is known. By means of rearranging equation (32), $I = V/R$. This intensity would be the one going through each of the coils whose previous voltage was larger than 20 V. The dimensions of the coils are exactly the same as discussed above. Thus, the magnetic field and energetic requirements of the coils in such analysis are the following:

Property	Coil 1	Coil 2	Coil 3
Intensity (I)	20 A	10.32 A	3.05 A
Magnetic field at center (B_0)	618.60 Gauss	311.75 Gauss	91.35 Gauss
Resistance (R)	0.547 Ω	1.938 Ω	6.554 Ω
Necessary Voltage (V)	10.94 V	20.00 V	20.00 V
Necessary Power (P)	218.79 W	206.41 W	61.03 W

Table 3.5: Energetic cost for 600/600/600 Magnetic Nozzle operating at limited voltage V=20 A and AWG 12

The energetic restriction strongly reduces the maximum available magnetic field generated by the second and third coils, being the outer the most severely affected, dropping to less than a sixth of the nominal value. Thus, it was concluded that generating a 600/600/600 magnetic nozzle was not possible with the proposed architecture, and alternative solutions needed to be investigated.

Three Coil Magnetic Nozzle (600/300/150)

As the intended magnetic nozzle of 600/600/600 was not possible, an based on the results for a maximum of 20 volts per coil, it was decided to relax the initial requirements and generate a magnetic nozzle of the type 600/300/150. By relaxing the maximum magnetic field to be generated by each of the coils, the dimensions of these were expected to reduce too.

In order to decide on the arrangement of the coils, an analysis comparing the 600/300/150 versus the 150/300/600 arrangements was performed (taking into consideration the first field to be of the smallest coil and the last the one of the biggest one). For this new analysis, a 5mm width aluminum cylindrical structure was considered to be inside each coil, supporting the wiring. However, the spacing between two consecutive coils radii was still considered to be $3D_{sec}$. An intensity of 20A and a wire AWG 12 was considered, with an insulating material 0f 10% the conductor diameter thickness. Thus, the obtained radii, mass, magnetic field generation and energetic cost obtained for both arrangements are:

Property	Coil 1	Coil 2	Coil 3
Inner radius (R_i)	4 cm	8.565 cm	12.391 cm
Outer radius (R_o)	7.449 cm	11.275 cm	14.115 cm
Mass (m)	3.20 kg	4.44 kg	3.95 kg
Magnetic field at center (B_0)	618.60 Gauss	296.92 Gauss	149.40 Gauss
Resistance (R)	0.547 Ω	0.758 Ω	0.675 Ω
Necessary Voltage (V)	10.94 V	15.16 V	13.51 V
Necessary Power (P)	218.79 W	303.31 W	270.14 W

Table 3.6: Results for 600/300/150 Copper Magnetic Nozzle

Property	Coil 1	Coil 2	Coil 3
Inner radius (R_i)	4 cm	5.608 cm	8.695 cm
Outer radius (R_o)	4.493 cm	7.580 cm	15.59 cm
Mass (m)	0.47 kg	2.21 kg	13.13 kg
Magnetic field at center (B_0)	153.70 Gauss	323.44 Gauss	604.13 Gauss
Resistance (R)	0.081 Ω	0.378 Ω	2.243 Ω
Necessary Voltage (V)	1.62 V	7.56 V	44.87 V
Necessary Power (P)	32.46 W	151.21 W	897.37 W

Table 3.7: Results for 150/300/600 Copper Magnetic Nozzle

From the results, it can be easily observed that not only the first arrangement gives a magnetic nozzle whose all energetic requirements can be easily met, but also one of less and better distributed weight. If fact, the outer coil of the second arrangement is too big and heavy, and requires huge voltages through it to work. Thus, it is concluded that the first arrangement is the better one.

Based on this one, a first preliminary CAD model was designed in order to have an idea of the desired magnetic nozzle and possible physical constraints. In this model, the 33 mm diameter plasma source of the EP2 laboratory was included. This allowed for a smaller inner radius of the smaller coil, reducing the size and energetic requirements of the whole magnetic nozzle. Since the distance between coils at the most critical position explained in section 3.4 was not still implemented, an iteration between the model interference and the code was done, obtaining the following design:

Property	Coil 1	Coil 2	Coil 3
Coil width (L)	4.93 cm	4.93 cm	4.93 cm
Inner radius (R_i)	2.70 cm	6.50 cm	9.80 cm
Outer radius (R_o)	5.164 cm	8.717 cm	11.278 cm
Packing factor (R_o/R_i)	1.912	1.341	1.151
Turns by row (n)	20	20	20
Number of rows (m)	11	10	7
Mass (m)	1.61 kg	2.84 kg	2.75 kg
Magnetic field at center (B_0)	605.29 Gauss	316.35 Gauss	162.85 Gauss
Resistance (R)	0.275 Ω	0.485 Ω	0.470 Ω
Necessary Voltage (V)	5.51 V	9.69 V	9.40 V
Necessary Power (P)	110.20 W	193.87 W	187.97 W

Table 3.8: CAD dimensions for 600/300/150 Copper Magnetic Nozzle

The heating analysis is done with this design also. Considering an initial temperature of $T_0 = 20^{\text{o}}\text{C}$, and the following heating characteristics of copper:

c [41]	384 $\frac{J}{KgK}$
α_0 (at 20ºC and 100% conductivity) [43]	0.00394 K^{-1}

Table 3.9: Heating properties of Copper

A limit in the temperature has been set at T=180ºC, as it is a critical temperature for most insulators of wires. In such a way, the system is prevented from overheating and breaking through the insulator failure. In this case, it shows that the time to reach T=180ºC is 11.6153 minutes. Thus, the magnetic nozzle allows for a little more than 11 minutes of continuous operation before overheating, which is low to perform all validation tests.

The CAD model is included next. Its shows that although there is no actual interference between the coils and their structures, their assembly might be extremely complicated. Deflections of the coils might be introduced after introducing one into another.

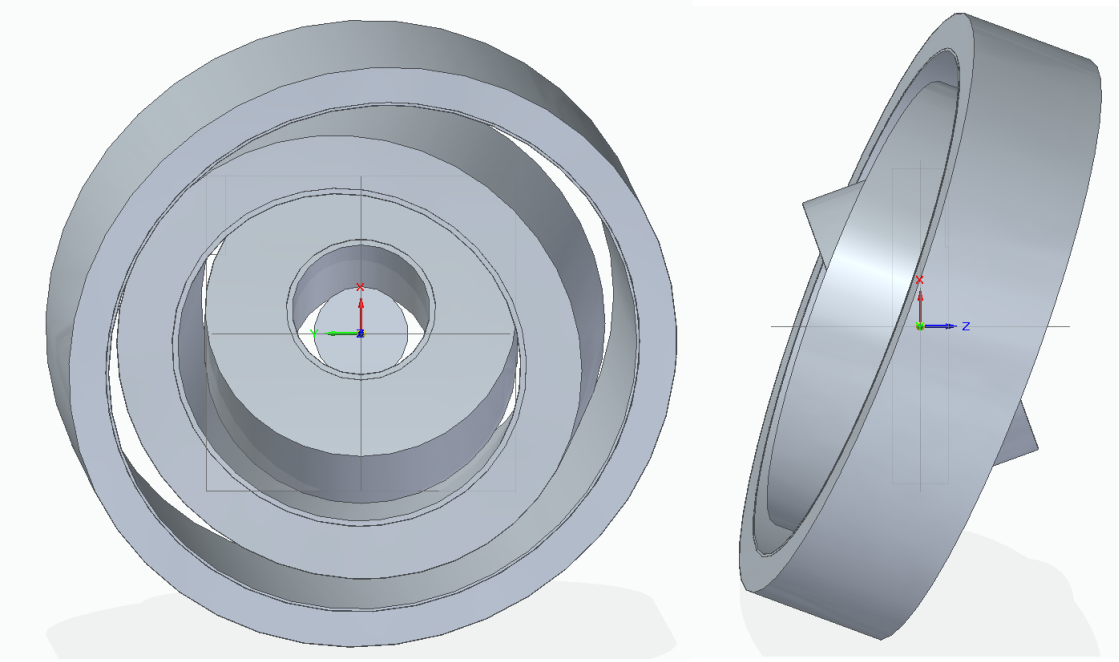

Figure 3.19: Preliminary three coil magnetic nozzle CAD model

For simplicity reasons, then, it would be interesting to generate a magnetic nozzle in such a way that the coils assembly is straight forward, meaning that can be introduced into some supports perpendicular to the plasma source plane without any interference. In fact, the most interesting way would be if they could be assembled with their deflection angle already introduced. Thus, the sizing of the coils explained in section 3.4 in which some spacing between the most critical positions of two consecutive coils is considered was introduced at this point. A final analysis of

sizing using this method with three coils was made, where the lateral structure of the aluminum support (5 mm) was also included in order to reach more detailed design, obtaining the following results:

Property	Coil 1	Coil 2	Coil 3
Coil width (L)	4.94 cm	4.94 cm	4.94 cm
Inner radius (R_i)	3.81 cm	10.95 cm	18.59 cm
Outer radius (R_o)	8.00 cm	15.63 cm	22.04 cm
Packing factor (R_o/R_i)	2.099	1.427	1.186
Turns by row (n)	16	16	16
Number of rows (m)	18	20	15
Mass (m)	3.17 kg	7.93 kg	9.08 kg
Magnetic field at center (B_0)	603.04 Gauss	302.51 Gauss	148.18 Gauss
Resistance (R)	0.542 Ω	1.355 Ω	1.553 Ω
Necessary Voltage (V)	10.83 V	27.10 V	31.05 V
Necessary Power (P)	216.64 W	541.92 W	621.05 W

Table 3.10: Sizing of 600/300/150 Copper Magnetic Nozzle with no-interference in oblique position (20^{o})

Based on these results, the sizes of the coils are too big to be manufactured and the energetic cost too high to be achievable. Thus, the change of the wire into an 10 AWG and a current of 25 A was considered. However, the results obtained for such wire require even bigger coil sizes and energy (outer radius of third coil of 28.53 cm and this same coil needs 796.34 W).

Therefore, in conclusion from all these resulting data, it was not possible to generate a 3D magnetic nozzle made of three independent coils with normal-use conductors and with the resources of the laboratory or the subcontractors. The design still fails to fulfill all constraints. Thus, alternative solutions needed to be investigated.

Two Coil Magnetic Nozzle (600/300)

Considering the encountered problems, it was decided that a magnetic nozzle composed of only two coils, whose maximum magnetic field would be of 600 Gauss for the inner one and 300 for the outer one, will be designed. Following the line of reasoning of the paper of Merino and Ahedo [1], this would allow motion in all the points in the line joining the tips of the vectors of direction of the coils. However, this would easily demonstrate the proposition behind such paper that a directed magnetic field can be used to steer a plasma jet.

For this new design, it was decided to use a wire of rectangular cross-section in order to not waste space within the coil. In fact, after some investigation, it

was decided to use a specific wire of copper conductor and kapton insulator of cross section 5mmx1.2mm and an insulator thickness of 0.060 mm [44] from a company called Essex. With such cross-section dimensions, it would be equivalent to an AWG 10 bases o the cross-sectional area [37]. Thus, a 30A current was decided to be passed through it in order to generate the required magnetic field intensities. Although this surpasses the recommendations of MIL-STD-975M [38] (since more than 15 wires per bundle are surely to be used), it keeps below the maximum for an equivalent AWG wire.

In addition to this changes, it had to bee considered a maximum outer diameter (OD) of 240 mm of the outer coil, since it is the maximum windable size by the winding company considered for the winding of the coils (Elementos Magnéticos Navarra S.L.). Also, the width of the aluminum structures sustaining the wires, after contacting with Technical Office, were going to be retrieved from standard aluminum tubes [45]. 2.5mm thick structures are used in the limits of the coil to keep the wires packed. Under this considerations, the following dimensions were able to be reached:

Property	Coil 1	Coil 2
Coil width (L)	4.596 cm	4.596 cm
Inner radius (R_i)	3.566 cm	8.816 cm
Outer radius (R_o)	6.206 cm	11.324 cm
Packing factor (R_o/R_i)	1.740	1.284
Turns by row (n)	8	8
Number of rows (m)	21	22
Mass (m)	2.77 kg	5.44 kg
Magnetic field at center (B_0)	607.20 Gauss	294.853 Gauss
Resistance (R)	0.144 Ω	0.283 Ω
Necessary Voltage (V)	4.33 V	8.494 V
Necessary Power (P)	129.82 W	245.81 W

Table 3.11: Sizing of 600/300 Copper Magnetic Nozzle with standard aluminum tubes

The results showed a nozzle fulfilling all the constraints and magnetic field requirements, and with an energetic cost easily achievable by the motors of the EP2 laboratory. Thus, for this magnetic nozzle, two standard tubes of 70mm OD/65 mm ID and 180mm OD/170 mm ID (OD: Outer Diameter, ID: Inner Diameter). A manufacturable prototype was designed, which complies with all requirements and reaches the desired characteristics. However, once the design was completed, the wire provider Essex was contacted. Due to company politics, the minimum amount of wire that they would provide exceeded hugely from the UC3M project budget. Therefore, this design could not be continued in the design process: the wire provider step failed. A new one had to be iterated.

In order to solve the wire provider problem, the EP2 lab contacted with SENER, who ensured that they were able to provide with a 15 kg of copper wire of 3.12mm of outer diameter and 3mm of copper diameter. In addition to the wire change, another aluminum type of structure was selected of 3.5 mm width both in the cylindrical part and in the limits at the edges. This selected change from standard aluminum tubes was due to the decision from Technical Office of forming these tubes by the process of turning [46]. Also, it was decided that for increasing the maximum available magnetic field, the width of the coils in the longitudinal direction will exceed slightly the 5cm imposed by the previous requirements, since a trade-off between maximum radius versus length showed that 5 cm length restriction requires an outer maximum radius o similar dimensions but gives much less magnetic field. Based on these structure and wire considerations, the following performances of the coils were obtained:

Property	Coil 1	Coil 2
Coil width (L)	5.692 cm	5.692 cm
Inner radius (R_i)	3.67 cm	8.50 cm
Outer radius (R_o)	5.55 cm	11.93 cm
Turns by row (n)	16	16
Number of rows (m)	6	11
Mass of copper (m)	1.76 kg	7.15 kg
Magnetic field at center (B_0)	347.67 Gauss	318.08 Gauss
Resistance (R)	0.066 Ω	0.268 Ω
Necessary Voltage (V)	1.98 V	8.05 V
Necessary Power (P)	59.41 W	241.36 W

Table 3.12: Performance of Magnetic Nozzle (Copper Diameter 3mm, 30 A)

Although the desired 600/300 magnetic field were not available, a more equitable distribution of the maximum magnetic intensity between the two coils was obtained, without going below the 300 Gauss requirements limit. In addition, this arrangement gives a maximum outer radius for the big coil of 11.93 cm, which lies within the limits of the windable structures by Elementos Magnéticos Navarra S.L. It also shows some energetic requirements that are easily achievable by the already existing motors of the EP2 laboratory, with voltages much lower than the maximum 20 volts considered. Finally, it can be seen how the amount of copper needed in total is below the maximum allowable by SENER, which is 15 kg. As such, this last design model, which fulfills all the imposed restraints and whose performances lie within acceptable limits of the intended ones, was decided to be the one of the prototype to be manufactured.

3.6 Final Design

Based on the coil sizing done in the previous section, the final design of the prototype can be performed. Next, an explanation of all its features will be given.

Wire characteristics

A short description of the wire, the conductor part and its insulator will be given.

A total of 27.8059 meters of wire are needed for the inner coil and 112.9688 meters are required for the second coil. Thus, a total amount of 140.7747 meters of wire are needed. Taking into consideration the copper part, a total amount of 1.76107 kg of copper are needed for the inner coil, while 7.15482 kg of copper are needed for the outer coil, making it a total of 8.9159 Kg of needed copper (below the maximum 15 kg available).

For the insulator part, a Kapton insulating material is considered, since it has good thermal properties (up to 200ºC) [47] and low outgassing, which is beneficial in vacuum conditions, it will not affect the vacuum chamber performances [48]. An insulator thickness of 1.92% of the copper conductor diameter was used.

A thermal analysis of the evolution of the wire heating can be used according to the one explained in 3.4 Considering a maximum temperature of 180ºC to leave some margin up to the critical 200ºC of Kapton, the following evolution is expected (considering a current of 30 A through both coils):

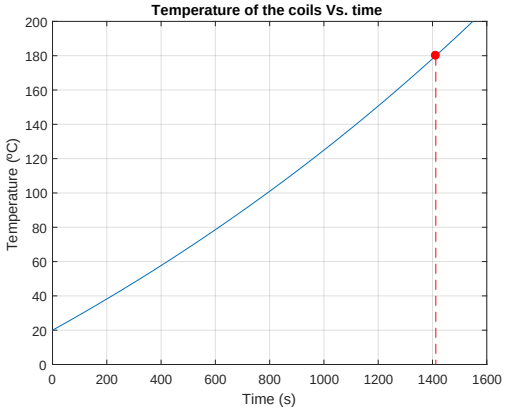

Figure 3.20: Temperature evolution of prototype Magnetic Nozzle

The figure shows how the magnetic nozzle can be safely operated up to 1412.3 seconds (23.5383 minutes), which is enough to do all the necessary validation tests.

Coil sizing

The physical properties of the coils (without any aluminum structure, that is only the wire pack), as well as the maximum magnetic field that they can generate, are summarized in the following table:

Property	Coil 1	Coil 2
Coil width (L)	4.992 cm	4.992 cm
Inner radius (R_i)	3.67 cm	8.50 cm
Outer radius (R_o)	5.55 cm	11.93 cm
Turns by row (n)	16	16
Number of rows (m)	6	11
Magnetic field at center (B_0)	347.67 Gauss	318.08 Gauss

Table 3.13: Characteristics of the coils of the magnetic nozzle prototype

With these data, the maximum magnetic field in each of the directions can be calculated by changing the 3x3 matrix in section 3.4 to a 3x2, and by specifying the direction of the selected position only by means of one angle α':

$$\begin{bmatrix} 0 & 0 \\ sin(\alpha) & -sin(\alpha) \\ \cos(\alpha) & \cos(\alpha) \end{bmatrix} \begin{bmatrix} B_1 \\ B_2 \end{bmatrix} = \begin{bmatrix} 0 \\ \sin(\alpha') \\ \cos(\alpha') \end{bmatrix} \tag{54}$$

Which considers a magnetic coil whose coil's axes lie on the Y-Z plane. Based on this, the maximum available magnetic fields in each direction can be obtained. The figure considers the direction towards the axis of the inner coil (higher magnetic field) to be positive.

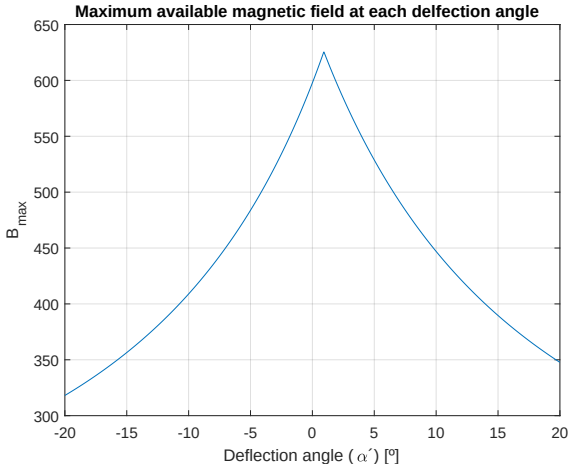

Figure 3.21: Maximum magnetic field available (in Gauss) in each direction from prototype center

It is observed how the maximum is closer to the direction of the coil that generates a higher maximum magnetic field. However, being the ones of both coils so similar in both coils of the prototype, it is close to the 0^{o} direction (straight flow of plasma from its source). Strong magnetic fields are generated in all directions, being the minimum the one of pure outer coil contribution (318 Gauss).

Supporting structure

In this section, the design of the structure to support the coils of the magnetic nozzle. On the one hand, it is important to discuss the aluminum spools around which they will be winded. Their dimensions have been sized in parallel with the ones of the coils, since they were essential for the configuration non.interference. Thus, the following dimensions were obtained:

Property	Spool 1 (for coil 1)	Spool 2 (for coil 2)
Width (L)	5.692 cm	5.692 cm
Thickness	3.5 mm	3.5 mm
Inner radius (R_o)	3.32 cm	8.15 cm
Outer radius (R_o)	3.67 cm	8.50 cm

Table 3.14: Dimensions of aluminum spools of the magnetic nozzle prototype

In addition to this, it was necessary to develop a fastening system for the whole magnetic nozzle. Based on the already existing plate for mounting coils of the EP2 laboratory (Appendix A), a gripping system had to be design.

A first idea consisted on reusing the four bars of the plate assembly to fasten the outer coil and then look for a way of attaching the inner one to those bars. The bars would sustain the coils by introducing them into holes on one side of the aluminum spool. However, due to the small thickness of these spools, additional structure would be needed to be added at the end of these in such a way that holes could be drilled through. These protrusions, however, should be in such a way that no interference would be caused between them and with the plasma source tube.

However, it was observed that the outer coil could not be attached in such a way as it would need of additional structures at the end of the coil that would cause interference. Thus, it was decided to build an auxiliary structure which would be attached to the already existing plate and to which the coils would be fastened. In such a way, these structure allows for flexibility in the decision of where are the attached bars located to optimize non-interference. It was decided to build bars perpendicular to the plate and the additional structure at a specific position and drill the wholes in the additional supporting part of the coils with a 20^{o} angle. In such a way, mounting of the coils could be done straight forward and perpendicular to the plasma source exit. The additional structures built on the end of the spools

would be located in the upper and lower parts of the coil, since the angle of the coil is in the horizontal direction, to avoid any type of interference. In addition it would only be of a width and thickness sufficient to pass the supporting bar and the necessary fixing screws (above and below the bars). An additional benefit of this auxiliary structure is that it allows to mount first the inner coil and then the outer one, also enabling independent adjustment of both by varying the length of the bars that support them.

Taking all this into account, it had to be considered the manufacturing process of the spools. After discussing with the Technical Office, the spool shape would be formed by turning [46], and the additional structure to introduce the bars by milling. In addition to this, the winding company required the aluminum spool surface to be hard anodized. This surface treatment ensures electric isolation between the wires and the aluminum structure [49]. When winding around a conductive material (such as aluminum) there is always some risk of electric contact as the isolation of the wires may have some porosities.

For the bars supporting the coils, aluminum bars of 10 mm diameter for the outer coil and aluminum bars of 6 mm diameter for the inner coil have been considered. The auxiliary structure has been decided to be of stainless steel. For the fixing screws, ISO metric screws M4 have been selected for the outer coil and ISO metric screws M3 for the inner one [50].

Finally, a last parameter to be considered in the design of the structure support is the plasma source itself. Since it requires an antenna and a tool box, one side of the source tube could not be accessible. Also, an antenna space should be considered, modeled as a tube of 35 mm outer diameter. This last one is also included in the model with the plasma source exit to check for interference. The drawings of the additional structure, inner coil and outer coil are included in Appendix B.

Final drawing

Thus, after all the design process, the magnetic nozzle prototype was developed. The sketch of the whole system, including the plasma source exit and antenna and the auxiliary structure are shown in the drawing of the following page. It is observed how no interference occurs. The auxiliary structure designed was subcontracted for forming by laser cutting.

Manufacturing

As a conclusion for the final design, the manufacturing and delivery must be discussed. Due to the outsourcing of all the manufacturing processes, longer times are required to get the magnetic nozzle done and mounted. Therefore, the manufactured piece was neither finished nor delivered to its complete validation, and it is still in such process.

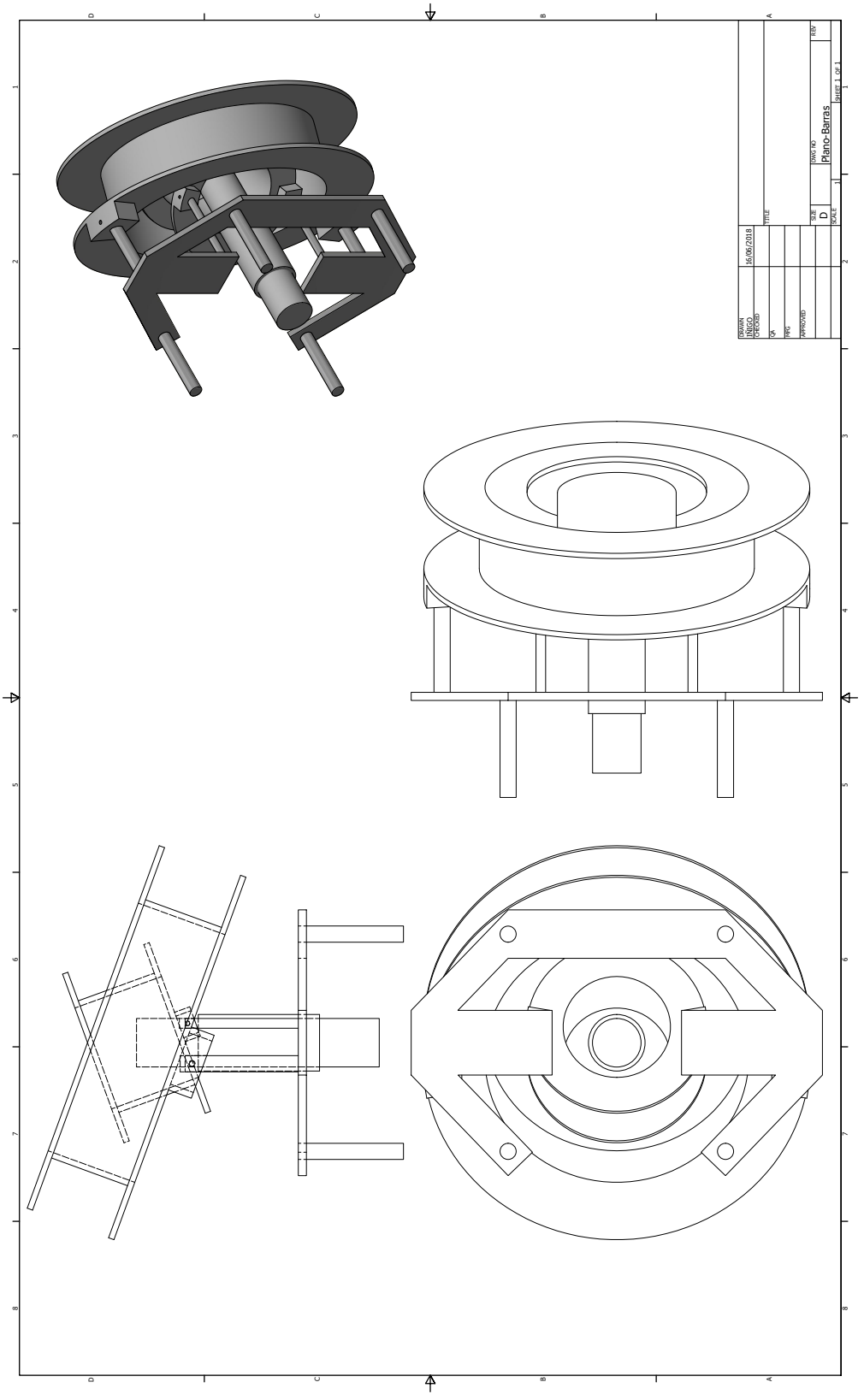

Figure 3.22: Final Drawing of Magnetic Nozzle Prototype

4 Prototype Validation

After building the prototype, it is of interest to validate its usefulness and whether it fulfills the requirements specified when designing it. In order to do so, a validating method has been designed and will be used when the prototype is fully manufactured and sent to the EP2 laboratory.

4.1 Magnetic Field Measuring Device: Gaussmeter

In order to measure the magnetic field, it was decided to use a Gaussmeter distributed by the company Lake Shore. This magnetic field measuring device works under the principle of the Hall effect sensors.

The Hall effect was first observed by E. H. Hall [51]. It states that when a current passes through a sample which is located in a magnetic field, an electric potential proportional to both the intensity of the current and the magnitude of the magnetic field is generated across it. This potential occurs in the direction perpendicular to both the magnetic field and the current.

Based in this concept, the Hall effect sensors on which the gaussmeter relies for measuring the magnetic field [52] are solid-state sensors providing an output voltage proportional to the magnetic flux passing through it. The output Hall voltage can be expressed as:

$$V_H = \gamma_B B \cos\theta \tag{55}$$

Where V_H is the Hall voltage given in mV, γ_B is the magnetic sensitivity of the sensor given in mV/kG at a given current, B is the magnetic flux density in kG and θ is the angle between the magnetic flux direction and the vector normal to the plane of the sensor. Thus, the gaussmeter measures this Hall voltage and uses the linear relationship to retrieve the magnetic field. Hence, it is important to keep the sensor perpendicular to the magnetic flux so that the magnetic field calculated completely relates to the measured voltage. However, this problem does not affect 3-dimensional probes due to the nature of the sensor (there will always be a certain angle between the magnetic flux direction and any of the faces of the sensor).

The sensor contains a semiconductor sheet on which the Hall voltage is measured, which is called “Hall plate”. Most of the sensitivity to the magnetic field is contained in a surface approximated by a circle centered at the plate and whose diameter is equal to the plate width.

The 3-dimensional Hall probes relies on three different Hall sensors (each one with its respective plate), each one with its own output voltage and corresponding magnetic flux measurement.

Based on these operation basics, the specific device selected for measuring the magnetic field was the Model 460 3-Channel Gaussmeter [53], since it allows for three-dimensional measurements of the magnetic field and for communication with a computer. The performance specifications can be seen in Appendix C, although the main characteristics are summarized in the following table:

Lake Shore model 460 Gaussmeter Main Specifications
3 axes and 3 independent channels
Displays the axes simultaneously
Displays Vector Magnitude (based on independent channel readings)
Resolution up to 5 digits
IEEE-488 and Serial interfaces
Measurements in Gauss (G) or Tesla (T)

Table 4.1: Main Specifications of the Lake Shore model 460 Gaussmeter. Retrieved from [53]

In the following parts, a brief explanation of the characteristics of the device which were necessary for measuring the magnetic field will be given. Thus, the measurement mode considered, as well as the probe used and the specific interface will be defined.

Measurement Mode

As the magnetic field generated by the designed magnetic nozzle coming from two coils is continuous, the DC measurement mode was selected. The device is well suited for this DC since the measurements that it makes rely on accuracy and resolution which are best for this mode. In addition, the noise floor produced by the operation in such mode is so low that the device allows up to 5 digit measurements.

In a parallel way, the gaussmeter allows for ranging of the measurements, from 300 mG to up to 300 kG. In the DC mode, variations approaching as low as 0.010 mG can be detected by the device. If the DC magnetic field is larger (which is the case of the magnetic nozzle), this resolution lowers to 1 part in 300,000 maximum.

Probe

The probe used for the magnetic field measurement is of crucial importance, since each one of the possible ones have different range and resolution specifications, as well as having a different amount of axes readings possible. In fact, each probe has a 512-byte Electrically Erasable Programmable Read Only Memory (EEPROM) included, whose information is downloaded to the device when it is turned on. This memory stores the specific information that the gaussmeter needs for operation,

such as the configuration of multi-axis measurements and the field ranges available for display. If the probe is connected when the device is already powered up, this memory may be erased and the sensor would become useless.

It is important, when handling the probes, to consider their fragility, especially at the sensor tip. It must be at all times protected from abrasion, blows, bends, stress and excessive temperature. In fact, no pressure should be exerted on the tip and the probe should only be held in place for measurement by securing the handle. Any strain on the sensor or its stem alters the calibration of the probe and, if excessive force is exerted, may produce the Hall generation destruction.

The probe selected for the magnetic field measurements for the validation of the 3D magnetic nozzle is the model MMZ-2508-UH, which is a High Sensitivity Probe whose measurements allow ranges up to 30 kG. The stem to hold the Hall sensor is made of aluminum. It also ensures a 0.25 % accuracy of the measurement reading up to 20 kG (which completely covers the limits expected for the magnetic nozzle). It must be taken into account, however, that this accuracy may be altered by the environment temperature. The following figure shows a picture of the probe and the three channels (wires) for each of the measurable axes.

Figure 4.1: 3-Axis Hall probe used

The resolution of this probe depends on the range of magnetic field selected, and is summarized is the following table:

Range	MMZ-2508-UH Resolution (Filter Off)
± 30 kG	± 0.01 kG
± 3 kG	± 0.0001 kG
± 300 G	± 0.01 G
± 30 G	± 0.001 G

Table 4.2: Resolution of the measurements of the MMZ-2508-UH probe. Retrieved from [53]

In addition to these characteristics, it must be taken into account the sensors "active area" when measuring the magnetic field, as explained before. This "active area" is the one over which the Hall sensor averages the magnetic field value, as it is the portion of the Hall plate where the majority of the magnetic sensitivity occurs. The specific ones for the selected probe can be seen in the following figure:

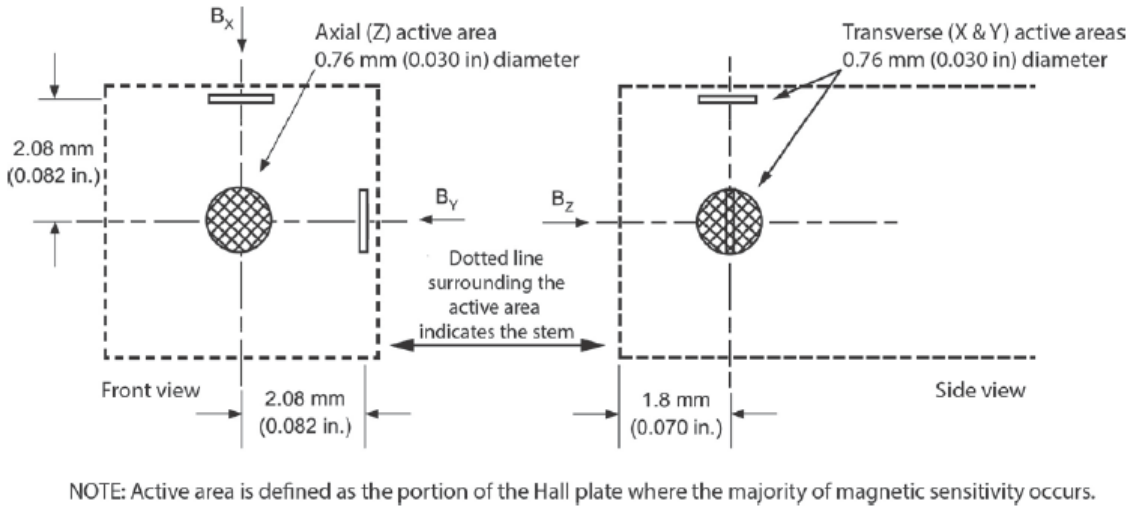

Figure 4.2: Active areas of the 3-axis probe. Retrieved from [53]

As it can be observed, these active areas are not at the tip of the probe, and thus this offset must be taken into account when relating the magnetic field to the specific location in space measured.

A final remark considering the probes must be made. These must be zeroed before the measurements by means of a Zero Gauss Chamber. This chamber completely blocks any magnetic field, such that it calibrates the sensors before any measurement. In addition to that, both the instrument and the probe must warm up for 5 minutes before zeroing the probe and at least 30 minutes to comply with the rated accuracy. The Zero Gauss Chamber and the probe must be at the same temperature to ensure correct calibration.

4.2 Gaussmeter Control

Considering all the characteristics and specifications of the device, it was of interest to control the magnetic field measurements by means of a computer. To do so, it was decided to create a LabVIEW environment able to control both the gaussmeter and the physical device, i.e. translational arm or probe holder, which would move the probe inside the magnetic field to different positions. LabVIEW is a graphical programming tool developed by National Instruments which enables a simple and intuitive way to control instrumentation devices [54].

All the details concerning the communication between the Gaussmeter and the computer by means of the interface are explained in Appendix E.

The Hall probe to measure the magnetic field was decided to be placed in a robotic arm located in from of the magnetic nozzle and which can move axially and azimuthally with respect to a center located at the plasma source. Thus, the LabVIEW program was designed to control both the gaussmeter and the robotic arm in each magnetic field retrieval movement. Thus, a LabVIEW program with the following user interface was created:

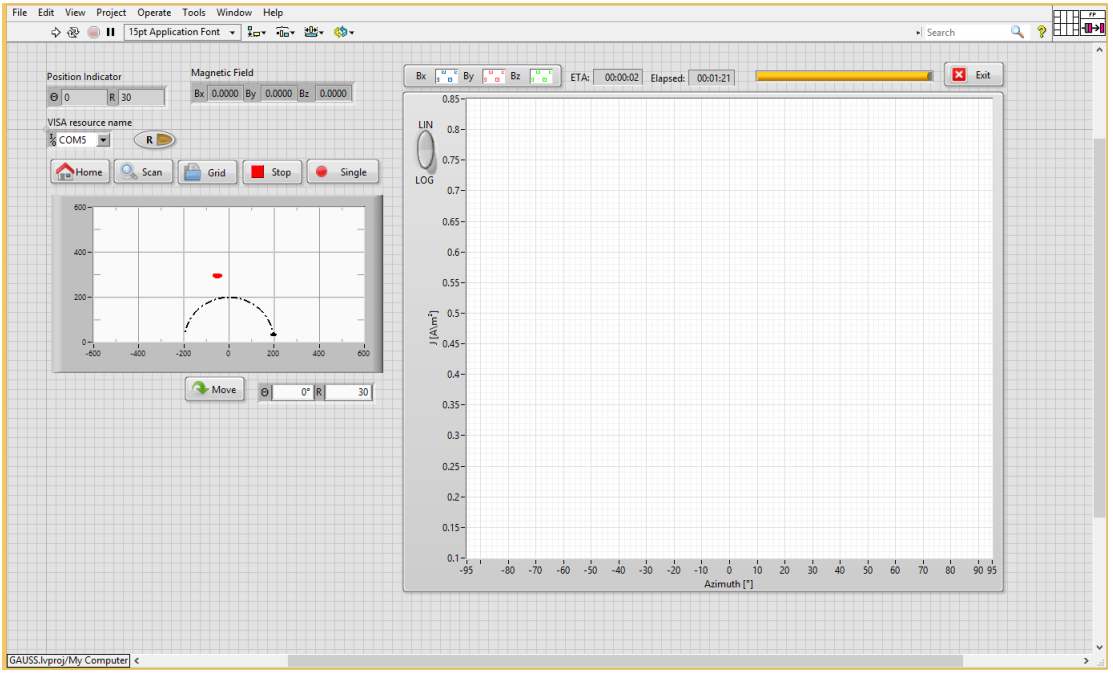

Figure 4.3: Gaussmeter Control LabVIEW Interface

This program allows for many different functions and gives different data. In the following lines, the different buttons, graphs and text boxes will be explained. Among the information boxes, one finds the position indicator, which specifies in which position the robotic arm is located at a given time. Next to it, the magnetic field indicator shows the magnetic field magnitude measured by the Hall probe and

the gaussmeter in each of the axes for a single measurement. Below, one can find the "VISA resource name" box, which serves to specify the income port of the device to be used (as specified before, *COM5* for the gaussmeter). Considering the buttons, the first one is the "Home" button, which automatically moves the robotic arm to an already specified initial position. The "Scan" button starts the measurement of the magnetic field at the points in space determined by a given grid of azimuthal and radial points. The "Grid" button enables to upload a given grid of points for the program to measure at. Next to it, the "Stop" button completely stops the scan process but enables a continued use of the program. Finally, the "Single" button makes a single measurement of the magnetic field at whichever position the robotic arm is and displays that information in the magnetic field indicator explained before. The button above all these with an "R" is the "Reverse" button, which turns upside down the grid loaded, allowing for another scan in the opposite sense and avoiding the need of time to reach again the "home" position. The last button is the "Move" one, which moves the robotic arm to the specific azimuthal and radial position specified by the user in the text boxes next to it.

Considering now the graphs, the first one to be explained is the one located below the buttons. This one shows the set of points specified by the loaded grid, so that the user can see whether the grid is the correct one. The bigger graph on the right shows the measured magnetic field on each of the axes at each point for visual interpretation of the results. This way, the user can see the different components of the magnetic field measured by the gaussmeter in each of the points of the specified grid, either in linear of logarithmic scales. This has the benefit of allowing the user to decide whether they want to repeat the measurements before exporting and post-processing the results.

Lastly, the "Exit" button on top of the big graph stops the whole program and stops running it. A flowchart explaining how the program works is shown in the following page (Figure 4.4).

It is important to notice how, after the scan is performed, the program exports a *.txt* file automatically to a given documents folder with the measured data. This is the one read in the post-process of the measurements in order to be analyzed. Another important characteristic of the program is that it initializes and finalizes communication with both the device and the robotic arm at the start and end of the program. Doing so is important to tell the devices when they should be aware of possible communications with them, as well as ensuring good performance. Failure to end communication with the devices may result in inability of further measurements by means of the LabVIEW program since new initialization of communication cannot be made.

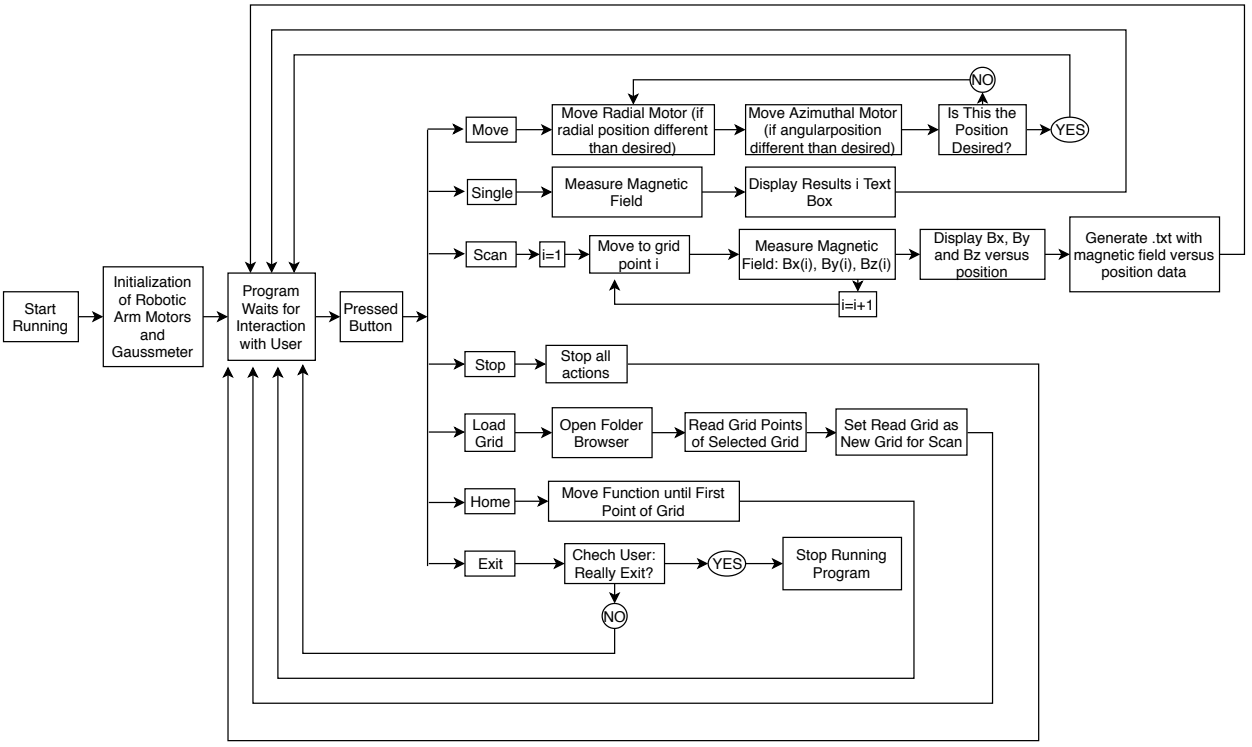

Figure 4.4: LabVIEW Program for Control of Gaussmeter and Robotic Arm Flowchart

Once the complete LabVIEW program was developed, it was necessary to physically fasten the Hall probe of the Gaussmeter to the robotic arm.

In order to do so, it was decided to design a 3D-printed piece which would enable to hold the probe to the arm and keep it well adjusted. Therefore, it was determined that two fastenings would be done: one above the probe, to adjust it, and another one below, to attach it. The design of the piece considered holding the probe at the start of its handler, since, as it has been already explained, attaching it by the stem would generate strains that could affect the measurement readings. In addition to that, both the upper and lower subjection systems will be comprised of a M3 screw and its respective bolt [50]. However, all the dimensions of the generated CAD design are slightly bigger than the ones necessary for the piece since the poor precision of the 3D printer may cause the holes to be too small to fit the different bodies. Making them slightlyy bigger ensures that they will fit and, since the adjustments are made by screws, the is no problem o looseness.

The final 3D-printed piece is shown in the following figure. A drawing of the piece with the different measures is attached in Appendix D.

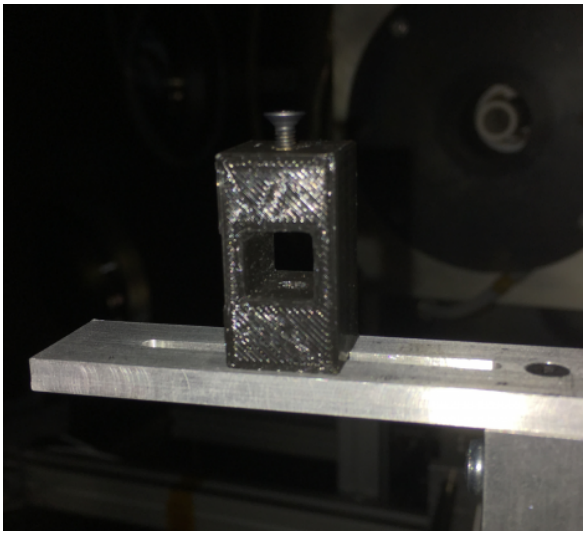

Figure 4.5: 3D printed probe-holding piece

4.3 Magnetic Field Measurements Process

In order to check the validation process designed for the 3D magnetic nozzle, it was of interest to try it with a coil already placed with the Helicon Plasma Thruster of the EP2 laboratory. In such a way both the validation process and the theories regarding the magnetic field produced by a coil, necessary for the correct performance of a magnetic nozzle, could be demonstrated.

In order to validate the magnetic field of the coil currently being used by the Helicon Plasma Thruster of the EP2 group, the magnetic probe and the Gaussmeter were used. The experiment was performed inside the vacuum chamber of the EP2 laboratory and the control of the different devices (gaussmeter, coil and robotic arm) was performed by means of a set of digital computers next to the chamber. In addition, the vacuum chamber was at all times open as there was no need to generate vacuum for magnetic field measurements (it is not affected by whether there is a medium such as air or not). Therefore, controlling the systems close to the devices and having the chamber opened allowed also for visual checking of the correct performance of the whole set-up and immediate action (physical or of computer control) if errors occurred. A representative image of the testing environment and the computer control setup is shown in the following image:

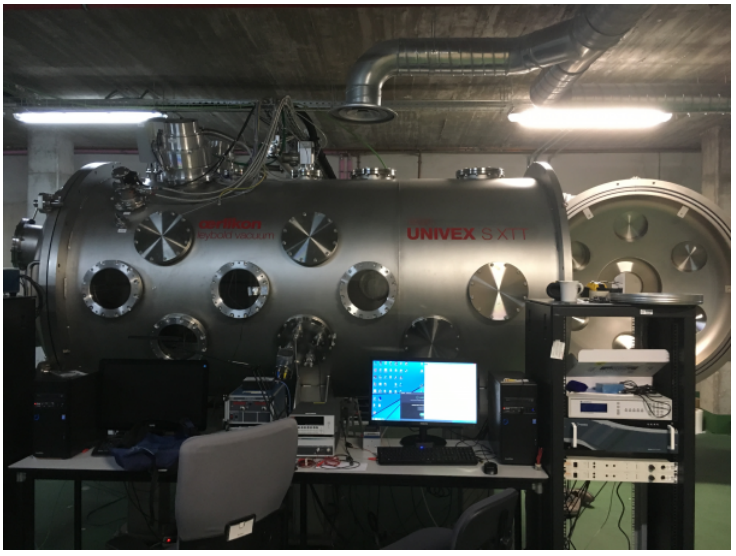

Figure 4.6: Testing Environment and Vacuum Chamber

As it was discussed in the previous section, both the gaussmeter and the robotic arm were controlled by means of a LabVIEW program. This program was run by the computer shown in the right, closer to the two power sources feeding energy to the two motors of the robotic arm and to the gaussmeter. The left computer was used to control the activation and deactivation of the magnetic coil in order to generate its magnetic field. This was done by means of a program which allowed to control the intensity going through the magnetic coil as well as a maximum allowable voltage.

If the program received a measure of a voltage of equal or higher value than the one set, it would automatically power the coil off in order to avoid overheating and possible damage to the equipment. Due to the characteristics of the coil, a current of 5 Amperes was directed through it in order to generate a magnetic field of about 250 Gauss at its center. Constant control of the voltage measured at the coil was needed in order to ensure that it did not overheat, breaking the whole system. Since the current going through it was relatively low, no actual risk of overheating under normal conditions should appear. However, as it was discussed in the design process, the temperature rises exponentially with time in a continuously working coil. Thus, it was better to constantly keep control before it increased further remarkably fast. As a rule of thumb, it was decided to note to let the voltage across the coil go higher than 1.3 times the intensity (V (V) =1.3 I (A)).

The robotic arm is located inside the vacuum chamber and it is mounted on a metallic structure on top of a circular-shaped rail. The arm was able to move along this circular track in an azimuthal fashion, being the center of rotation of the arm the center point of the "thruster" exhaust section (or center point of the coil). In addition, a vertical bar is mounted on the arm which can be moved forward and backward along the radial direction (being this movement controlled by a different motor as explained before). A small horizontal metallic tab (or probe holder) is attached to this vertical bar, which can be adjusted at several heights. The same horizontal tab has a groove on which any probe can be attached (allows for several positions) by means of adjustment with a screw and a nut. In the center of rotation of the robotic arm is located the magnetic coil and the plasma source, such that all measurements point towards them. In the following image, a picture of the set-up of this robotic arm within the vacuum chamber and its position relative to the magnetic coil is showed:

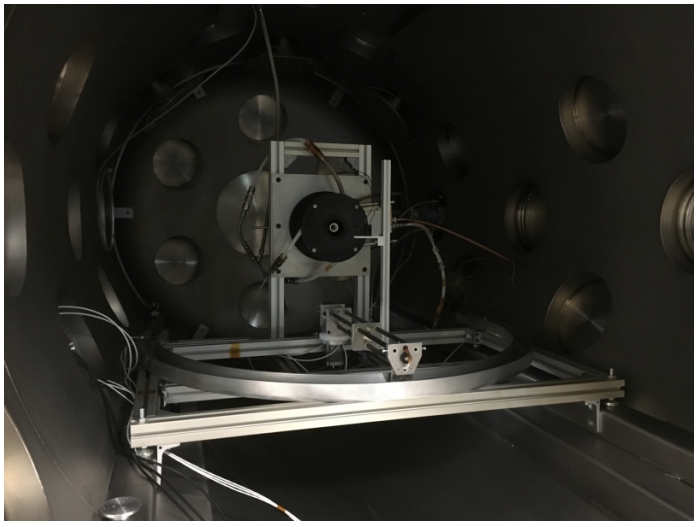

Figure 4.7: Set-Up of the Robotic Arm and Thruster Within the Vacuum Chamber

Once the operating systems were established, the probe was set on the robotic

arm. In order to do so, the 3D printed piece defined in the previous section was used. This way, the Hall probe handler can be attached to the horizontal part of the robotic arm and also be adjusted to limit possible movements or looseness. The final set-up is shown in the following figure 4.8. It is important to note the necessity of locating the cable of the wire fixed with the robotic arm in order to avoid any interference and possible obstruction in the correct operation of the robotic arm. This was done by means of insulated adhesive tape, since only temporary positioning of the cable was needed, for simplicity.

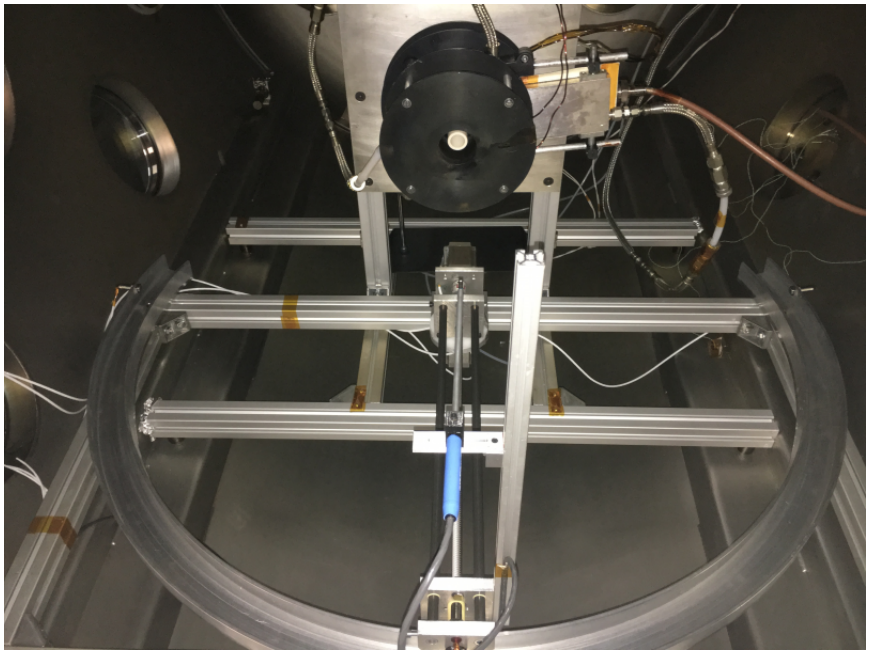

Figure 4.8: Robotic Arm and Probe Set-Up

Once all connections seemed to be correct, it was decided to place the probe at a height of the robotic arm vertical structure such that the center of the probe was completely aligned with the center of the coil when the arm was located in its axis of symmetry (or 0^{o} azimuthal angle). A picture showing such arrangement is shown as follows:

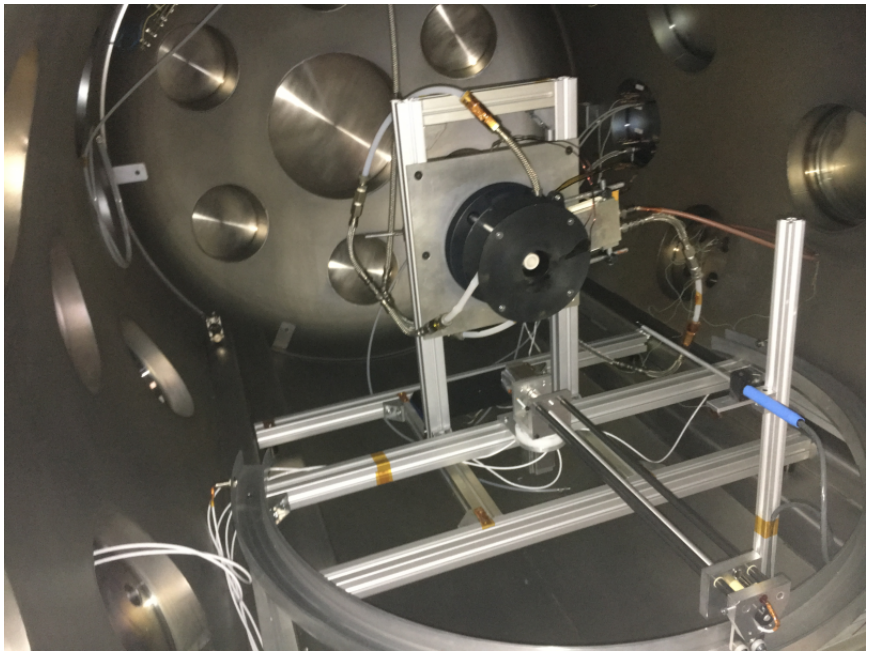

Figure 4.9: Position of the Probe with Respect to Coil being validated

In the LabVIEW program, the position measured of the robotic arm in the radial direction is with respect to the exit plane of the magnetic coil, being the center at the exit the zero position. It is important to remark here that the LabVIEW program considers an offset from the known position of the robotic arm to the "active area" of the probe (see section 4.1). In such a way, the distance from the exit plane of the coil written in the output of the program is not actually the distance to the arm but to the "active area" of the probe, which is the point actually being measured.

At this moment, all the necessary devices and connections were in place and the validation of the coil map could be performed. However, in order to ensure the reliability of the validation, a test measurement was made. Knowing that the magnetic coil was generating a magnetic field of approximately 250 Gauss in its center, and according to the distance squared decay of magnetic field as described in section 3.2, the magnetic field along the axial line of the coil was measured. It was decided to start the measurements in the far field (300 mm away from the coil exit plane) and stop them after exiting the coil through the other side. Measurements at several distance steps were obtained, although the steps where smaller near the coil due to the higher gradients in the magnetic field according to the the theory. The following axial magnetic field distribution was obtained:

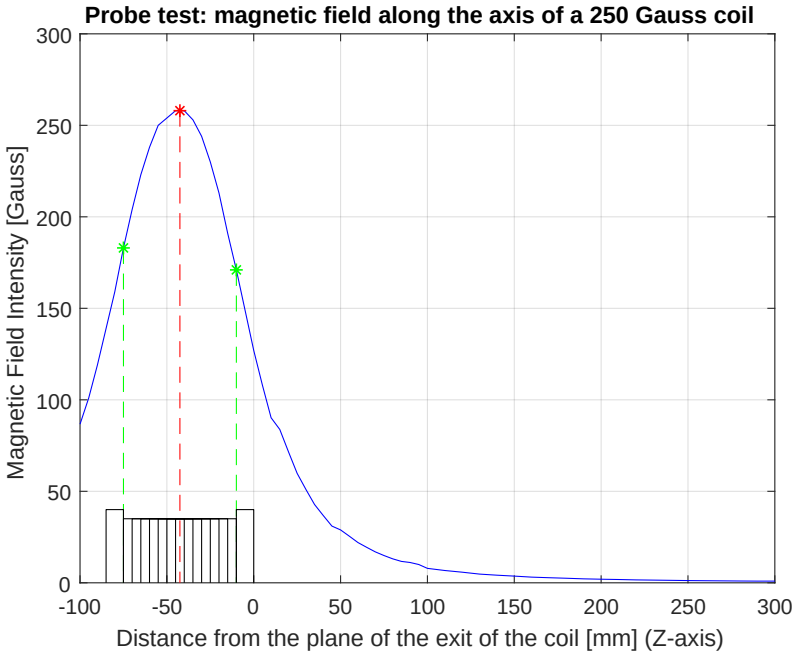

Figure 4.10: Test of the Axial Magnetic Field of a 250 Gauss coil along its axis

In the plot, the coil dimensions and positions are shown for reference. It is observed how the maximum magnetic field intensity is experienced at the center of the coil, with a value of intensity of 258 Gauss, which is close to the theoretical 250 Gauss predicted. In addition, close symmetry can be seen along both sides of the axis from the center of the coil, which corresponds to what is known about the magnetic field along the axis of a coil. In fact, it can be observed also how quickly decreases the intensity of the field as the distance from the center increases, approaching asymptotically the zero value. Such behavior correlates with the decrease proportional to the square of the distance predicted. Therefore, according to the similitudes observed between the measured field and the theoretical one, it was determined that the validating method was operating correctly, and so did the programs and all the devices needed. Thus, the mapping of the whole magnetic field of the coil could be performed.

4.4 Validation of the Magnetic Field of a 250 Gauss Magnetic Coil

As a preliminary validation of the operation characteristics and performances of the designed 3D magnetic nozzle, it was of interest to check the real magnetic field generated by a coil. The ultimate goal by means of this experiment was to check the validity of the magnetic field following the axis of symmetry line of the coil. Showing the veracity of such hypothesis would allow to finally determine that the magnetic field actually follows such line in physical experimental environments (and not only in theory), proving the validity of the underlying logic of the 3D magnetic nozzle.

The experiment was performed by means of the process explained in the previous section. In order to map the maximum amount of area in front of the coil, a sweep of different scans was performed. It was decided to measure the magnetic lines along the radial direction from a point close to the coil to one far enough for the effect of the magnetic coil to be negligible. This measurements were to be done along several azimuthal angles to validate the whole space.

In order to perform such experiment it was decided to measure the magnetic field along lines from a distance of 10 mm to the center of the coil to up to 300 mm from the center of the coil. It was decided not to measure from the exact center (0 mm) to avoid interference with the limiting structure of the coil at higher angles from the central axis. Impact between the probe and the coil would severely alter the magnetic field readings, giving useless measurements, and could even break the probe since the robotic arm is not able to sense this problem and would try to continue moving forward (stressing even more the probe tip and causing irreparable damage). The measured lines would be located at each 5^{o} azimuthal angle between each other, being the zeroth angle along the axis of the coil. Although 5^{o} may seem relatively big steps, the concentration of points measured close to the coil exit is high enough to accurately map the sharp changes in the magnetic field at such distance. The behavior of the magnetic field at higher distances is of less relevance, since the plasma is mostly affected by the exit shape of the field and the changes between steps are much less pronounced, allowing for accurate interpolation of data between distant points. However, to ensure even more precision, it was decided to make steps of 5 mm distance from 10 mm to 100 mm positions to better measurement of the field changes, while steps from 100 mm to 300 mm were of 10 mm (less accuracy was needed). Azimuthal angles between $+80^{o}$ and -80^{o} from the axis line will be considered, since it gives the most information about the field and to avoid any possible obstruction of the probe with the coil. Thus, a total of 33 different directions will be made.

The probe was zeroed in the Zero-Gauss chamber before performing the experiment. In each direction scan two different measurements were made: one with the magnetic coil powered up and one without its magnetic field. The purpose of this was to measure the effect of the Earth-generated magnetic field inside the vacuum

chamber and then measure the total field followed by the plasma when the coil is active. The magnetic field generated only by the coil is then the one measured when it is active minus the one produced by the Earth. Thus, it is of interest to check the three possible magnetic fields existent

It was decided to set the range of the z-axis and x-axis of the probe (radial direction and azimuthal direction respectively) at ±300 G, giving a resolution of ±0.01 G, which is good enough for the purposes of the validation of this coil. The range of the y-axis (measuring the direction perpendicular to the plane of movement of the probe) was set to ±30 G giving a resolution of ±0.001 G, since theory expects magnetic fields in this direction to be zero (although some fluctuations may be expected due to intrusion of other magnetic fields).

It must be also considered the necessity to transform the results obtained by the probe into Cartesian coordinates for its correct plotting and analysis. Taking into account that measurements are being obtained in a polar fashion (radial and azimuthal position), the Cartesian position can be easily obtained as:

$$x = R\sin(\theta) \tag{56}$$

$$y = 0 \tag{57}$$

$$z = R\cos(\theta) \tag{58}$$

In order to transform the magnetic field measurements from the radial, azimuthal and out-of-plane directions to the Cartesian ones, a rotation must be made between both sets of coordinates. Thus, one must consider the way in which the probe is measuring the fields. It was set that the z-axis of the probe measured the radial component, the x-axis of the probe measured the azimuthal component and the y-axis of the probe measured the out-of-plane component. To make the rotation change, one must take into account the directions in which the probe considers the magnetic field to be positive. The positive directions are in the increasing radial direction for the radial component, in the clockwise direction for the azimuthal component and in the downwards direction or the out-of-plane component. The plane vectors' relative position to obtain the rotation matrix are shown in the figure 4.11. Thus, according to this figure, the rotation between both sets of axes is given by:

$$\begin{bmatrix} B_x \\ B_y \\ B_z \end{bmatrix} = \begin{bmatrix} -\cos\theta & 0 & \sin\theta \\ 0 & 1 & 0 \\ \sin\theta & 0 & \cos\theta \end{bmatrix} \cdot \begin{bmatrix} B_{azimuthal} \\ B_{out-of-plane} \\ B_{radial} \end{bmatrix} \tag{59}$$

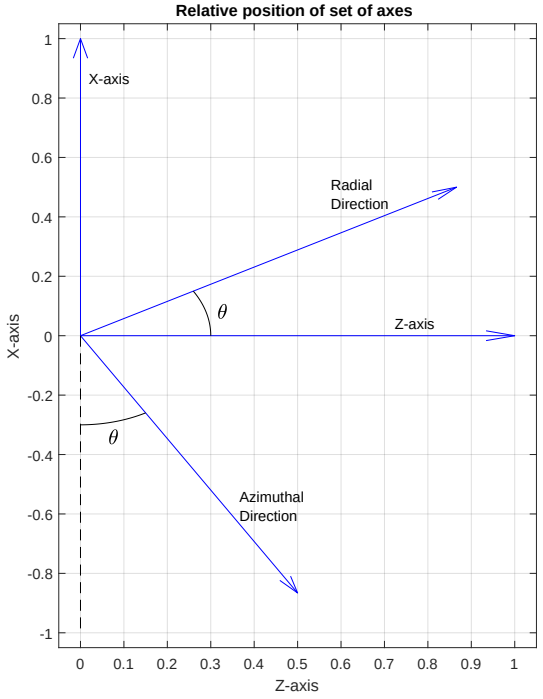

Figure 4.11: Position of sets of axes for the rotation matrix

Based on all the necessary conditioning of the data, a post-processing code was used to perform all the changes. This code reads the data exported by the LabVIEW program for both the background and the total magnetic field measurements for each of the angles. Once it has this data, it makes the changes to the Cartesian axes and performs the calculations needed. All the results are stored in matrices which have the whole data, which are the ones used for plotting. This is summarized into the following flowchart of functioning of the post-processing program:

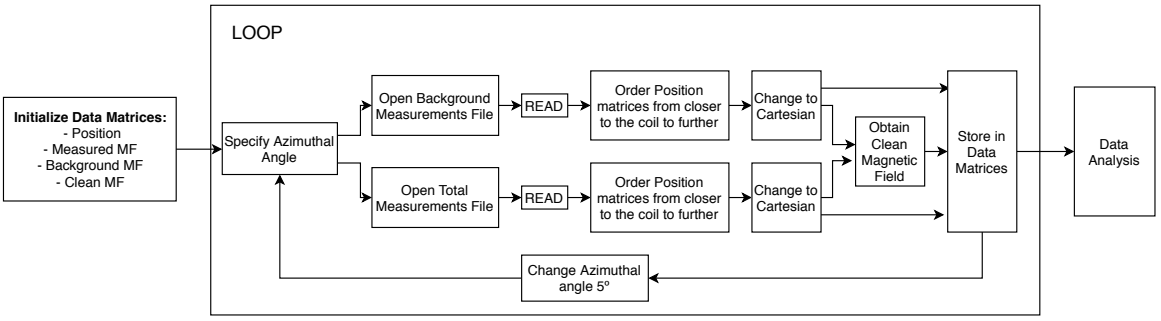

Figure 4.12: Flowchart of Post-Processing Program

Considering all this, a total of 66 different scans were made by means of the LabVIEW program. The results obtained are shown and discussed in the following lines.

Discussion of the Measurements

Once all the measurements obtained by the probe were post-processed, the different results can be analyzed. The first important measurement to discuss is the distribution of the total magnetic field measured in the area in front of the magnetic coil. The results are shown in figures 4.13 and 4.14:

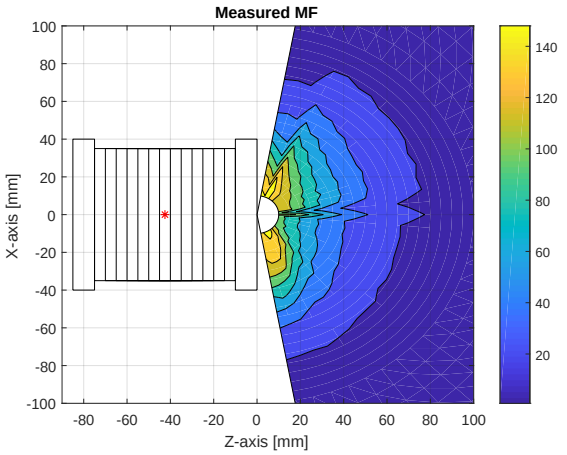

Figure 4.13: Total Magnetic Field Measured (Gauss)

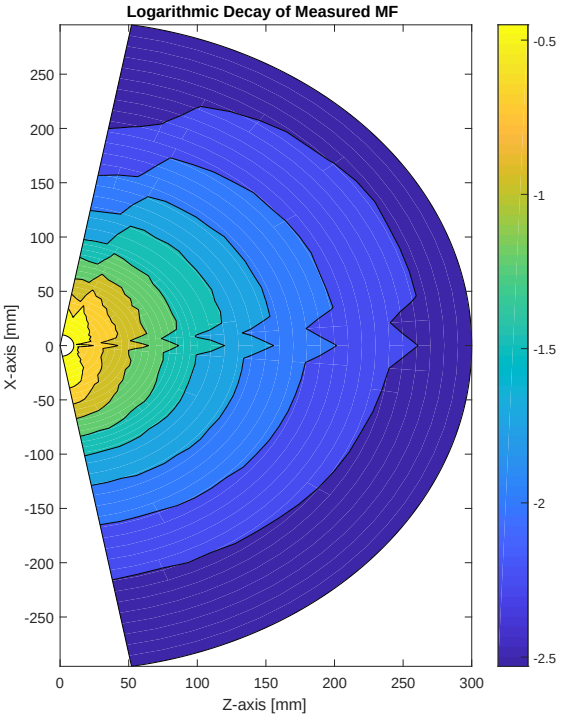

Figure 4.14: Logarithmic Decay of Total Magnetic Field Measured with Respect to Maximum Available at the Center of the Coil

Figure 4.13 shows the actual distribution of the intensity of the magnetic field in the measured points in the near region of the exit of the coil. The coil is showed to represent the actual distance from the point of maximum magnetic field (red asterisk) with respect to the measured points. It can be observed how points closer to the exit of the coil have the greatest magnitudes and a fast decrease is experimented as the distance increases. This goes in correlation with the theory presented in previous sections, as the magnetic field decreases proportional to the square of the distance. Higher magnetic fields are experimented on the sides of the coil axis, however. This is mainly due to the fact that measuring in an azimuthal way provokes that at higher angles, the probe is actually closer to the exit of the coil as the latter is not a single point but a circle.

The plot shown in figure 4.14 represents the logarithmic decay of the mag-

netic field intensity measured in the whole sector relative to the maximum available magnetic field in the center of the coil (measured to be 258 gauss in the previous section). The plot shows a more distributed evolution, in contrast with the left one which shows that almost all changes are experienced near the exit. It is remarkable how the maximum magnetic field intensities are one third of the maximum. This right-hand-side plot shows how magnetic field go from intensities of the order of one third the intensity in the center near the exit to intensities of less than two orders of magnitude below at the largest radial positions. However, this evolution seems to be experienced almost uniformly, being the differences near the exit still larger than far from it.

These results show in fact that in the total obtained magnetic field, the intensities generated correlate to those expected in front of a theoretical coil. It is now interesting to examine how the background magnetic field affects this total measurements.

The background magnetic field can be defined as the one that is affecting the space in front of the coil but that it is being generated by external sources, such as the Earth magnetic field or those generated by electronic and electrical instrumentation inside or near the vacuum chamber. The magnetic field in the area in front of the coil was measured while having the coil powered off. The measurements are shown in figure 4.15.

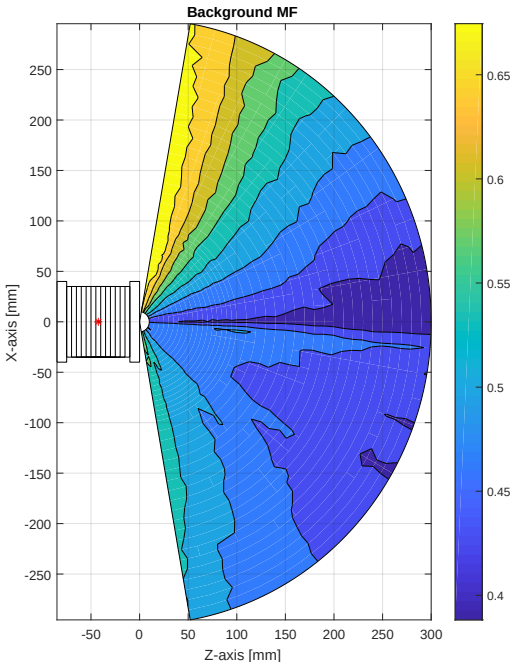

Figure 4.15: Background Magnetic Field Measured (Gauss)

As before, figure 4.15 shows the magnetic field measurements. It can be seen that a more random distribution of magnetic field intensities is experienced in front

of the coil, producing the greatest ones near 80^{o} azimuthal angle and the lowest along the 0^{o} and close to it. Such a distribution could be inherent to the magnetic field of the Earth at the location and relative position of the vacuum chamber with respect to it, or could be generated by the electronic and electric components located near the 80^{o} angle that power up the coil and the plasma source. Magnitudes of lower than the gauss unity are measured throughout the sector area. Low impact in the near region is thus predicted in the magnetic field of the coil that would guide the plasma thrust vector.

Taking into account both measured distributions, one can analyze the actual magnetic field generated only by the coil (or "clean" magnetic field) by subtracting the total measured one by the background one. The results are shown in figures 4.16 and 4.17.

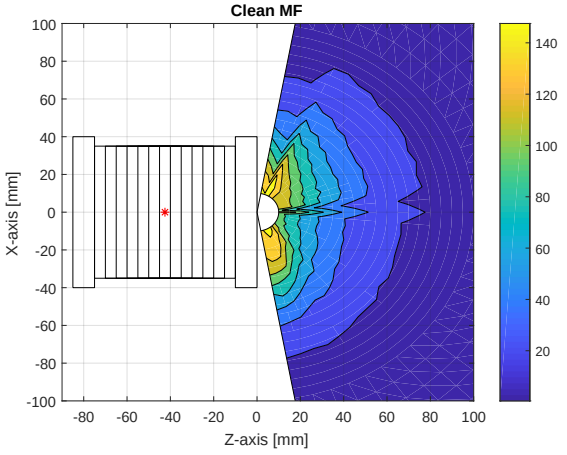

Figure 4.16: Clean Magnetic Field Measured (Gauss)

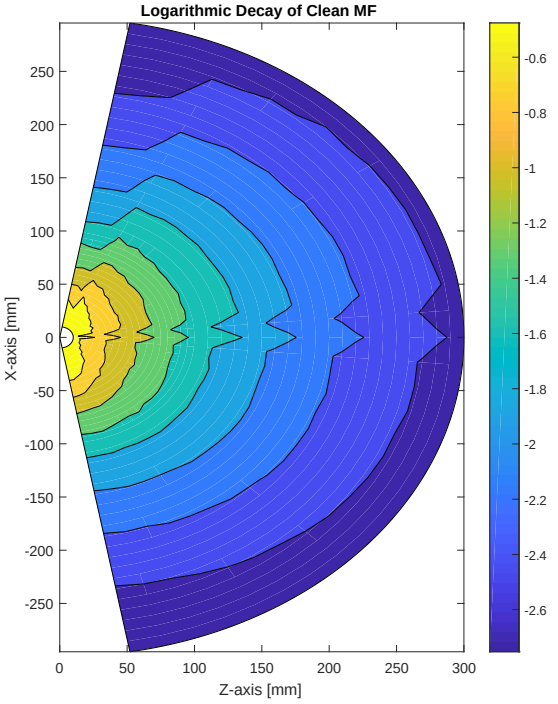

Figure 4.17: Logarithmic Decay of Clean Magnetic Field Measured with Respect to Maximum Available at the Center of the Coil

The measurements of the magnetic field of the coil shown in figure 4.16 show a distribution very similar to that obtained in 4.13. In fact, they are almost the same, since most of the change in magnetic field intensities is experienced near the coil exit, where it is not easy to check visually for differences. However, when one considers the logarithmic decay relative to the maximum available magnetic field intensity at the middle of the coil shown in figure 4.17, more differences between the total measured magnetic field intensities and the "clean" ones are observed. The main

remark consists on the slight drop of intensities in the "clean" magnetic field. This drop is more accentuated as one moves further from the coil exit. This translates into the fact that background magnetic field seems to affect greater the far regions from the coil, while leaving almost unbothered the near region. It is interesting to check up to what point the background magnetic field is comparable to the magnetic field generated by the coil. In addition, a peak in the magnetic field is observed along the axis of the coil, however, which does not correlate with the theoretical smooth continuous distribution. This peak, could be due to irregularities in the winding of the coil which may produce differences in the intensities of magnetic field. These differences may be more pronounced closer to the axis, showing therefore the peaks in the distribution.

In the following figure 4.18 the relative effect of the background magnetic with respect to the calculated "clean" magnetic field of the coil itself is shown in a logarithmic fashion, to check for relationship of orders of magnitude.

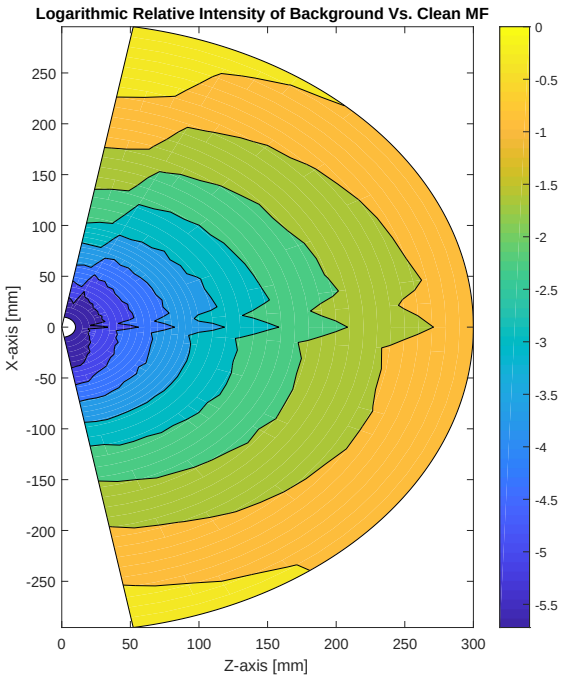

Figure 4.18: Logarithmic Relative Intensity of Background Vs. Clean Magnetic Field

Due to the natural distribution of the magnetic field generated by a coil, the results obtained are as expected. Being the magnetic field of the background of the order of tenths of gauss, the relative effect with respect to the one generated at the coil is maximum in the far region, where orders of magnitude are comparable. However, the closer one gets to the coil, the less the background affects the magnetic field being applied, where the relative effect drops to more than five orders of magnitude

of difference. The results translate directly into understanding that the background magnetic field has little effect in the near region of the magnetic coil exit, thus little effect into the vectoring of the plasma plume is expected. In fact, since the effect of steering the thrust vector relies on the strength and direction of the magnetic field in the near region, no effective influence of the background magnetic field should be expected. In the other hand, while both being of equivalent orders of magnitude in the far region, the magnetic field at such distance has very little effect in the control of the thrust vector. In conclusion, small effect of background magnetic field is expected in the performance of the magnetic nozzle applied magnetic field.

Although the magnetic field expected in the plane of symmetry of the coil is expected to be completely in plane, some out of plane components were measured. Thus components may be due to asymmetries in the coil itself or to small relative rotations of the probe within the handler which may have generated small magnetic field errors. These errors were tried to be reduced to the minimum by means of the 3D printed securing handler and the screws. It is interesting, however, to check the relative intensity of the out-of-plane magnetic field with respect to that of the in-plane magnetic field. This ratio is obtained as $(B_y/\sqrt{B_x^2 + B_z^2})$, where the x and z components are the ones in-plane and the y component is the one out-of-plane. This analysis is performed with the "clean" magnetic field intensities and is shown in figures 4.19 and 4.20.

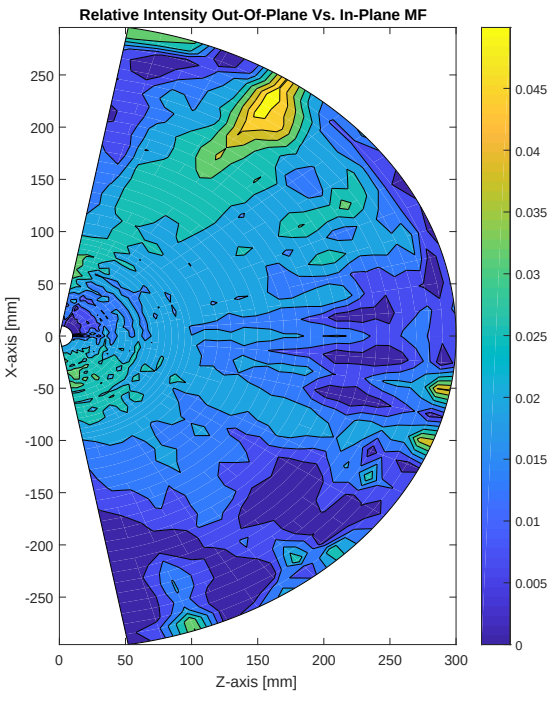

Figure 4.19: Relative Intensity Out-Of-Plane Vs. In-Plane MF

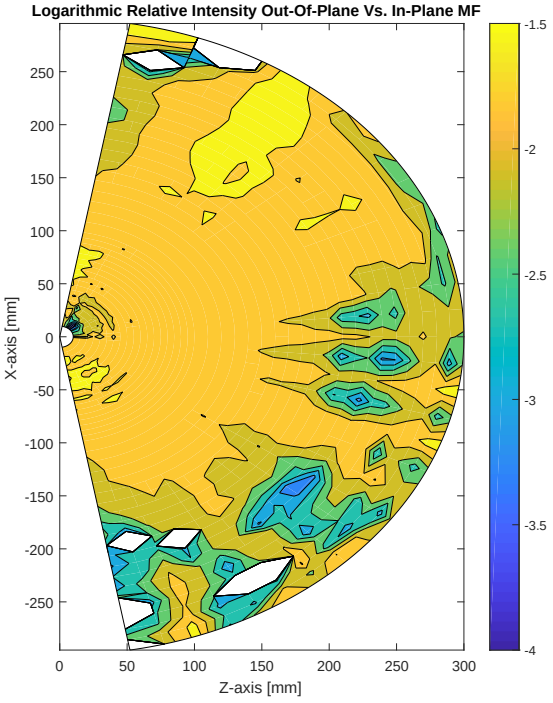

Figure 4.20: Logarithmic Relative Intensity Out-Of-Plane Vs. In-Plane MF

The left-hand-side figure 4.19 shows how the out-of-plane component, in general,

has little effect compared to the magnetic field generated in-plane. In fact, the maximum relative magnetic field is observed in far-regions from the magnetic coil exit. In addition, the distribution itself shows certain level of randomness and not a specific trend, thus meaning that these out-of-plane magnetic components can actually be produced by the sensitivity of the probe itself, which generates the error, or by irregularities in the winding of the coil. Thus it can be concluded that the tested coil presents very small asymmetries. Looking to the right-hand-side figure 4.20 which shows the same results as the other plot but in logarithmic scale, it can be seen that the maximum effect is always at least one order of magnitude below for the out-of-plane component, being this situation in the far-field. This correlates with the results seen in the other plot. The white spots are those where the relative strength is 0 and the logarithm thus goes to negative infinity. Based in these low relative values, most of the magnetic field keeps being in-plan with the plane of symmetry of the magnetic nozzle, steering the plasma thrust vector within it, which is the desired one.

In order to finish this analysis, it is of interest to check how the magnetic field is directed in the whole space in front of the magnetic nozzle and how the plasma plume is expected to behave by following it. This is shown in figures 4.21 and 4.22, for which the in-plane "clean" magnetic field (the one of the magnetic coil by itself) has been used.

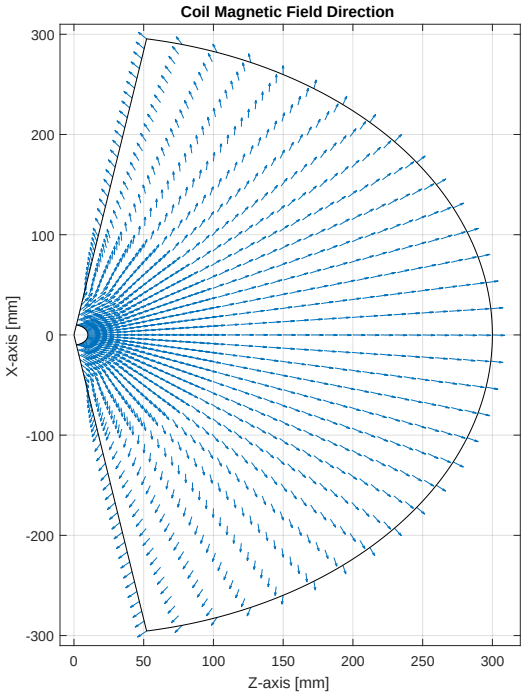

Figure 4.21: Direction of the Magnetic Field Generated by the Coil

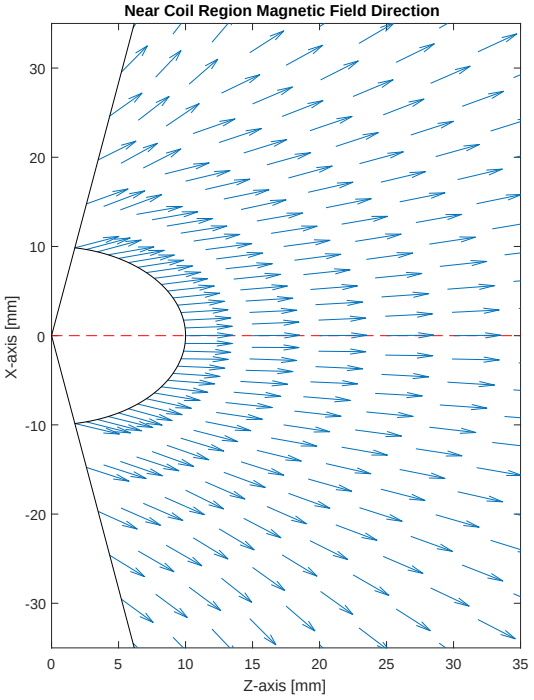

Figure 4.22: Direction of the Magnetic Field in the Region Near the Coil Exit

In Figure 4.21 the whole behaviour of magnetic field in the measured area can be

observed. It shows how near the axis of the coil the magnetic field is almost purely axial. As one moves towards large azimuthal angles, the magnetic field direction starts turning towards the backwards direction. This effect is most extreme at the $\pm 80^{o}$ positions. This behaviour in the whole sector is exactly the one expected by a magnetic coil by the closing magnetic lines effect. This shows that the validating process shows accurately the behaviour of a coil. However, the most interesting magnetic field directions are those in the near.region of the coil exit, shown in Figure 4.22.

In order for a magnetic nozzle to work in the intended way and for the proposed 3D magnetic nozzle designed in this work, it is of interest that the magnetic field in the central axis of the coil (and near it) closely follows the axis line. Looking to the plot of the near region, one perfectly sees how the magnetic line of the axis follows exactly the axis of symmetry of the magnetic coil. In fact, all lines at angles close to the central axes are closely followed by the magnetic field lines starting at them. This proves the theoretical description of a magnetic coil and a 3D magnetic nozzle that the coil generates a magnetic field which is aligned with its axis in the center line.

This behaviour validates the principles of magnetic field deflection of the magnetic nozzle, since it proves that the magnetic field is axial in the axis of symmetry of the coil. It serves as a first validating test of its correct performance.

4.5 Proposed Experiments for Validation of the 3D Magnetic Nozzle

As it has been stated in the Design section, the prototype was not delivered to the EP2 group for validation. However, it is of interest to develop a validation process through several experiments in order to ensure future works are coordinated and specified. The proposed validating experiments consist on two different parts: magnetic field validation and plasma deflection validation. In the following lines, the description of such experiments and its objectives will be stated.

Considering the magnetic field validation of the 3D magnetic nozzle prototype, it is interesting to study the intensity and direction of the field both in the near-region of the magnetic nozzle and in the far one. In order to do so, the magnetic field will be measured by means of the validation process designed and demonstrated in the previous sections. In such a way, the plane in which both axes of the coils composing the magnetic nozzle and the one of the plasma source will be studied. This is the plane of symmetry of the whole magnetic nozzle system and thus will give the most information of how the magnetic field is actually being deflected. As for the already performed validating experiment, a sweep of magnetic field measurements at several radial distances from the plasma source exit throughout several azimuthal angles will be performed in each experiment. Measuring such an extensive area in front of the magnetic nozzle will allow for a complete analysis of the magnetic field that it applies.

These measurement sweeps should be checked in at least four different experiment scenarios for complete validation of the magnetic nozzle. Such cases are the following:

1. **Axial magnetic field**: It is essential to check the ability to generate an axial magnetic field of the magnetic nozzle. To do so, the same amount of magnetic field intensity must be generated by both coils (although the intensity through both will not be the same). Comparison of the results of this experiment with those of a single-coil magnetic nozzle would give an insight in the differences of the field in the near-region of the exit and far from it.

2. **Only inner coil powered up**: Powering only the inner coil is necessary to study the actual maximum deflection of the magnetic field that it can generate, as well as its intensity. This experiment is crucial to check whether the magnetic nozzle can actually deflect the field the desired amount. It is also important to analyze the whole magnetic field in front of the magnetic nozzle that is being generated in order to observe how it starts turning back the magnetic lines and how one may expect the plasma to behave.

3. **Only outer coil powered up**: the same experiment reasons and objectives as for the previous case are applicable to this one. However, it is interesting to analyze also the outer coil by its own.

4. **Both coils powered up to generate intermediate deflection angle**: For this last experiment, it is interesting to pass a different intensity through the coils, so that they generate different magnetic field intensities and, thus, a magnetic field directed towards an intermediate angle between axial and maximum deflection angle. This is crucial to prove the theory behind the 3D magnetic nozzle that different magnetic field generated by coils can generate intermediate deflections. As for the previous cases, both the intensity and the behaviour of the magnetic field lines are of interest.

To analyze all of the cases, a mapping of the magnetic field measured throughout the area in front of the coil is of interest, for visual analysis. In addition, to check the experimental results, it would be interesting to compare the obtained experimental measurements with the theoretical ones obtained by the design code. In particular, the most interesting one would be to compare the direction and intensity of the magnetic line that passes through the exit of the plasma source. This way, it would be demonstrated the actual ability of the magnetic nozzle to create a deflected magnetic field.

By means of such experiments, the magnetic field performance would be completely demonstrated and validated, proving the theoretical characteristics of the magnetic nozzle.

In the other hand, the validation of the plasma thrust steering performance of the 3D magnetic nozzle requires different experiments. While having the Helicon Plasma Thruster of the EP2 powered up, several experiments studying the correct behavior of the magnetic nozzle must be presented. As for the previous magnetic field validation processes, the measurements of the plasma should be performed on the plane containing the two axes of the coils and the one of the plasma source. Sweeps at different azimuthal angles should be used to properly characterize the plasma expansion.

Two different characteristics of the plasma plume should be studied. On the one hand, a Faraday cup [55] is to be used in order to characterize ion current density in the far region. At a constant radius far from the plasma source, azimuthal sweeps of the device will allow to obtain the ion current density at each angular position showing the direction in which most of the plasma is being directed. The azimuthal angle in which the peak of the ion current density is located will be that of the "direction" of the plasma plume. Therefore, this experiment will show the actual deflection of plasma. On the other hand, as only forward thrust can be measured by using a conventional thrust balance, thrust vectoring will be detected by the decrease in axial thrust. In such a way, if F_{max} is the thrust when the thrust vector is aligned with the thruster axis (symmetric magnetic field), F_{meas} is the measured thrust when plasma plume has been deflected and θ is the deflection angle from the axial line, one expects that by geometry $F_{meas} = F_{max} \cos\theta$. The deflection of the thrust vector is therefore simply $\theta = \arccos(F_{meas}/F_{max})$.

These two types of measurements should be performed in four different cases,

at least, which are exactly the same as those of the magnetic field validation:

1. **Axial magnetic field**: This case is interesting to evaluate the behaviour of the 3D magnetic nozzle as if it was a single coil magnetic nozzle. Study the behavior of the plasma expansion and compare it to already performed experiments of magnetic nozzle performance will allow to analyze the effect of generating a straight-forward magnetic field which is being generated by two different coils. It is also important to measure the axial maximum thrust available, such that in the experiments at certain azimuthal deflection of the plume the thrust vector angular deflection can be obtained.
2. **Only inner coil powered up**: Powering up just one coil will allow to check for the maximum available plasma plume deflection and thrust vector deflection. It will also enable an analysis of the plasma particles in such a configuration, studying the detachment of ions to the desired maximum deflection.
3. **Only outer coil powered up**: The same reasons and objectives as for the previous case apply to this one, but it is considered important to study the behavior of the maximum deflection available by this outer coil. In addition, due to the differences in size and therefore in the magnetic field, the plasma expansion may be slightly different, thus an analysis is of interest.
4. **Both coils powered up to generate intermediate deflection angle**: It is interesting, finally, to check the ability of the 3D magnetic nozzle to steer plasma jet in an intermediate direction between the axial direction and the maximum deflection. Stating that at intermediate angles the magnetic nozzle can actually move the thrust vector and plasma plume to directions between the zero and the maximum one will prove that, in fact, the 3D magnetic nozzle is useful to use in maneuvering. It will show that all the range of angles between the maxima given by the two coils is available for thrust steering.

In the results given by these experiments, however, it must be considered that the non-symmetric effect of the use of the two coils may produce undesirable effects in the plasma expansion, which produces asymmetries in it too. This relates into possible negative effects in the thrust vector that could affect its intensity when it is being deflected. This may produce lower measured force and incite to thinking that lower thrust vector steering is being done.

From the results obtained in these plasma expansion characterization experiments, several results should be discussed. Firstly, it would be of interest to compare the actual thrust deflection against the magnetic field deflection that is being applied. This will give an insight of how the ions are sticking to these magnetic field lines and evaluate how much defection of magnetic field is needed to generate a certain thrust deflection. Secondly, it will be interesting to check the measurements with the results obtained using the code FUMAGNO of Merio Merino [31]. Since this code assumes fully magnetized ions, its results are limited. Thus, the measurements will allow for a more exact behavior of plasma in the characteristics of the

magnetic field of the 3D magnetic nozzle and to correct the code for more exact results.

The results of these plasma expansion characterization experiments will completely validate the perfromance of the 3D magnetic nozzle, proving its usefulness. In such a way, the theoretical approach of Merino and Ahedo would be completely demonstrated experimentally, and 3D magnetic nozzles will be proven to be an effective way of steering plasma in spaceborn maneuvers.

5 Regulatory Framework

According to the regulatory framework, the work presented has been under consideration of laws applying to security and health of work in laboratory environments. Thus, the following legislation is applicable for implementing and testing the prototype:

- *Law 31/1995, of November the 8th, on Prevention of Workplace Risk (BOE nº 269 10/11/1995).* This law regulating at country level (Spain) specifies the conditions to ensure work safety. Application of this law is mandatory whenever work is going to be performed, as in the process of working in the laboratory of EP2.
- *Directive 2013/35/EU of the European Parliament and of the Council of 26 June 2013 on the minimum health and safety requirements regarding the exposure of workers to the risks arising from physical agents (electromagnetic fields) (20th individual Directive within the meaning of Article 16(1) of Directive 89/391/EEC) and repealing Directive 2004/40/EC.* This European directive establishes the threshold magnetic field intensities to ensure security of workers working under their effects. It is important since all validation processes demand the application of high magnetic fields to operate the magnetic nozzle and the plasma source.

Based in these two applicable laws, the work performed in the laboratory was guided in order to ensure safety. In addition to this, it must be noted that in the design process the used auxiliary parts (such as screws and nuts) followed the *International Organization for Standardization (ISO)* guidelines to ensure compatibility and simplification of the manufacturing process.

As a final remark, it must be considered that all magnetic field simulations and data post-processing have been regulated under the *MatLab* standard programming language, while all validation devices controls have been regulated under the *LabVIEW* standard programming language.

6 Budget

The budget of this project is shown in Table 6.1.

As it is observed, most of the costs come from experimenting needs, such as the operation of the plasma thruster and that of the DC sources. Also, it must be considered the manufacturing cost and the man-work that it implies, adding several costs of both engineering, production and material treatment. Finally, it is important to consider all the equipment (hardware) and programs (software) needed to simulate and test the prototype.

Concept		**Cost**	
Coils		1250 €	
	Wire		300 €
	Spool Material (Aluminum Blocks)		150 €
	Machining		400 €
	Anodizing		100 €
	Winding		300 €
PM Cost		2400 €	
Electronic Equipment		311.2 €	
	Equipment (PCs) Amortization		170 €
	RJ-11 cable		2 €
	RJ-11 to female DB9 adapter		4.2 €
	Prologix PGIB-USB Controller		135 €
Computer Programs Licensing		1000 €	
	LabVIEW License (One year)		1000 €
	MatLab Student License		Free
Experimenting Cost		3000 €	
	Helicon Plasma Thruster Operation (2 weeks)		3000 €
Total Cost of Project		**7961.2 €**	

Table 6.1: Project Budget

7 Conclusions

The work performed in this project has successfully shown the design of a prototype for a 3D magnetic nozzle as proposed by Merino and Ahedo, as well as the development of a complete validation process to prove its performance.

Taking into account the design phase of the 3D magnetic nozzle, it has been shown how the use of coils, whose magnetic field in the center is in the direction of the axis, are the best option to generate an applied magnetic field for a 3D magnetic nozzle. Also, the decision on mounting three independent magnetic coils one within another to generate the 3D magnetic field has been discussed as being due to manufacture constraints. How the magnetic field at any point in space was calculated has also been shown. In addition, the design of straight coils whose loops are perpendicular to the axis of the coil has been demonstrated to better deflect and be more manufacturable than the field against coils whose loops are at the desired deflection angle with respect to the axis. However, these showed good performance (enough for the purposes of the 3D magnetic nozzle), and the causes of the differences between both arrangements has been successfully explained.

Once the basic coil design decisions were discussed, the design iterations were presented, including the design process itself and the many agents involved. The characteristics of the magnetic nozzle being designed were shown, followed by the decisions made based in such characteristics and the manufacturing constraints. It was discussed how at each iteration the original requisites of design, especially in terms of number of coils used and generated magnetic field, had to be reconsidered. The requisites had to be relaxed but without penalizing in the validation of the 3D magnetic nozzle. A final design was achieved and its characteristics were examined. A fastening mechanism to hold the coils to the plasma source was discussed and presented.

In such a way, all the objectives concerning the design of the 3D magnetic nozzle were fulfilled, as the design achieved the manufacturing level.

Considering the validating process developed, the gaussmeter has been described, as well as the characteristics of the probe used and the interface with the digital computer. In addition, a LabVIEW program was created for the control of the measurements in the validation process and its characteristics were explained. In order to finish the setup of the validation process, an explanation about the robotic arm on which the probe is mounted and how the latter is fastened was given, as well as how all these bodies ere located within the vacuum chamber.

The designed magnetic field validation process was tried with a single coil on its horizontal plane of symmetry, showing the expected results and proving the usefulness of the process. The magnetic field of the coil was validated in the near-region between 10 mm to 300 mm from its exit and at several angular positions. Both the total magnetic field and the background magnetic field were measured. It

was shown that the maximum magnetic field intensity was being generated next to the coil exit, but its magnitude was one third of that available in the center of the coil. It was also shown compliance of the coil-induced magnetic field in front of it as the magnitudes showed a fast decrease as the radial distance from the coil increased. Drops to less than two orders of magnitude with respect to the field at the center of the coil were measured in the limits of the measured area. The background magnetic field measurements showed a more random distribution, of higher intensities near the 80^{o} azimuthal position but always within limits of the gauss unity. Considering the magnetic field generated by the coil only, it was shown that there was a small overall drop in the intensities with respect to the ones measured for the total field, being more representative in the far-region. The effect of the background magnetic field was then studied against the "clean magnetic" field, showing almost no effect in the regions near the coil, and increasing as radial distance increases, up to being of similar order of magnitude in the far-region. However, since plasma thrust steering is mostly done in the region near the coil, the background field effects are of little importance. The effect of out-of-plane magnetic field contribution with respect to in-plane contribution was then discussed, considering these as the own irregularities of the winding of the coil. Finally, the magnetic field directions of the measured coil were discussed, showing compliance with the theoretical magnetic lines of a single coil.

As a final remark, a complete validating process was discussed and explained in order to finish validating the 3D magnetic nozzle prototype. The experiments proposed would completely validate the magnetic nozzle and prove the performance of the magnetic nozzle described by Merino and Ahedo. Thus, all the objectives concerning the validation process were achieved.

Future Work

In this last section, the main activities to continue the study of a 3D magnetic nozzle are discussed, directed towards its intended possible applications.

The main work that must be done based in the project presented consists on performing the developed validation process proposed, based on the experiments for magnetic field and plasma characterization, of the manufactured prototype. Since the prototype is still in this manufacturing stage, proving its validity is still an objective to fulfill. In such a way, the basic principles of operation of the 3D magnetic nozzle would be proven, showing the electric propulsion community its usefulness.

Once this complete validation is done, efforts should be directed towards a magnetic nozzle able to steer plasma in three directions by means of joining at least three coils. In such a way, a study of possible different configurations should be done in order to reduce the size of the magnetic nozzle. Among these, it would be interesting to study the possible use of superconductors, the implementation of an efficient cooling system or the possibility of putting the coils interwined instead of

nested. Generating a more compact and light 3D magnetic nozzle able to generate higher intensity magnetic field would actually shown that it is possible to implement it into the propulsion system of space systems for maneuvering activities.

Finally, considering the hypothesis that this kind of magnetic nozzle is effective, its performance should be improved. Efforts should then be put by the whole electric propulsion sector in order to include such nozzles even in larger spacecrafts for its propulsion in space. Also, due to its high lifetime, more hours of continuous operation can be ensured by this system. Implementation of the 3D magnetic nozzle would allow for longer missions to further places, while maintaining the simplicity of operation explained throughout this work.

References

[1] M. Merino and E. Ahedo. "Contactless steering of a plasma jet with a 3D magnetic nozzle". In: *Plasma Sources Sci. Technol.* 26 (Aug. 2017). 095001.

[2] M. Merino and E. Ahedo. *Sistema sin partes móviles ni electrodos y procedimiento para vectorizar el empuje en motores espaciales de plasma.* P201331790. July 2015.

[3] M. Merino and E. Ahedo. "Encyclopedia of Plasma Technology". In: J L Shohet. Vol. 2. Taylor & Francis, 2016. Chap. Magnetic Nozzles for Space Plasma Thrusters, pp. 1329–1351.

[4] G. P. Sulton and O. Biblarz. *Rocket Propulsion Elements.* 7th ed. John Wiley & Sons, 2001. Chap. 19: Electric porpulsion.

[5] R.Jahn. *Physics of Electric Propulsion.* New York: Dover Publications, 2006.

[6] E. Ahedo. "Plasmas for space propulsion". In: *Plasma Physics and Controlled Fusion* 53.12 (2011), p. 124037.

[7] M. Martinez-Sanchez and J. E. Pollard. "Spacecraft electric propulsion - an overview". In: *Journal of Propulsion & Power* 14 (Sept. 1998), pp. 688–699.

[8] C.Charles. "Plasmas for Spacecraft Propulsion". In: *Journal of Physics D: Applied Physics* 42 (2009), p. 163001.

[9] D. M. Goebel and I. Katz. *Fundamentals of Electric Propulsion: Ion and Hall Thrusters.* JPL, 2008.

[10] Mario Merino Martínez. "Analysis of Magnetic Nozzles for Space Plasma Thrusters". PhD thesis. Universidad Politécnica de Madrid, June 2013.

[11] E. Ahedo. "Plasma dynamics in a helicon thruster". In: *EUCASS Proceedings Series* 4 (Mar. 2013), pp. 337–354.

[12] E. Ahedo and J. Navarro. "Helicon thruster plasma modeling: Two-dimensional fluid-dynamics and propulsive performances". In: 20 (Apr. 2013).

[13] D. Pavarin; F. Ferri; M. Manente; D. Curreli; Y. Guclu; D. Melazzi; D. Rondini; S. Suman; J. Carlsson; C. Bramanti; E. Ahedo; V. Lancellotti; K. Katsonis; K. Markelov. "Design of 50 W Helicon Plasma Thruster". In: *31st International Electric Propulsion Conference.* Vol. 20. Ann Arbor, MI, 2009.

[14] Kazunori Takahashi et al. "Performance improvement of a permanent magnet helicon plasma thruster". In: *Journal of Physics D: Applied Physics* 46.35 (2013), p. 352001.

[15] G. Krülle, M. Auweter-kurtz, and A. Sasoh. "Technology and Application Aspects of Applied Field Magnetoplasmadynamic Propulsion". In: *Journal of Propulsion and Power* 14.5 (1998), pp. 754–763.

[16] F. Chang-Diaz et al. *The physics and engineering of the VASIMR engine.* July 2000.

[17] A. Arefiev and B. Breizman. "Theoretical components of the VASIMR plasma propulsion concept". In: *Physics of Plasmas* 11.5 (2004), pp. 2942–2949.

[18] L. Cassady et al. "VASIMR Technological Advances and First Stage Performance Results". In: (Aug. 2009).

[19] R.A. Gerwin et al. *Characterization of plasma flow through magnetic nozzles*. Tech. rep. LANL report AL-TR-89-092. Los Alamos National Laboratory, 1990.

[20] M. Merino. *Magnetic Nozzles for Electric Propulsion*. EPIC lecture series at CDTI, Madrid; European Strategic Research Cluster EPIC. Oct. 2017.

[21] C. Deline et al. "Plume detachment from a magnetic nozzle". In: *Physics of Plasmas* 16 (2009). p. 033502.

[22] K. Terasaka et al. "Experimental studies on ion acceleration and stream line detachment in a diverging magnetic field". In: *Physics of Plasmas* 17 (2010). p. 072106.

[23] R. Moses, R. Gerwin, and K. Schoenberg. "Resistive plasma detachment in nozzle based coaxial thrusters". In: *AIP Conference Proceedings* 246.1 (1992), pp. 1293–1303. DOI: 10.1063/1.41752.

[24] B. Breizman, M. Tushentsov, and A. Arefiev. "Magnetic nozzle and plasma detachment model for a steady-state flow". In: *Physics of Plasmas* 15.5 (2008), p. 057103. DOI: 10.1063/1.2903844.

[25] M. Merino and E. Ahedo. "Plasma detachment in a propulsive magnetic nozzle via ion demagnetization". In: *Plasma Sources Science and Technology* 23.3 (2014), p. 032001.

[26] M. Merino and E. Ahedo. "On plasma detachment in propulsive magnetic nozzles". In: *Physics of Plasmas* 18 (2011), p. 053504.

[27] E. Ahedo and M. Merino. "Preliminary Assessment of Detachment in a Plasma Thruster Magnetic Nozzle". In: *46th AIAA/ASME/SAE/ASEE Joint Propulsion Conference & Exhibit*. Nashville, TN, July 2010.

[28] M. Merino and E. Ahedo. "Towards thrust vector control with a 3D steerable magnetic nozzle". In: *34th Int. Electric Propulsion Conf.* Fairview Park, OH: Electric Rocket Propulsion Society, 2015.

[29] B. Wood et al. "The development of a multi-purpose thruster orientation mechanism". In: *14th European Space Mechanisms and Tribology Symp.* 2011.

[30] A. Wittman. *Redundant system for satellite inclination control with electric thrusters*. US Patent 6565043. 2003.

[31] Mario Merino (2017). mariomerinomartinez/fumagno: First release, DOI: 10.5281/zenodo.593787.

[32] Paul A. Tipler and Gene P. Mosca. *Physics for Scientists and Engineers (Vol. 2)*. 6th ed. W. H. Freeman and Company, 2008.

[33] Mario Merino (2017). mariomerinomartinez/magnetic_field: First release, DOI:10.5281/zenodo.496131.

[34] Peter J. Mohr; Barry N. Taylor; and David B. Newell. *CODATA recommended values of the fundamental physical constants: 2010*. Tech. rep. Committee on Data for Science and Technology (CODATA). NIST., 2012.

[35] Dr. Sen-ben Liao; Dr. Peter Dourmashkin; and John W. Belcher. *Course notes for Physics 8.02 Electricity and Magnetism; module 9: Sources of Magnetic Fields*. Tech. rep. http://web.mit.edu/viz/EM/visualizations/

coursenotes/modules/guide09.pdf. Massachusetts Institute of Technology (MIT), 2004.

[36] Frank W. J. Olver; Daniel W. Lozier; Ronald F. Boisvert; and Charles W. Clark. *NIST Handbook of Mathematical Functions*. Chapter 19: Elliptic Integrals. Cambridge University Press, 2010.

[37] *Standard Specification for Standard Nominal Diameters and Cross-Sectional Areas of AWG Sizes of Solid Round Wires Used as Electrical Conductors*. Designation: B 258 – 02. ASTM International. June 2002.

[38] *NASA Standard Electrical,Electronic, and Electromechanical (EEE) Parts List (MIL-STD-975M)*. pp. A.35. NASA. 1994.

[39] Frank P. Incropera ... [et al]. *Fundamentals of Heat and Mass Transfer*. 6th ed. John Wiley & Sons, 2007.

[40] M.R. Ward. *Electrical Engineering Science*. pp. 36–40. McGraw-Hill, 1971.

[41] David R. Lide, ed. *CRC Handbook of Chemistry and Physics*. Internet Version 2005, ¡http://www.hbcpnetbase.com¿. Boca Raton, FL: CRC Press, 2005.

[42] *National Electrical Code*. Table 310.16. NEC. 2005.

[43] J. H. Dellinger. *The temperature Coefficient of Resistance of Copper*. Bulletin of the Bureau of Standards, Vol. 7, pp. 83 (1911) Scientific Paper 147 (S147). 1910.

[44] Superior Essex. *MAGNEBOND AB-220*. Tech. rep. Retrieved from http://www.essexeurope.com/EU/products.aspx?id=2147484354.

[45] Alu-Stock. *Standard aluminum profiles: Aluminum Round Tubes*. http://www.alu-stock.es/en/aluminium-industry/standard-profiles/round-tubes/.

[46] Robert H. Todd; Dell K. Allen and Leo Alting. *Manufacturing Processes Reference Guide*. Industrial Press, 1994.

[47] *Dupont Kapton Summary of Properties*. http://www.dupont.com/content/dam/dupont/products-and-services/membranes-and-films/polyimde-films/documents/DEC-Kapton-summary-of-properties.pdf. DuPont. 2017.

[48] G. Lee. *Materials for Ultra-High Vacuum*. Fermi National Accelerator Laboratory. 1989.

[49] Anesdur. *Hard anodizing*. http://www.anesdur.com/en/industrial-technical-anodizing/hard-anodizing.html.

[50] International Organization for Standardization. *ISO general purpose screw threads; ISO 68-1:1998*. Part 1: Metric screw threads.

[51] E. H. Hall. "On a New Action of the Magnet on Electric Currents". In: *American Journal of Mathematics* 2.3 (1879), pp. 287–292. ISSN: 00029327, 10806377. URL: http://www.jstor.org/stable/2369245.

[52] Lake Shore Cryotronics Inc. *Hall Sensors; Magnetic Field Sensors*. Tech. rep. Retrieved from https://www.lakeshore.com/products/hall-magnetic-sensors/pages/Overview.aspx. 575 McCorkle Blvd. Westerville; Ohio 43082-8888 USA, Aug. 2017.

[53] *User's Manual Model 460 3-Channel Gaussmeter*. Lake Shore Cryotronics Inc. 575 McCorkle Blvd. Westerville; Ohio 43082-8888 USA, July 2017.

[54] National Instruments. *What is LabVIEW?* `http://www.ni.com/en-gb/shop/labview.html`. Accessed: 2018-06-01.

[55] K. L. Brown and G. W. Tautfest. "Faraday-Cup Monitors for High-Energy Electron Beams". In: *Review of Scientific Instruments* 27.9 (1956), pp. 696–702.

[56] "IEEE Standard Codes, Formats, Protocols, and Common Commands. for Use With ANSI/IEEE Std 488.1-1987 IEEE Standard Digital Interface for Programmable Instrumentation". In: *ANSI/IEEE Std 488.2-1987* (1988). DOI: `10.1109/IEEESTD.1988.120316`.

[57] *EIA standard RS-232-C: Interface between Data Terminal Equipment and Data Communication Equipment Employing Serial Binary Data Interchange*. Washington, USA: Electronic Industries Association, Engineering Department, 1969.

[58] RS Components. *RS Pro 9 Way D-sub Female, RJ11 Adapter, Unshielded*. `https://uk.rs-online.com/web/p/rj-adapters-couplers-extensions/0818665/`. Accessed: 2018-06-01.

[59] National Instruments. *Instrument Driver Network: Lake Shore Cryotronics 460 Meter*. `http://sine.ni.com/apps/utf8/niid_web_display.model_page?p_model_id=11873`. Accessed: 2018-06-01.

[60] Prologix; LLC. *GPIB-USB (HPIB-USB) Controller*. `http://prologix.biz/gpib-usb-controller.html`. Accessed: 2018-06-01.

Appendix A: Drawing of Existing Plate

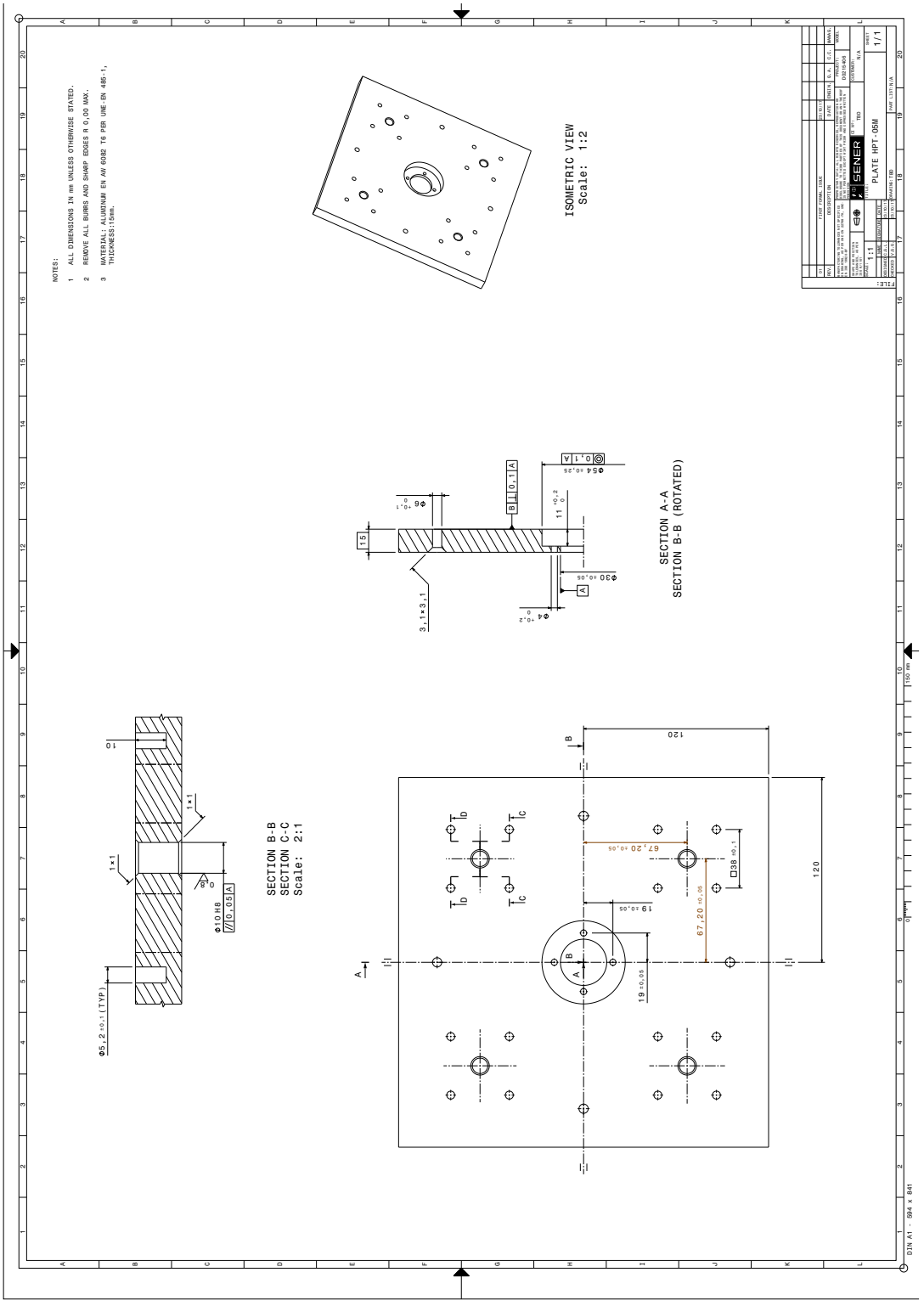

Appendix B: Drawing of Designed Structures

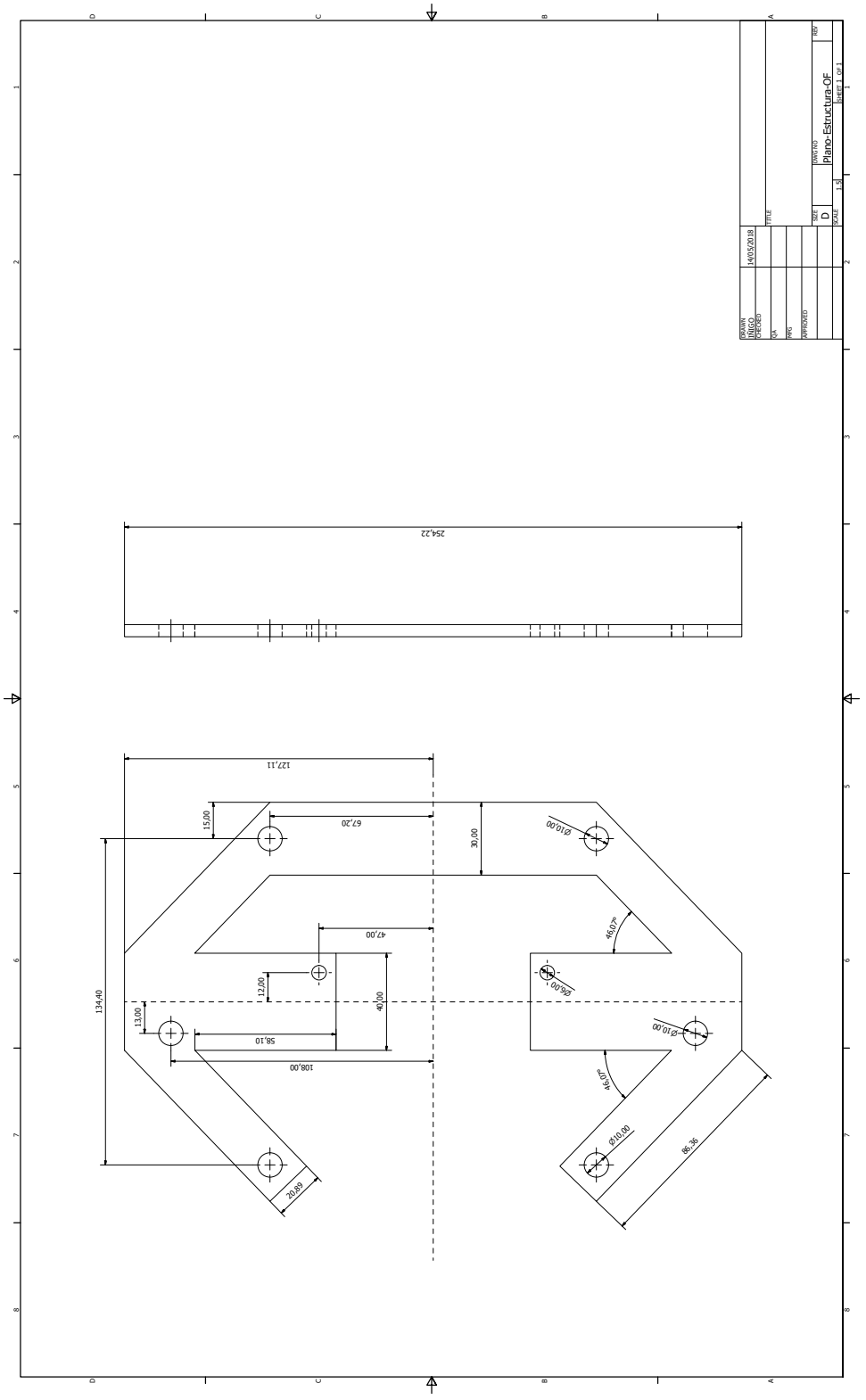

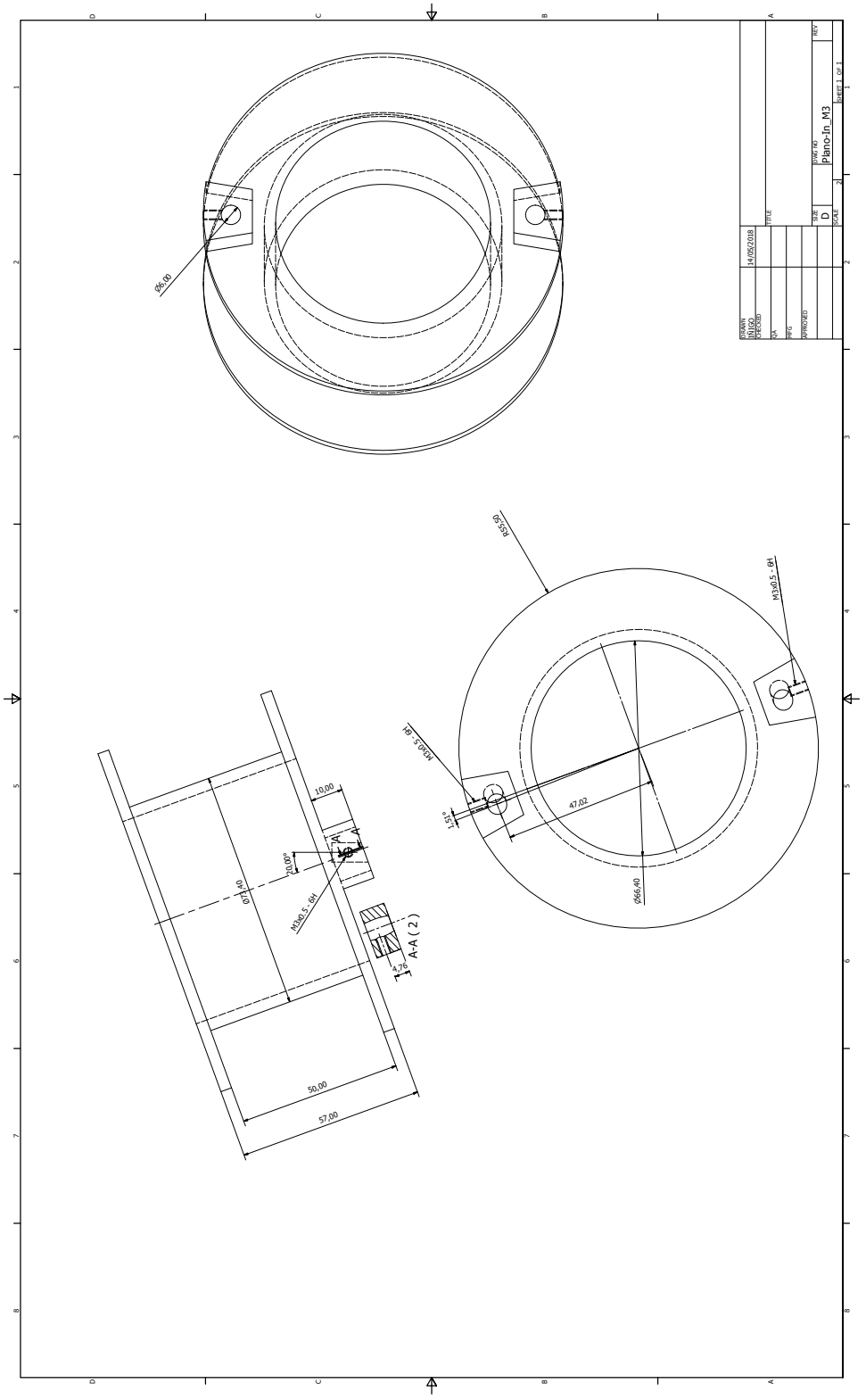
Ø66,80
R53,50
M30x0,5 -6H
M30x0,5 -6H
47,02
1,75
Ø66,40
10,00
20,00°
Ø74,40
M30x0,5 -6H
A-A (2)
4,76
50,00
57,00
14/05/2018
D
Plano-In_M3
Sheet 1 of 1

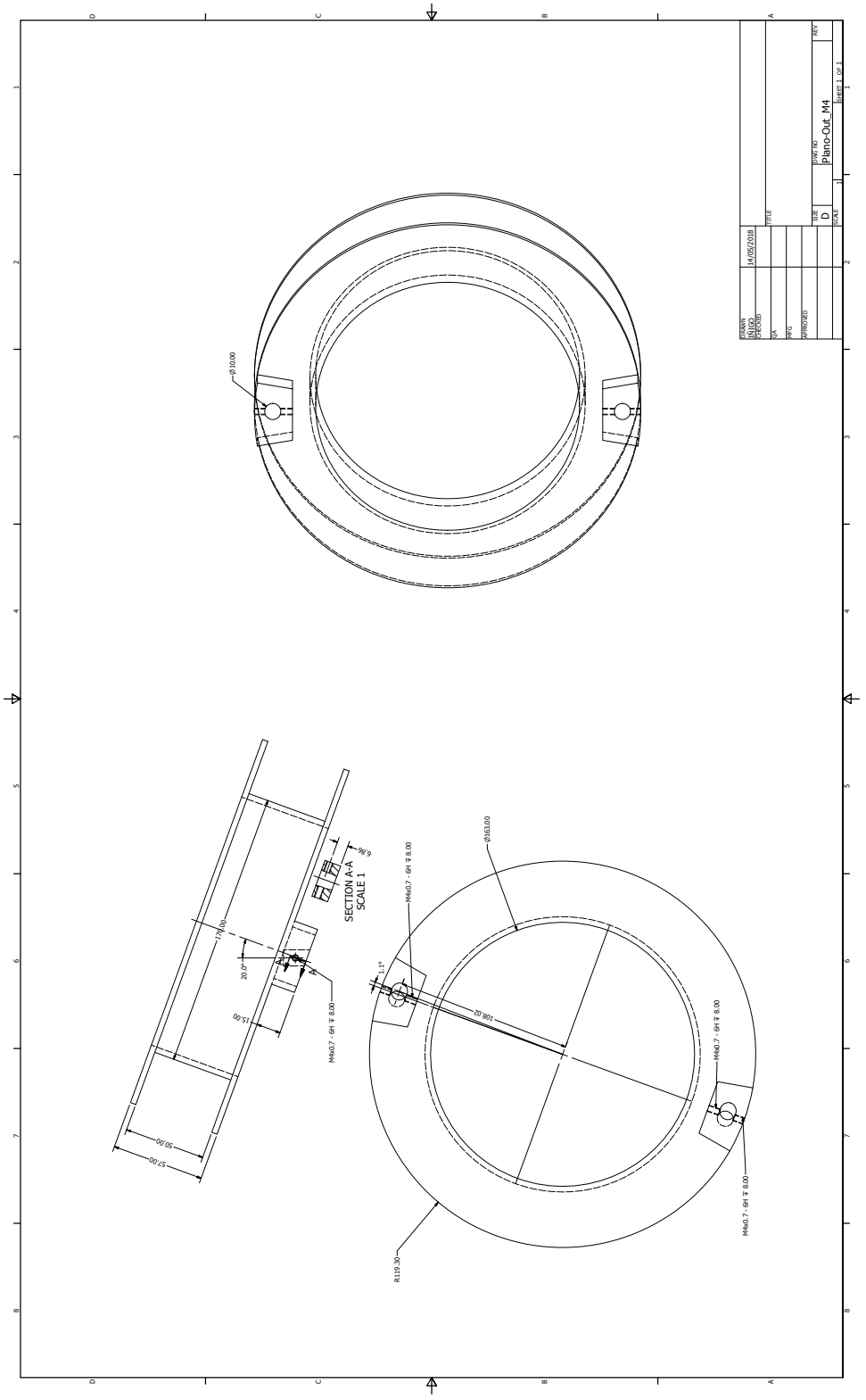
Ø10.00
SECTION A-A
SCALE 1
M4x0.7 - 6H ↧ 8.00
Ø163.00
108.02
R119.30
1.1°
20.0°
15.00
170.00
50.00
57.00
6.98

Appendix C: Model 460 3-Channel Gaussmeter Specifications [53]

1.2 SPECIFICATIONS

General Measurement
Number of Inputs: 3
Update Rate: up to 4 readings per second on display;
up to 14 readings per second with IEEE-488 interface
Measurement Modes: DC, RMS, Peak
Probe Compatibility: Standard, multi-axis, and custom probes
Probe Features: Linearity Correction, Temperature Correction, Auto Probe Zero, Differential Reading, Vector Magnitude
Measurement Features: Auto Range, Max Hold, Relative Mode, Filter
Probe Connector: 15 pin D style

DC Measurement
DC Display Resolution: 5¾ digits with filter, 4¾ digits without filter

Range	Resolution w/ Filter	Resolution w/out Filter
HST Probe		
300 kG	0.001 kG	0.01 kG
30 kG	0.0001 kG	0.001 kG
3 kG	0.00001 kG	0.0001 kG
300 G	0.001 G	0.01 G
HSE Probe		
30 kG	0.0001 kG	0.001 kG
3 kG	0.00001 kG	0.0001 kG
300 G	0.001 G	0.01 G
30 G	0.0001 G	0.001 G
UHS Probe		
30 G	0.0001 G	0.001 G
3 G	0.00001 G	0.0001 G
300 mG	0.001 mG	0.01 mG

DC Accuracy: ±0.10% of reading ±0.005% of range
DC Temperature Coefficient: ±0.05% of reading ±0.03% of range/°C

AC RMS & Peak Measurement
AC Display Resolution: 4¾ digits

Range	RMS Resolution	Peak Resolution
HST Probe		
300 kG	0.01 kG	0.01 kG
30 kG	0.001 kG	0.001 kG
3 kG	0.0001 kG	0.0001 kG
300 G	0.01 G	—
HSE Probe		
30 kG	0.001 kG	0.001 kG
3 kG	0.0001 kG	0.0001 kG
300 G	0.01 G	0.01 G
30 G	0.001 G	—
UHS Probe		
30 G	0.001 G	0.001 G
3 G	0.0001 G	0.0001 G
300 mG	0.01 mG	—

AC Frequency Range: 10 – 400 Hz
AC RMS Accuracy: ±2% of reading (50 – 60 Hz)
AC RMS Freq. Response: 0 to -3.5% of reading (10 – 400 Hz)
(All AC RMS specifications for sinusoidal input >1% of range)
AC Peak Accuracy: ±5% typical
AC Peak Speed: 5 ms for single peak

Front Panel
Display Type: 4 line by 20 character, vacuum fluorescent
Display Resolution: Up to ±5¾ digits
Display Update Rate: 4 rdgs/sec. Vector Off, 3 rdgs/sec On
Displays Units: Gauss (G), Tesla (T)
Units Multipliers: µ, m, k
Annunciators:

RMS	AC input signal
DC	DC input signal
MAX	Max Hold value
°	Relative reading
R	Remote operation
a	Alarm on

Keypad: 25 full travel keys
Front Panel Features: Intuitive operation, display prompts, front panel lockout, brightness control

Interfaces
RS-232C Capabilities:
Baud: 300, 1200, 9600
Connector: RJ-11 configuration
Update Rate: Up to 14 readings per second
IEEE-488 Capabilities:
Complies with IEEE-488.2: SH1 AH1 SR1 RL1 PP0 DC1 DT0 C0 E1
Software Support: LabView Driver
Update Rate: 18 rdgs/sec. Vector Off, 14 rdgs/sec. Vector On
Alarm:
Settings: High and low set point, Inside/Outside, Audible
Actuators: Display annunciator, beeper
Monitor Analog Output (3)
Configuration: Real-time analog voltage output
Scale: ±3 V = ±FS on selected range
Frequency Response: DC to 400 Hz
Accuracy: Probe dependent
Minimum Load Resistance: 1 kΩ (short circuit protected)
Connector: BNC
Corrected Analog Output (1)
Configuration: Voltage output generated by DAC
Range: ±3 V; ±10 V for Model 460-10
Scale: User defined
Resolution: 0.366 mV of ±3 V
Update Rate: Same as field measurement
Accuracy: ±0.1% of full scale in addition to measurement error
Minimum Load Resistance: 1 kΩ (short circuit protected)
Connector: BNC

General
Ambient Temperature: 15 – 35 °C at rated accuracy.
5 – 40 °C with reduced accuracy
Power Requirement: 100, 120, 220, 240 VAC (+5%, -10%), 50 or 60 Hz, 40 watts
Size: 434 W x 89 H x 369 mm D (17.1 x 3.5 x 14.5 in.), half rack
Weight: 7.5 kilograms (16.5 pounds)
Approval: CE Mark

Ordering Information

Part number	*Description*
Instrument	
460	Model 460 Gaussmeter, ±3 V corrected analog output
460-10	Model 460 Gaussmeter, ±10 V corrected analog output
Accessories Included	
115-006	Detachable line cord (U.S.)
115-007	Detachable line cord (European)
4060	Zero gauss chamber
MAN-460	Model 460 Gaussmeter User's Manual
Accessories Available	
4001	RJ-11 cable assembly
4002	RJ-11 to DB-25 adapter
4003	RJ-11 to DE-9 adapter
4004	IEEE-488 cable, 1 meter (3 feet)
4065	Large zero gauss chamber for Gamma probe
RM-1	Rack mount kit for one 460 gaussmeter
MCBL-6	User programmable cable with PROM (6' long)
MCBL-20	User programmable cable with PROM (20' long)
MPEC-10	Probe extension cable with EEPROM (10' long)
MPEC-25	Probe extension cable with EEPROM (25' long)
MPEC-50	Probe extension cable with EEPROM (50' long)
MPEC-100	Probe extension cable with EEPROM (100' long)

(Extension cables must be matched to probes)

Probes Ordered Separately
Custom Probes Available (Consult Lake Shore for more information)
Specifications are subject to change without notice.

Appendix D: 3D Printed Probe Holder Drawing

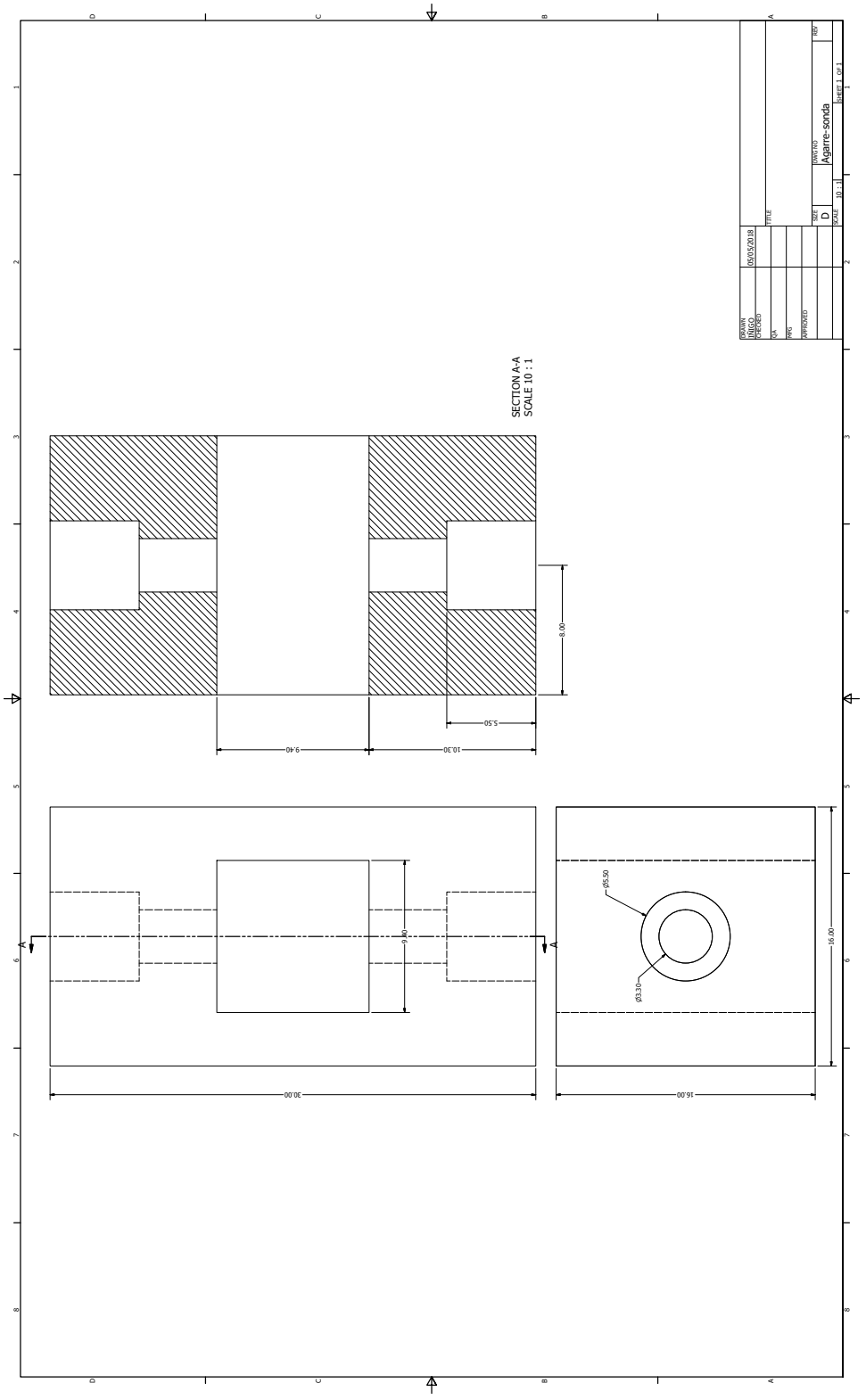

Appendix E: Gaussmeter Interface

Interface

The Lake Shore model 460 Gaussmeter offers two different interface ways: IEEE-488 and Serial interface.

IEEE-488 is an 8-bit communication bus used for instrumentation with a hardware and specific programming standards that simplify interfacing between the device and a computer. This bus is also commonly called GPIB (General Purpose Interface Bus). In particular, the used device complies with the IEEE-488.2-1987 standard [56]. Thus, it incorporates its functional, electrical and mechanical specifications. In this interface mode, all instruments connected perform one or more of the interface functions of "talker" (transmits data onto bus to other devices), "listener" (receives data) or "bus controller" (designates to the devices which function they must perform). In order to use this interface, IEEE-488 address of the device and the IEEE-488 terminators must be specified within the device. These serve for the bus to locate the specified device and to know when a message string is finished respectively.

The serial interface of the device is a RS-232C. This interface is described as a standard of the Electronics Industries Association (EIA) [57]. It requires a connection from an RJ-11 wire (which is the exit provided by the gaussmeter) to a 9-pin or 25-pin connector. For this type if interface, a clamp-on ferrite filter provided by Lake Shore must be attached to the RJ-11 wire near the rear panel of the device in order to maintain electromagnetic compatibility. To use this interface, the baud rate (number of units of signal per second) must be specified within the device. The system allows baud rates of 33, 1200 and 9600.

By means of the two types of interface, the communication between the gaussmeter and the computer consists on two types of functions. The first consists on "commands", by which the computer instructs the device to perform a certain function or change the settings of some parameters. The second ones consist on "queries" by which the computer instructs the device which response it needs to send (such as a measurement, inform about the range used, etc.). These are followed by "responses", in which the instrument responds to these "queries" with the information asked.

Communication with the Computer

On a first trial, it was considered to do the connection via serial interface by means of an RJ-11 wire and 9-pin connector. Thus, an adapter from RJ-11 to female DB9 connector was needed to communicate the computer of the EP2 laboratory with the gaussmeter. Such a device was retrieved from RS Components, from its web site [58]. Once this adapter was acquired it wad to be wired accordingly with the

interface specifications. The wired required was detailed in the manual of the model 460 gaussmeter [53] and is sketched as follows:

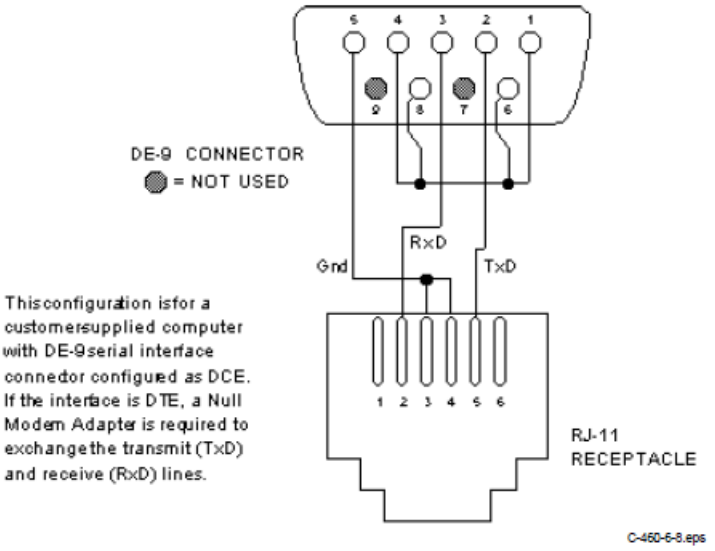

Figure 7.1: RJ-11 to DB9 wiring. Retrieved from [53]

However, since the computer of the EP2 laboratory is catalogued as DTE (Data Terminal Equipment) the transmit channel (TxD) and the receive channel (RxD) had to be wired on the contrary to the specified on the drawing.

A multimeter was used to correlate each of the wires of the acquired adapter to the number of pin of RJ-11. The relationship between the pin number of the drawing and the respective color of the wire in the adapted is summarized in the following table:

Pin number	Color
1	Black
2	Yellow
3	Red
4	Orange
5	Green
6	Brown

Table 7.1: Relationship between wire color and RJ-11 pin number

The colour wires were welded to a female DB9 adapter and an auxiliary four-end wire was made to join pins 1,4,6 and 8 of the DB9. Once all the wires were welded, the multimeter was used, once again, to check for correct contact between the RJ-11 pins and the correspondent DB9 pins. The final weld can be seen in the following figures:

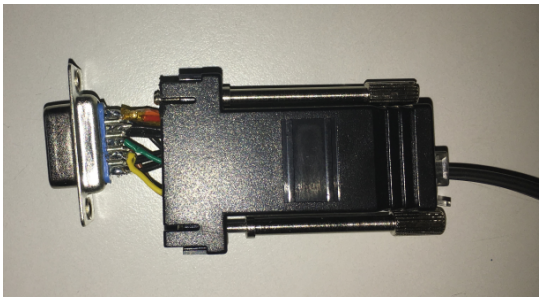

Figure 7.2: RJ-11 to DB9 welded connection

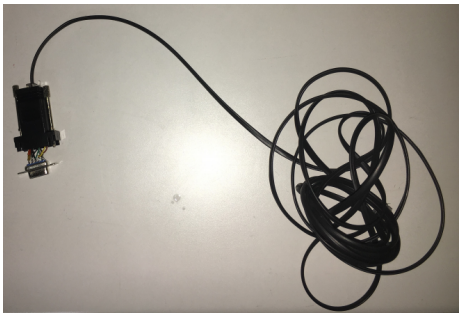

Figure 7.3: Connection with RJ-11 cable

The communication between the computer and the device had to be ensured and a correct program had to be developed. To develop the program, some specific functions of the gaussmeter were needed, such as measuring the magnetic field and correctly displaying such in the screen. To do so, different already created "drivers" for such functions were retrieved for use [59]. These were observed to be useful both for a serial interface and for IEEE-488.2 interface.

After several trials of connection, correct communication between both was achieved. However, the serial interface show some communication problems when trying the LabVIEW program for single measurements. Thus, it was decided to acquire a GPIB connector cable and use the IEEE-488.2 bus interface. A connector of these characteristics that allows IEEE-488.2 standard communication by means of an adapter to USB cable was retrieved from Prologix, LLC, web site [60]. By means of this adapter to USB, easy connection with the rear panel of the digital computer was enabled. This connector is the following:

Figure 7.4: Prologix GPIB-USB connector for IEEE-488.2 interface

Once again, it was necessary to reach communication between the digital computer and the gaussmeter via the bus interface. This was done using the National

Instruments Launcher. However, it was needed to download a program called "Prologix GPIB Configurator" (retrieved from [60]) in order to configure the different characteristics of the IEEE-488.2 interface needed for communication. The GPIB address was needed to be specified as well as the terminator (as explained for the IEEE-488 interface), as well as the number of bits if data. This configuration can be seen in figure 7.5. Once this was done, the NI Max function of the National Instruments Launcher allowed to communicate the device (which was introduced in *COM5* port) to the LabVIEW program. This connection can be seen in figure 7.6. Port settings in this last configuration of communication are not important since all the needed characteristics have already been specified in the "Prologix GPIB Configurator".

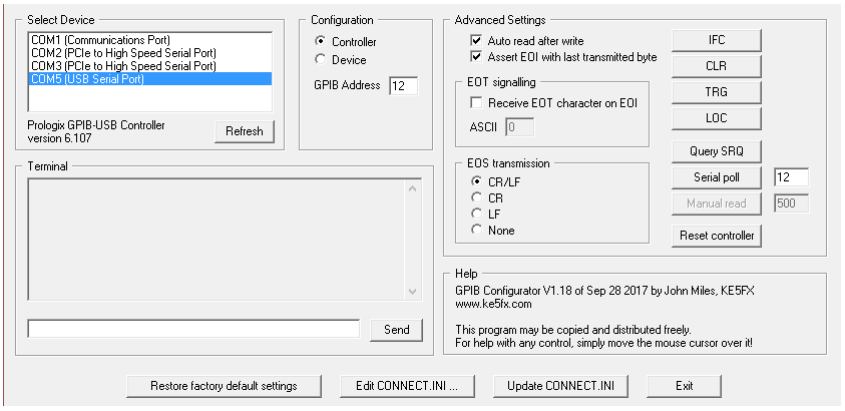

Figure 7.5: Prologix GPIB-USB configuration

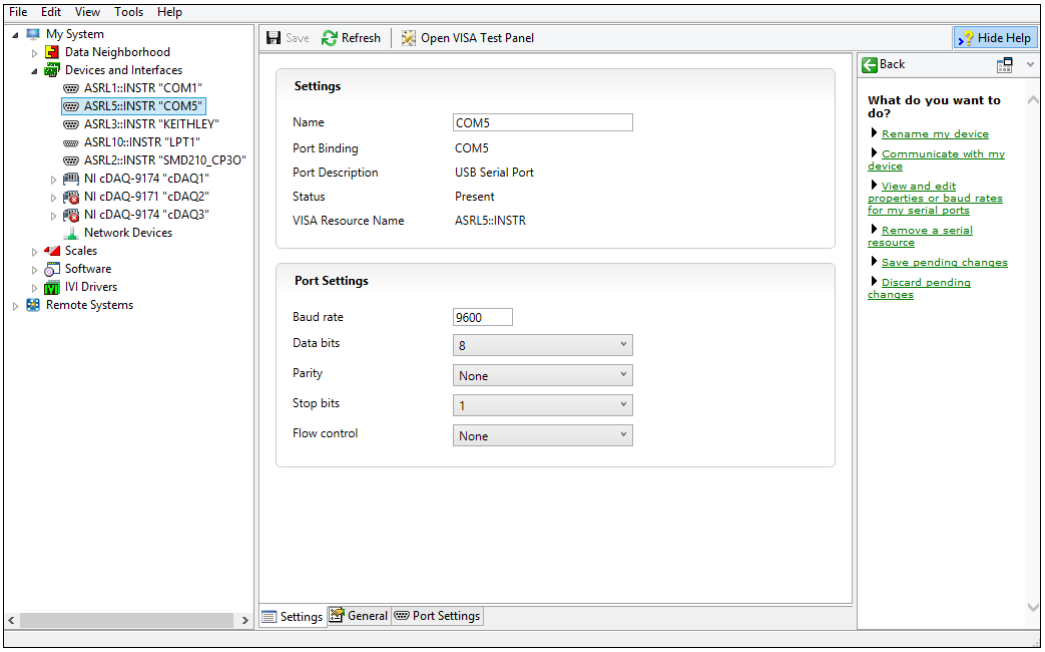

Figure 7.6: National Instruments Launcher configuration